

วิธีการใหม่สำหรับการสกัดแยกถนนจากข้อมูลภาพถ่ายดาวเทียมรีออส



วิทยานิพนธ์นี้เป็นส่วนหนึ่งของการศึกษาตามหลักสูตรปริญญาวิทยาศาสตรดุษฎีบัณฑิต

สาขาวิชาภูมิสารสนเทศ

มหาวิทยาลัยเทคโนโลยีสุรนารี

ปีการศึกษา 2554

**A NEW APPROACH FOR ROAD EXTRACTION FROM
THEOS IMAGES**

Satith Sangpradid



A Thesis Submitted in Partial Fulfillment of the Requirements for the

Degree of Doctor of Philosophy in Geoinformatics

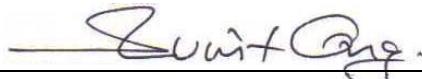
Suranaree University of Technology

Academic Year 2011

A NEW APPROACH FOR ROAD EXTRACTION FROM THEOS IMAGES

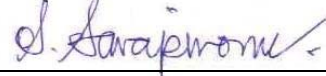
Suranaree University of Technology has approved this thesis submitted in partial fulfillment of the requirements for the Degree of Doctor of Philosophy.

Thesis Examining Committee



(Asst. Prof. Dr. Suwit Ongsomwang)

Chairperson



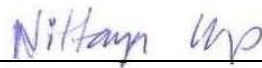
(Asst. Prof. Dr. Sunya Sarapirome)

Member (Thesis Advisor)




(Asst. Prof. Dr. Songkot Dasananda)

Member



(Assoc. Prof. Dr. Nittaya Kerdprasop)

Member




(Dr. Taravudh Tipdecho)

Member



(Prof. Dr. Sukit Limpijumnong)

Vice Rector for Academic Affairs



(Assoc. Prof. Dr. Prapun Manyum)

Dean of Institute of Science

สาธิต แสงประดิษฐ์ : วิธีการใหม่สำหรับการสกัดแยกถนนจากข้อมูลภาพถ่ายดาวเทียม
ธีออส (A NEW APPROACH FOR ROAD EXTRACTION FROM THEOS IMAGES)
อาจารย์ที่ปรึกษา : ผู้ช่วยศาสตราจารย์ ดร.สัญญา สราภิรมย์, 145 หน้า.

การสกัดแยกลักษณะข้อมูลจากระยะไกลโดยอัตโนมัติ ให้ประโยชน์ในแง่ของเวลาและ
ค่าใช้จ่าย มากกว่าการสกัดแยกแบบดั้งเดิมเช่นการแปลงข้อมูลเป็นดิจิทัลด้วยมือ วัตถุประสงค์ของ
งานวิจัย คือการปรับปรุงวิธีการ Fast Intensity Hue Saturation สำหรับกระบวนการทำ pan-
sharpening บนข้อมูลธีออส และเพื่อพัฒนาโมดูลสำหรับการจัดกลุ่มข้อมูลภาพและสกัดแยกถนน
อัตโนมัติ กระบวนการประกอบด้วย การทำ pan-sharpening จากภาพหลายช่วงคลื่นและภาพแพน
โครมาติก เทคนิคการจัดกลุ่มประยุกต์ใช้กับภาพ pan-sharpened เพื่อหากลุ่มตัวแทนเครือข่ายถนน
การทำ morphological และการแบ่งส่วนแบบ edge-aid ประยุกต์ใช้กรองและลบวัตถุที่ไม่ใช่ถนน
และ morphological thinning ใช้สำหรับการสกัดแยกเส้นกลางของถนน

เทคนิคและโมดูลที่พัฒนาประยุกต์ใช้กับชุดข้อมูลธีออส ในอำเภอเมืองนครราชสีมา ใน
กระบวนการนี้ทำการทดลอง 3 ครั้ง สำหรับการทดลองครั้งที่ 1 และ 2 ให้ กำหนดแบนด์ Green
และ Blue ปรับด้วยการคูณ 0.75 และ 0.25 ตามลำดับ ในการทดลองครั้งที่ 3 ไม่ปรับใน 2 แบนด์นี้
สำหรับการทดลองทั้งหมด แบนด์ Red และ NIR ปรับด้วยการคูณ a และ b ตามลำดับ โดยค่า a และ
b ได้จากค่าเฉลี่ย CCs สูงสุดของภาพหลายช่วงคลื่นและภาพ pan-sharpened ของแต่ละการทดลอง
ผลที่ได้คือ $a = 0.05 \ 0.55 \text{ และ } 1.05$ และ $b = 0.95 \ 0.45 \text{ และ } 1.45$ นำไปใช้ในการทดลองครั้งที่ 1 ถึง
3 ตามลำดับ ภาพ pan-sharpened ที่ได้จากการทดลอง นำมาตรวจสอบด้วยการวิเคราะห์ด้วย
สายตาจากภาพสีผสมเท็จและภาพแพนโครมาติก เปรียบเทียบค่าสัมประสิทธิ์ความสัมพันธ์ของ
ภาพ pan-sharpened และภาพแพนโครมาติก เปรียบเทียบจากผลการจัดกลุ่มของภาพ โดยการ
ทดลองครั้งที่ 3 ให้ผลลัพธ์ที่ดีกว่าการทดลองทั้งสองวิธี

การจัดกลุ่มของตัวแทนเครือข่ายถนนและการสกัดแยกถนนโดยอัตโนมัติ กระทำอยู่บน
ข้อมูลภาพ pan-sharpened จากการทดลองครั้งที่ 2 และ 3 โดยผลของการทดลองครั้งที่ 3 แสดงผล
ของการจัดกลุ่มข้อมูลดีกว่าและผลของการสกัดแยกถนนโดยอัตโนมัติดีกว่า จากการตรวจสอบด้วย
completeness correctness และ quality ของผลการสกัดแยกถนนเส้นหลักและเส้นรอง

สาขาวิชาการรับรู้จากระยะไกล
ปีการศึกษา 2554

ลายมือชื่อนักศึกษา 
ลายมือชื่ออาจารย์ที่ปรึกษา 

SATITH SANGPRADID : A NEW APPROACH FOR ROAD
EXTRACTION FROM THEOS IMAGES. THESIS ADVISOR : ASST.
PROF. SUNYA SARAPIROME, Ph.D. 145 PP.

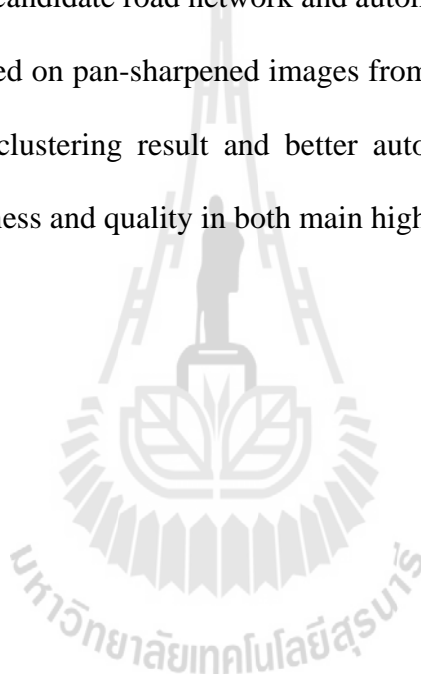
THEOS IMAGES/IHS TRANSFORMATION/PAN-SHARPENED IMAGES/
FUZZY C-MEANS/SIMULATED ANNEALING/ROAD EXTRACTION/
MATHEMATICAL MORPHOLOGY/EDGE-AID SEGMENTATION

Automated extraction of features from remotely sensed data can provide more benefit, in terms of time and budget consumption, than the conventional extraction such as manual digitization. The research objectives were to improve Fast Intensity Hue Saturation (FIHS) transformation for pan-sharpening process operating on THEOS data and to develop extension modules for image clustering and automated road extraction. The processes included image pan-sharpening process from multispectral images and panchromatic image, the clustering techniques applied to pan-sharpened images to generate clusters of candidate road network, the morphological operations and edge-aid segmentation applied to filtering and remove non-road objects and morphological thinning for road centerline extraction.

The developed techniques and modules were applied to THEOS datasets in Amphoe Maung Nakhon Ratchasima. There were 3 trials to perform. For the trials no.1 and no.2, the Green and Blue bands were adjusted by multiplying with 0.75 and 0.25, respectively, while the trial no.3, no adjustment was applied for these 2 bands. For all trials, Red and NIR bands were adjusted by multiplying with a and b , respectively. Using the highest average correlative coefficient (CCs) of original

multispectral images and pan-sharpened images of each trial, $a = 0.05, 0.55, \text{ and } 1.05$ and $b = 0.95, 0.45, \text{ and } 1.45$ were applied to the trials no.1 to no.3, respectively. Pan-sharpened images resulted from each trial were examined by visual comparison to their color composite images and panchromatic image, comparing CCs of pan-sharpened and panchromatic images, clustering results comparison. The trial no.3 can provide the best result among all examined methods.

Clustering for candidate road network and automatic road centerline extraction processes were operated on pan-sharpened images from trials no.2 and no.3. The trial no. 3 showed better clustering result and better automated extraction in terms of completeness, correctness and quality in both main highway and local road network.



School of Remote Sensing

Academic Year 2011

Student's Signature

Satith Sangpradid

Advisor's Signature

S. Sangpradid

ACKNOWLEDGEMENTS

I am grateful to all the people who helped me in various stages of this project. Without their help and support, I could never have reached a successful conclusion to the project.

The work would not be possible without the guidance and direction of my supervisor Asst. Prof. Dr. Sunya Sarapirome who has been strongly supportive of my work and overall concern for me from the first day and encouragement throughout the time of the research. I am also thankful to Asst. Prof. Dr. Suwit Ongsomwang and Asst. Prof. Dr. Songkot Dasananda for several useful given discussion and comments. I would also like to thank Assoc. Prof. Dr. Nittaya Kerdprasop, Lt. Col. Dr. Sompoch Pantavungkour, and Dr. Taravudh Tipdecho for their support, guidance and the time despite their own busy schedule.

I give my special thanks to my friends and colleagues in the research office for the joyful and supportive environment they created all these years. The financial support from the Maharakham University, is also very thankful.

Finally, I can never thank enough to my parents. They are the best parents I could have asked for. They have been giving me the endless supports and devoting all their love to me since I was born.

Satith Sangpradid

CONTENTS

	Page
ABSTRACT IN THAI.....	I
ABSTRACT IN ENGLISH	II
ACKNOWLEDGEMENTS.....	IV
CONTENTS.....	V
LIST OF TABLES.....	X
LIST OF FIGURES	XIII
LIST OF ABBREVIATIONS.....	XXII
CHAPTER	
I INTRODUCTION.....	1
1.1 State of the problem	1
1.2 Research objectives.....	3
1.3 Benefits of the study	3
II LITURATURE REVIEW.....	4
2.1 Related concepts and theories	4
2.1.1 THEOS satellite images	4
2.1.2 Pan-sharpening	5
2.1.3 The evaluation of pan-sharpening image	9
2.1.3.1 Correlation coefficients (CCs).....	9

CONTENTS (Continued)

	Page
2.1.4 Clustering techniques	10
2.1.4.1 Fuzzy C-means	10
2.1.4.2 Clustering validity	11
2.1.4.3 Simulated annealing	13
2.1.5 Road extraction methods	14
2.1.5.1 Road tracking methods	16
2.1.5.2 Dynamic programming and snakes	16
2.1.5.3 Segmentation and classification	17
2.1.6 Mathematical morphology	18
2.1.7 Difference-of-Gaussians algorithm for edge detection	19
2.2 Literature reviews	21
2.2.1 Pan-sharpening model	21
2.2.2 Fuzzy clustering model	22
2.2.3 Mathematical morphology of road extraction model	24
2.3 Synthesis for the research approach	26
III DATA, EQUIPMENT AND RESEARCH METHODOLOGY	28
3.1 Equipment and data used for the study	28
3.1.1 Software	28
3.1.2 Data	29
3.2 Research methodology	30

CONTENTS (Continued)

	Page
3.2.1 Pan-sharpening	33
3.2.2 Image clustering approach	37
3.2.3 Road extraction	39
3.2.3.1 Appropriate structure element acquiring	40
3.2.3.2 Morphological opening and closing	41
3.2.3.3 Morphological top-hat	43
3.2.3.4 Edge-aid segmentation	45
3.2.3.5 Morphological thinning	45
3.2.4 Accuracy assessment	46
3.2.4.1 Completeness	46
3.2.4.2 Correctness	47
3.2.4.3 Quality	48
IV RESULT AND DISCUSSION	49
4.1 Pan-sharpening, fuzzy c-means simulated annealing of trial no.1	49
4.1.1 Pan-sharpening	48
4.1.2 The evaluation of image pan-sharpening	54
4.1.3 Fuzzy c-means clustering and simulated annealing	57
4.2 Pan-sharpening, fuzzy c-means and simulated annealing of trial no.2	60
4.2.1 Pan-sharpening	60
4.2.2 The evaluation of image pan-sharpening	64

CONTENTS (Continued)

	Page
4.2.3 Fuzzy c-means clustering and simulated annealing	66
4.3 Pan-sharpening, fuzzy c-means simulated annealing of trial no.3.....	69
4.3.1 Pan-sharpening	69
4.3.2 The evaluation of image pan-sharpening	74
4.3.3 Fuzzy c-means clustering and simulated annealing	76
4.4 The comparison of image quality of all trials	79
4.4.1 Visual comparison of composite images from all Trials.....	79
4.4.2 The CCs of the pan-sharpened and panchromatic images	80
4.4.3 Consideration on clustering results of all Trials.....	85
4.5 Image clustering.....	86
4.5.1 Comparison based on descriptive statistics	87
4.5.2 Visual comparison of the clustering results	93
4.5.3 Comparison of the clustering results with the accuracy assessment	96
4.6 Road extraction	100
4.6.1 Mathematical morphology operation for candidate road network	102
4.6.2 Edge-aid segmentation	103
4.6.3 Automated extraction of road centerline	106
4.6.4 Accuracy assessment.....	109

CONTENTS (Continued)

	Page
V CONCLUSIONS AND RECOMMENDATIONS	113
5.1 Conclusions	113
5.1.1 Pan-sharpening image	113
5.1.2 Image clustering	114
5.1.3 Road extraction	115
5.2 Recommendations	116
REFERENCES	117
APPENDICES	124
APPENDIX A THE DATA SET OF THE PANCHROMATIC AND MULTI-SPECTRAL IMAGES	125
APPENDIX B THE COMPARISON OF THE CCs OF THE ORIGINAL MS AND THE PAN-SHARPENED IMAGES	131
APPENDIX C THE MODULE OF FCM AND SA, ROAD EXTRACTION DEVELOPED BY IDL PROGRAMMING	134
CURRICULUM VITAE	145

LIST OF TABLES

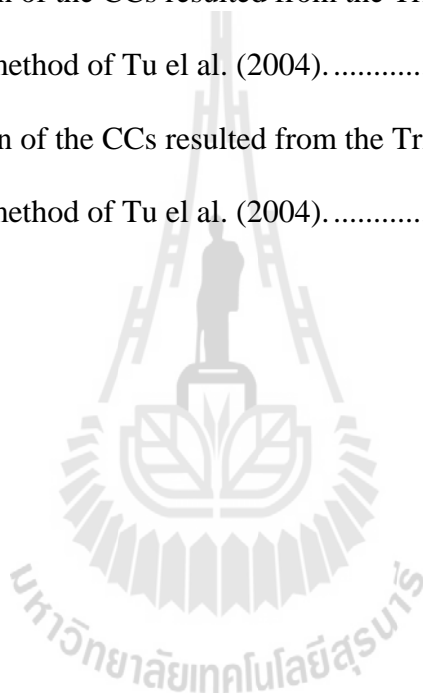
Table	Page
2.1 The characteristics of THEOS.	4
2.2 General classification of road extraction methods.....	15
4.1 Average correlation coefficients (CCs) between resembled original and pan-sharpened images of 10 sets of THEOS images of the trial no.1, with varying spectral weights.	50
4.2 The comparison of the CCs resulted from the trial no.1 and the FIHS method of Tu et al. (2004).	55
4.3 Average correlation coefficients (CCs) between resembled original and pan-sharpened images of 10 sets of THEOS images of the trial no.2, with varying spectral weights.	60
4.4 The comparison of the CCs resulted from the trial no.2 and the FIHS method of Tu et al. (2004).	65
4.5 Average correlation coefficients (CCs) between resembled original and pan-sharpened images of 10 sets of THEOS images of the trial no.3, with varying spectral weights.	69
4.6 The comparison of the CCs resulted from the trial no.3 and the FIHS method of Tu et al. (2004).	75
4.7 The comparison CCs between pan-sharpened images of all trials and the panchromatic images.....	81

LIST OF TABLES (Continued)

Table	Page
4.8	The comparison of the descriptive statistics measurement on clustering results on the Red band using ISODATA, K-means, and FCM and SA. 91
4.9	The comparison of the descriptive statistics measurement on clustering results on the Green band using ISODATA, K-means, and FCM and SA. 92
4.10	The comparison of the descriptive statistics measurement on clustering results on the Blue band using ISODATA, K-means, and FCM and SA. 92
4.11	The comparison of the descriptive statistics measurement on clustering results on the NIR band using ISODATA, K-means, and FCM and SA. 93
4.12	Error matrixes and accuracy assessment of the result of clustering image using ISODATA technique..... 97
4.13	Error matrixes and accuracy assessment of the result of clustering image using K-means technique..... 97
4.14	Error matrixes and accuracy assessment of the result of clustering image using FCM and SA technique..... 98
4.15	Summarized overall accuracy and kappa statistics of clustering image using ISODATA, K-means, and FCM and SA techniques..... 98
4.16	Summarized producer's and user's accuracies of clustering image using ISODATA, K-means, and FCM and SA techniques..... 99
4.17	The comparison of accuracy assessment of the road centerline extraction between the trials no.2 and no.3..... 111

LIST OF TABLES (Continued)

Table	Page
B.1 The comparison of the CCs resulted from the Trial no.1 and the FIHS method of Tu el al. (2004).....	132
B.2 The comparison of the CCs resulted from the Trial no.2 and the FIHS method of Tu el al. (2004).....	132
B.3 The comparison of the CCs resulted from the Trial no.3 and the FIHS method of Tu el al. (2004).....	133



LIST OF FIGURES

Figure	Page
2.1	The relative radiometric responses of the THEOS images (GISTDA, 2009)... 5
2.2	The relative spectral responses of IKONOS images (Teague, 2001). 7
2.3	An example of the edge DoG detection (a) the Gaussian 1, (b) the Gaussian 2, and (c) The result of the edge DoG detection (Narasimhan, 2006)..... 20
3.1	The study area is Nakhon Ratchasima city municipality and the vicinity 29
3.2	Conceptual framework of the study 31
3.3	Trials and errors of pan-sharpening process. 32
3.4	Pan-sharpening of high spatial resolution and multi-spectral image based on improved IHS transformation. 34
3.5	Image clustering approaches..... 37
3.6	Optimization of clustering methods..... 38
3.7	Automated road extraction using mathematical morphology and edge-aided segmentation. 39
3.8	Structure elements with (a) 3 by 3 square and (b) 8 by 8 square..... 41
3.9	The morphological opening operation with a 3 by 3 square..... 42
3.10	The morphological closing operation with a 3 by 3 square. 43
3.11	The original image (a) and the result of morphological top-hat operation of a 3 by 3 square (b). 44

LIST OF FIGURES (Continued)

Figure	Page
3.12 The original image (a) and the result of morphological top-hat operation of a 8 by 8 square (b).	44
3.13 The length matched reference road is the length of reference network falling in the buffer area of extracted data.....	46
3.14 The length of matched extraction is the length of extracted data falling in the buffer zone of the reference network.....	47
4.1 The image dataset 1 (a) Panchromatic image (b) Multi spectral images (c) pan-sharpened images from the trial no.1 using parameters 0.05 for a and 0.95 for b	51
4.2 The zoom-in image dataset 1 (a) Panchromatic image (b) Multi spectral images (c) pan-sharpened images from trial no.1 using parameters 0.05 for a and 0.95 for b	52
4.3 The image dataset 2 (a) Panchromatic image (b) Multi spectral images (c) pan-sharpened images from the trial no.1 using parameters 0.05 for a and 0.95 for b	53
4.4 The zoom-in image dataset 2 (a) Panchromatic image (b) Multi spectral images (c) pan-sharpened images from the trial no.1 using parameters 0.05 for a and 0.95 for b	54
4.5 The comparison of pan-sharpened images data set 1 (a) pan-sharpened images from FIHS (b) pan-sharpened images from the trial no.1 using parameters 0.05 for a and 0.95 for b	56

LIST OF FIGURES (Continued)

Figure	Page
4.6	The comparison of pan-sharpened images data set 2 (a) pan-sharpened images from FIHS (b) pan-sharpened images from the trial no.1 using parameters 0.05 for a and 0.95 for b 55
4.7	The result of unsupervised classification with 30 classes operated on pan-sharpened images resulted from the trial no.1 using FCM and SA (a), the zoom-in classified image (b), the zoom-in pan-sharpened images (c). 58
4.8	The result of unsupervised classification with 30 classes operated on pan-sharpened images resulted from the trial no.1 using FCM and SA (a), the zoom-in classified image (b), the zoom-in pan-sharpened images (c). 59
4.9	The image dataset 1 (a) Panchromatic image (b) Multi spectral images (c) pan-sharpened images from the trial no.2 using parameters 0.55 for a and 0.45 for b 61
4.10	The zoom-in image dataset 1 (a) Panchromatic image (b) Multi spectral images (c) pan-sharpened images from trial no.2 using parameters 0.55 for a and 0.45 for b 62
4.11	The image dataset 2 (a) Panchromatic image (b) Multi spectral images (c) pan-sharpened images from the trial no.2 using parameters 0.55 for a and 0.45 for b 63
4.12	The zoom-in image dataset 2 (a) Panchromatic image (b) Multi spectral images (c) pan-sharpened images from trial no.2 using parameters 0.55 for a and 0.45 for b 64

LIST OF FIGURES (Continued)

Figure	Page
4.13	The comparison of pan-sharpened images data set 1 (a) pan-sharpened images from FIHS (b) pan-sharpened images from the trial no.2 using parameters 0.55 for a and 0.45 for b 65
4.14	The comparison of pan-sharpened images data set 2 (a) pan-sharpened images from FIHS (b) pan-sharpened images from the trial no.2 using parameters 0.55 for a and 0.45 for b 66
4.15	The result of unsupervised classification with 30 classes operated on pan-sharpened images resulted from the trial no.2 using FCM and SA (a), the zoom-in classified image (b), the zoom-in pan-sharpened images (c). 67
4.16	The result of unsupervised classification with 30 classes operated on pan-sharpened images resulted from the trial no.2 using FCM and SA (a), the zoom-in classified image (b), the zoom-in pan-sharpened images (c). 68
4.17	The plot between different distance of average CCs and varying b . When a is bigger than 1 and b is less than 1.5, the turning point of the rate of increment of the different distance appeared at $b= 1.45$ 70
4.18	The image dataset 1 (a) Panchromatic image (b) Multi spectral images (c) pan-sharpened images from the trial no.3 using parameter 1.05 for a and 1.45 for b 71
4.19	The zoom in of image dataset 1 (a) Panchromatic image (b) Multi spectral images (c) pan-sharpened images from the trial no.3 using parameter 1.05 for a and 1.45 for b 72

LIST OF FIGURES (Continued)

Figure	Page
4.20 The image dataset 2 (a) Panchromatic image (b) Multi spectral images (c) pan-sharpened images from the trial no.3 using parameter 1.05 for a and 1.45 for b	73
4.21 The zoom in of image dataset 2 (a) Panchromatic image (b) Multi spectral images (c) pan-sharpened images from the trial no.3 using parameter 1.05 for a and 1.45 for b	74
4.22 The comparison of pan-sharpened images data set 1 (a) pan-sharpened images from FIHS (b) pan-sharpened images from the trial no.3 using parameter 1.05 for a and 1.45 for b	75
4.23 The comparison of pan-sharpened images data set 2 (a) pan-sharpened images from FIHS (b) pan-sharpened images from the trial no.3 using parameter 1.05 for a and 1.45 for b	76
4.24 The result of unsupervised classification with 30 classes operated on pan-sharpened images resulted from the trial no.3 using FCM and SA (a), the zoom-in classified image (b), the zoom-in color composite of the pan-sharpened images (c).	77
4.25 The result of unsupervised classification with 30 classes operated on pan-sharpened images resulted from the trial no.3 using FCM and SA (a), the zoom-in classified image (b), the zoom-in color composite of the pan-sharpened images (c).....	78

LIST OF FIGURES (Continued)

Figure	Page
4.26 The pan-sharpened images in the area representing local road network resulted from (a) the trial no.1, (b) the trial no.2, and (c) the trial no.3.....	79
4.27 The pan-sharpened images in the area representing main highway network resulted from (a) the trial no.1, (b) the trial no.2, and (c) the trial no.3.....	80
4.28 The comparison of panchromatic image (a) and the pan-sharpened images data set 1 of Red band from the trial no.1 (b), the trial no.2 (c), and the trial no.3 (d).....	82
4.29 The comparison of panchromatic image (a) and the pan-sharpened images data set 1 of NIR band from the trial no.1 (b), the trial no.2 (c), and the trial no.3 (d).....	83
4.30 The comparison the panchromatic image data set 1 (a) and the color composite images (R:G:B 4:2:1) of pan-sharpened images resulted from the trial no.1 (b), trial no.2 (c), and trial no.3 (d).	84
4.31 The extension interface of FCM and SA processes.	86
4.32 (a) The color composite of the pan-sharpened images from the trial no.3, the results of clustering using (b) ISODATA, (c) K-means, and (d) FCM and SA.....	88
4.33 The comparison of the descriptive statistics measurement on clustering results on the Red band using (a) ISODATA, (b) K-means, and (c) FCM and SA.....	89

LIST OF FIGURES (Continued)

Figure	Page
4.34 The comparison of the descriptive statistics measurement on clustering results on the Green band using (a) ISODATA, (b) K-means, and (c) FCM and SA.....	89
4.35 The comparison of the descriptive statistics measurement on clustering results on the BLUE band using (a) ISODATA, (b) K-means, and (c) FCM and SA.....	90
4.36 The comparison of the descriptive statistics measurement on clustering results on the NIR band using (a) ISODATA, (b) K-means, and (c) FCM and SA.....	90
4.37 The zoom-in images of (a) the color composite of the pan-sharpened images, the results of clustering using (b) ISODATA, (c) K-means, and (d) FCM and SA.....	94
4.38 The zoom-in images of (a) the color composite of the pan-sharpened images, the results of clustering using (b) ISODATA, (c) K-means, and (d) FCM and SA.....	95
4.39 The zoom-in images of (a) the color composite of the pan-sharpened images, the results of clustering using (b) ISODATA, (c) K-means, and (d) FCM and SA.....	96
4.40 The color composite of pan-sharpened images from (a) the trial no.2 and (b) the trial no.3.	100

LIST OF FIGURES (Continued)

Figure	Page
4.41 The results of 15 clusters classified using FCM and SA operated on pan-sharpened images from (a) the trial no.2 and (b) the trial no.3.....	101
4.42 The binary images of candidate road network (white) and non-road features (black) from (a) the trial no.2 (b) the trial no.3.....	103
4.43 The result of morphology top-hat operation for binary images from (a) the trial no.2 and (b) the trial no.3.....	106
4.44 The panchromatic image of the study area (a) and the edge image using edge DoG (b). The edge was displayed in white.....	104
4.45 The zoom-in images resulted from edge DoG detection.	104
4.46 The candidate road network (in white) resulted from morphology Top-Hat operation and edge-aid segmentation of images from (a) the trial no.2 and (b) the trial no.3.....	106
4.47 The extraction results of centerline road network using the morphological thinning operation on images (a) from the trial no.2 and (b) the trial no.3. .	107
4.48 The overlay of road centerline network from the trial no.2 on the panchromatic image.....	108
4.49 The overlay of road centerline network from the trial no.3 on the panchromatic image.....	108
4.50 The reference data of road centerline network.	109

LIST OF FIGURES (Continued)

Figure	Page
4.51	The result of the accuracy assessment of the road centerline extraction which is performed on the testing images of trial no.2 and the reference data. 110
4.52	The result of the accuracy assessment of the road centerline extraction which is performed on the testing images of trial no.3 and the reference data. 110
A.1	The image data set 1 (a) Panchromatic image (b) Multispectral images..... 126
A.2	The image data set 2 (a) Panchromatic image (b) Multispectral images..... 126
A.3	The image data set 3 (a) Panchromatic image (b) Multispectral images..... 127
A.4	The image data set 4 (a) Panchromatic image (b) Multispectral images..... 127
A.5	The image data set 5 (a) Panchromatic image (b) Multispectral images..... 128
A.6	The image data set 6 (a) Panchromatic image (b) Multispectral images..... 128
A.7	The image data set 7 (a) Panchromatic image (b) Multispectral images..... 129
A.8	The image data set 8 (a) Panchromatic image (b) Multispectral images..... 129
A.9	The image data set 9 (a) Panchromatic image (b) Multispectral images..... 130
A.10	The image data set 10 (a) Panchromatic image (b) Multispectral images.... 130

LIST OF ABBREVIATIONS

CCs	=	Correlation Coefficients
DoG	=	Edge Difference-of-Gaussians
FCM	=	Fuzzy c-means
FIHS	=	Fast Intensity Hue Saturation
GIS	=	Geographic Information System
GISTDA	=	Geo-Informatics and Space Technology Development Agency (public organization)
IDL	=	Interactive Data Language
IHS	=	Intensity Hue Saturation method
LoG	=	Laplacian-of-Gaussians
MS	=	Multispectral
NIR	=	Near Infrared
PAN	=	Panchromatic image
PCA	=	Principal Component Analysis
SA	=	Simulated Annealing
THEOS	=	Thailand Earth Observation System

CHAPTER I

INTRODUCTION

1.1 State of the problem

In recent years, an automated feature extraction from satellite image has been supplemental piece of technology used to achieve image information. It is able to facilitate the image analysis, the interpretation and the updating existing databases for the urgent information requirement of each organization. Currently, the image information extraction has mostly performed manually, which has been very expensive and time-consuming. To overcome this drawback, the automated thematic extraction from images is needed to develop.

As known, high spatial resolution and multi-spectral characteristics of remote imagery becomes a powerful tool to the understanding of phenomena on the ground. Several researchers have been using pan-sharpening images for object clustering and segmentation. Pan-sharpening is an image processing technique increasingly used to combine the available high spectral resolution images and high spatial resolution panchromatic image for both of the high spatial and the spectral resolutions. The pan-sharpening image technique used in this study is an improved IHS transformation technique.

The clustering procedure is the pre-processing method of basic image classification. Clustering involves the search for image points (DNs) that are similar

enough to be grouped together. In the analysis of an image, K-means, ISODATA, and fuzzy c-means are conventional clustering techniques. Conventional clustering techniques are always based on partitioning of the feature space. The most widely used fuzzy clustering algorithm is the fuzzy c-means algorithm proposed by Bezdek and Pal (1992). The determining of the optimal partition and optimal number are widely used to validate the problems of the fuzzy partitions, hence it is being one of the most important issues related to the fuzzy clustering analysis. However, the fuzzy c-means algorithm has no validity index to identify iteration of optimal partition.

The first try of automated feature extraction is generally started on road network because road in high-resolution remotely sensed image includes the following obvious characteristics: length, shape, boundary, long rectangular, its connectivity and etc. There are some researchers working on the same propose with IKONOS and QUICKBRID (Mohammadzadeh, Tavakoli, and Valadan Zoej, 2006; Ameri, Mobaraki, and Valadan Zoej, 2008; Lizarazo and Barros, 2008).

In this study, the fuzzy c-means, the simulated annealing technique, and cluster validity index are the three methods for improving the image clustering for road network extraction. The more proper the data are clustered, the more automated extraction is improved. To reach the study objectives the modules on image processing such as clustering and extraction with specific techniques will be developed under the IDL environment.

An automated road network extraction approach through mathematical morphology of this study will be applied on the high spatial resolution and multi-spectral images such as THEOS remotely sensed data. The THEOS data have their own spatial and spectral characteristics different from other mentioned. Finally,

extracted road centerline in form of vector from the road network in the image is expected. These road vectors can be directly imported into GIS for updating digital road maps.

1.2 Research objectives

The objective of this study is to present steps of effective approaches to automated road network extraction from pan-sharpened THEOS images. The main specific objectives of this study are as follows:

1.2.1 To improve IHS Transformation for pan-sharpening image technique.

1.2.2 To develop the extension module for image clustering using fuzzy c-means and simulated annealing algorithm.

1.2.3 To develop the extension module for automatic extraction of road network from image using mathematical morphology.

1.3 Benefits of the study

The benefits of the study include:

1.3.1 The image fusion technique of the IHS algorithm will be improved, so it can be applied efficiently to the pan-sharpening of multi-spectral and the high resolution images such as THEOS data.

1.3.2 The module of simulated annealing and fuzzy c-means methods used as a clustering approach of high resolution images will be developed.

1.3.3 The module for automated thematic extraction of road centerline as a GIS data layer will be developed using the mathematical morphology technique.

CHAPTER II

LITERATURE REVIEW

2.1 Related concepts and theories

The main related concepts and theories of this study are here summarized including THEOS satellite images, pan-sharpening, the evaluation of pan-sharpening image, clustering techniques, road extraction, mathematical morphology, edge detection, and accuracy assessment of image extraction.

2.1.1 THEOS satellite images

THEOS (Thailand Earth Observation System) satellite was launched on 1 October 2008 into a sun-synchronous orbit. The program is developed by the Geo-Informatics and Space Technology Development Agency (GISTDA), Ministry of Science and Technology, Thailand. The payload of THEOS satellite includes high spatial resolution panchromatic and multi-spectral images. Table 2.1 describes the characteristics of the THEOS satellite's sensor (GISTDA, 2009).

Table 2.1 The characteristics of THEOS.

	PAN	MS
Spatial resolution	2 m	15 m
Imaging swath	22 km	90 km
Spectral ranges	P : 0.45 – 0.90 μm	B1 (blue) : 0.45 -0.52 μm B2 (green) : 0.53 – 0.60 μm B3 (red) : 0.62 – 0.69 μm B4 (NIR) : 0.77 – 0.90 μm

The relative radiometric responses of the THEOS panchromatic and multi-spectral imagery are shown in Figure 2.1. It shows the spectral curves for the different bands of the satellite imagery. The spectral response of the pan is uniform in the entire wavelength; and covers the spectral response of Blue, Green, Red, and NIR bands. It is observable that the responses of Red and NIR are about 15-20% less than that of the panchromatic.

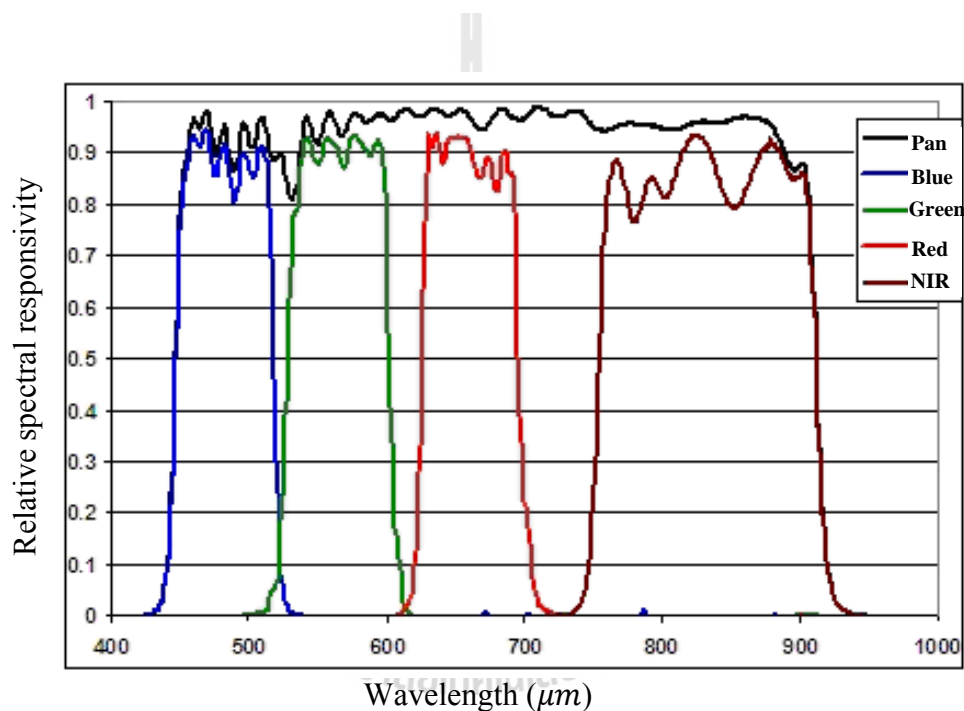


Figure 2.1 The relative radiometric responses of the THEOS images (GISTDA, 2009).

2.1.2 Pan-sharpening

Pan-sharpening is a technique to combine the available multi-spectral images and high spatial resolution panchromatic image to produce a synthetic image that has both high spatial and spectral resolutions. This image processing technique is known as pan-sharpening or resolution merge technique. Image pan-sharpening

technique has been developed by many researchers. The fusion techniques aiming at synthesizing multi-spectral images with a high spatial resolution one include for example, IHS transform, PCA, Brovey transform, and wavelet transform methods. The different aspects of data fusion were discussed in more detail in Zhang (1999) and Veeraraghavan (2004).

Intensity-Hue-Saturation (IHS) method is among the most popular fusion techniques for image pan-sharpening. The intensity-hue-saturation transform method is the replacement of the intensity band of multi-spectral image with a high resolution panchromatic band which is a simulation from color perception by human beings. The basic idea is as follows. Firstly, the low resolution pixel of multi-spectral images is resized to be the same of the high resolution panchromatic image. Secondly, the multi-spectral image composite is changed from the RGB color space to the IHS color space domain. Then, the intensity (I) element which is the spatial components is substituted by using histogram matched panchromatic image (high resolution image). At the same time the hue (H) and the saturation (S) parts are resampled to the resolution of the panchromatic image. Lastly, the inverse IHS transformation is used to get images back into RGB color domain to obtain a fusion image.

The problem of classical image fusion methods is distortion of the spectral characteristics of the multi-spectral image. This means that the variation on hue before and after the fusion process has appeared. Teague (2001) found the cause of this variation on hue and realized the influence of spectral response on the fused IKONOS images, the relative spectral responses, as shown in Figure 2.2. This study approach is to minimize the spectral distortion inherent in IHS based fusion methods.

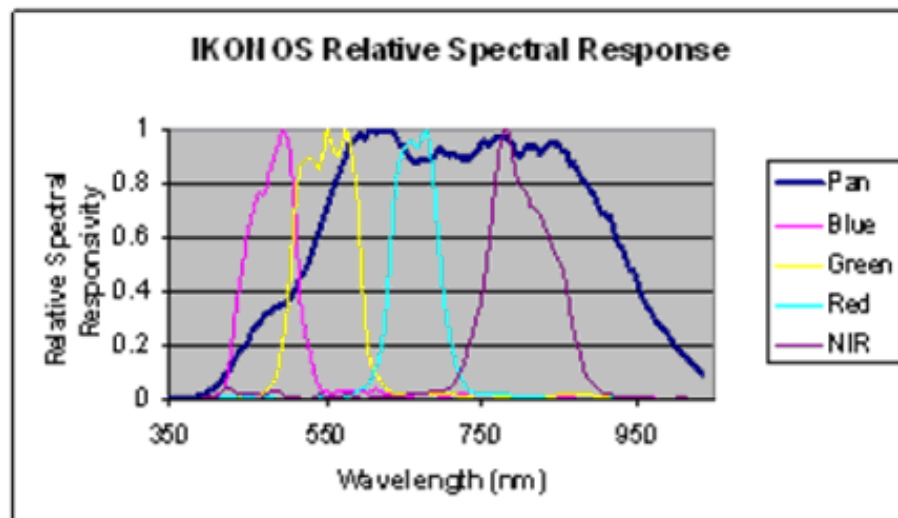


Figure 2.2 The relative spectral responses of IKONOS images (Teague, 2001).

Figure 2.2 shows the spectral curves for the different bands of the IKONOS satellite imagery. It shows that the spectral response of the panchromatic mode is not uniform in the entire wavelength; it is very low in the Blue band and maximum in the Green, Red, and NIR bands.

Zhang (2002) presented new automatic fusion approach together with input IKONOS multi spectral and panchromatic image. This new approach solved two problems of colour distortion and operator/data dependency. An approach based on least squares was developed to best approximate the gray value relation between the original multi-spectral, panchromatic and fused images to achieve the best colour representation.

Zhang and Hong (2005) utilized the IHS transform to fuse the high-resolution spatial information into low-resolution multi-spectral image and used the wavelet transform to reduce the color distortion in a way of generating a new high-resolution Pan image that correlates to the intensity image of the IHS transform. The

new Pan image is, then, used to replace the intensity image for a reverse IHS transform. The fused image is produced after the reverse IHS transform. The fusion results were better than the conventional IHS methods. Since the Pan and the intensity are not spectrally similar and the effect of the NIR bands is not included in intensity, from such mismatches, results of color distortion problem happen in this scheme.

The response of IKONOS panchromatic images (as shown in Figure 2.2) has an extensive range of wavelengths from visible to near-infrared. This difference obviously induces the color distortion problem in IHS fusion as a result of the mismatches. This is spectral dissimilarity of the Pan and I, a value transformed from IKONOS multi-spectral bands Blue, Green, and Red (Zhang, 2002). In particular, the gray values of Pan in the green vegetated regions are far larger than the gray values of I because the areas covered by vegetation are characterized by a relatively high reflectance of NIR and Pan bands as well as a low reflectance in the RGB bands. To minimize the radiance differences between Pan and I, Tu, Huang, Hung, and Chang, (2004) included the NIR band in the definition of the I component. Indeed, the fusion algorithm proposed by Tu et al. (2004) reduces the color distortions in fused images, especially on vegetated area.

In addition, Tu et al. (2004) introduced Fast Intensity Hue Saturation (FIHS) with spectral adjustment applied to the I image, considering that

$$\begin{bmatrix} R' \\ G' \\ B' \\ NIR' \end{bmatrix} = \begin{bmatrix} R + \delta'' \\ G + \delta'' \\ B + \delta'' \\ NIR + \delta'' \end{bmatrix} \quad (2.1)$$

when

$$\delta'' = PAN - I'' = PAN - \frac{R + a * G + b * B + NIR}{3} \quad (2.2)$$

where a and b are weighting parameters defined to take into account that the spectral response of the Panchromatic image does not fully cover that of the Blue and Green band. The values of these parameters were estimated experimentally after the fusion of 92 IKONOS images, covering different areas. According to the experimental results obtained by Tu et al. (2004), the best weighting parameters of a and b for Green and Blue bands are 0.75 and 0.25, respectively.

2.1.3 The evaluation of pan-sharpening image

The evaluation of pan-sharpening image is based on the experimental results of the factors, correlation coefficients (CCs), used in Zhou, Civco, and Silander, (1998) and Choi, Kim, Nam, and Kim, (2005).

2.1.3.1 Correlation coefficients (CCs)

The closeness between two images can be quantified in terms of the correlation function (Veeraraghavan, 2004). The CCs is computed from:

$$CCs(A,B) = \frac{\sum_{i,j} (A_{i,j} - \bar{A})(B_{i,j} - \bar{B})}{\sqrt{(\sum_{i,j} (A_{i,j} - \bar{A})^2)(\sum_{i,j} (B_{i,j} - \bar{B})^2)}} \quad (2.3)$$

Where A and B are the two images between which the correlation is computed.

\bar{A} and \bar{B} are the mean value of the images A and B .

i and j are the number of column and row of the image.

The best spectral information is available in the multi-spectral image and the pan-sharpened image bands should have a correlation closer to that between the multi-spectral image bands (Veeraraghavan, 2004).

2.1.4 Clustering techniques

The clustering is the most important unsupervised learning technique. In this study the combination of the fuzzy c-means algorithm and the simulated annealing algorithm is applied to develop an optimized clustering technique. Theories of the fuzzy c-means, the clustering validity, and the simulated annealing are introduced as follows:

2.1.4.1 Fuzzy c-means

Fuzzy c-means (FCM) clustering proposed by Dunn (1973) is the most widely used algorithm of fuzzy data partitioning. While considering the fuzzy set logic, the algorithm is developed based on k-means clustering. In this algorithm, each pixel does not belong exclusively to any one cluster but is represented by several memberships of each cluster instead. For a pixel, membership of each cluster is [0, 1] and the sum of those memberships is defined to be 1. The algorithm is performed with an iterative optimization of minimizing a fuzzy objective function (Bezdek, 1981).

$$J_m = \sum_{k=1}^n \sum_{i=1}^c (\mu_{ik})^m \|x_k - v_i\|^2, \quad m > 1 \quad (2.4)$$

Where J_m = minimized the objective function,
 c = number of clusters,
 n = total number of pixels,

μ_{ik} = degree of membership of pixel x_k in the cluster i ,

$\|x_k - v_i\|^2$ = the Euclidean distance between pixel x_k and cluster center v_i .

m = an exponential weight (or fuzziness) for each fuzzy membership, degree of fuzziness of each cluster increases along with the m .

Fuzzy partitioning is carried out through an iterative optimization of the objective function J_m in Eq. (2.4), with the update of membership μ_{ik} and the cluster centers v_i by:

$$\mu_{ik} = \frac{1}{\sum_{j=1}^c \left(\frac{d(x_k, v_j)}{d(x_k, v_i)} \right)^{\frac{2}{m-1}}}, \quad 1 \leq i \leq c, 1 \leq k \leq n \quad (2.5)$$

$$v_k = \frac{\sum_{k=1}^n (u_{ik})^{m x_k}}{\sum_{k=1}^n (u_{ik})^m}, \quad 1 \leq i \leq c \quad (2.6)$$

Therefore, Eq. (2.4) can be minimized by the Picard iteration through Eq. (2.5) and Eq. (2.6). The iteration analysis starts with two initial guesses which is including of the random initial guess of the number of classes (c) and an initial center for each cluster using Eq. (2.6) and Eq. (2.5). This was achieved by improving the iterations until the value of v_i got below threshold. Finally, each pixel is classified into a combination of memberships of clusters.

2.1.4.2 Clustering validity

Clustering validity is a concept used to evaluate the quality of clustering results. If the number of clusters is not known prior to commencing an algorithm, the clustering validity index may be used to find the optimal number of clusters. This can

be achieved by evaluating all of the possible clusters with the validity index and then the optimal number of clusters can be determined by selecting the minimum value of the index.

Several clusters validation indices have been developed for FCM, for an example, Bezdek (1974) proposed partition coefficient and partition entropy. The optimal partition (or the optimal value of c) is obtained by maximizing partition coefficient (or minimizing partition entropy) for $c = 2, 3, \dots, c_{max}$. Xie and Beni (1991) proposed a validity index that focused on compactness and separation. Kwon (1998) extended the index of Xie and Beni to eliminate its tendency to monotonically decrease by introducing a punishing function to Xie-Beni validity. In this research, the Xie-Beni index has been chosen as the cluster validity measurement because it is able to indicate when the clustering is optimized.

Xie-Beni validity is the combination of two functions. The first function calculates the compactness of data in the same cluster and the second one computes the separateness of data in different clusters. Let S represent the overall validity index, π be the compactness and s be the separation of the fuzzy c -partition of the data set. The Xie-Beni validity can now be expressed as:

$$S = \frac{\pi}{s} \quad (2.7)$$

Where

$$\pi = \frac{\sum_{j=1}^c \sum_{i=1}^n \mu_{ij}^2 \|x_i - v_j\|^2}{n}$$

and

$$S = (d_{\min})^2$$

d_{\min} is the minimum distance between cluster centres, given by $d_{\min} = \min_{ij} \|v_i - v_j\|$

Smaller values of π indicate that the clusters are more compact and larger values of s indicate the clusters are well separated. Thus a smaller S reflects that the clusters have greater separation from each other and are more compact.

2.1.4.3 Simulated annealing

A simulated annealing (SA) algorithm searches for the optimum solution to a given problem in an analogous way to heating and controlled cooling process in metallurgy. Specifically, it moves about randomly in the solution space looking for a solution that minimizes the value of some objective function. Because it is generated randomly, a given move may cause the objective function to increase, to decrease or to remain unchanged (Kirkpatrick, Gelatt, and Vecchi, 1983; Metropolis, Rosenbluth, Rosenbluth, Teller, and Teller, 1953).

According the minimized objective function, the new Xie-Beni index will be accepted when it is lower than the former index. This is processed using a simulated annealing method. In addition the new index can be accepted as well if possibility of acceptance (P) is less than a generated random number in the interval uniform (0, 1). The possibility of acceptance is determined using the function below Eq. (2.8):

$$P = \frac{1}{1 + (\exp^{-(E(j)-E(i))/T})} \quad (2.8)$$

where P = the probability of acceptance

$E(j) - E(i)$ = the change in the value of the objective function

- $E(j)$ = the new objective function
 $E(i)$ = the old objective function
 T = a control parameter called the temperature.

The most commonly used annealing schedule is called exponential cooling. It begins at some initial temperature, T_0 and decreases the temperature in steps according to $T_{k+1} = \alpha T_k$ where $0 < \alpha < 1$. Typically, a fixed number of moves must be accepted at each temperature before proceeding to the next. The algorithm terminates either when the temperature reaches some final value, T_f , or when some other stopping criterion has been met.

However, empirical evidence suggests that a good value for α is 0.95 and that T_0 should be chosen so that the initial acceptance probability is 0.8. The search is terminated typically after some fixed, total number of solutions has been considered (Kirkpatrick et al., 1983).

2.1.5 Road extraction methods

There are several researches working on automated road extraction from kinds of remotely sensed data which are reviewed accordingly.

Mena (2003) had reviewed some of these approaches. At present, the general extraction of road network has many techniques on the automatic, semi-automatic and related works which are given the variety of existing proposals in the literature. However, the principal factors can be selected in order to achieve it. These factors are grouped into the present objective, the extraction technique applied, and the type of sensor utilized as displayed schematically in Table 2.2.

Table 2.2 General classification of road extraction methods.

Classification of methods and works on road extraction

According to the present objective

- Road extraction general methods
- Road network reconstruction methods
- Segmentation general methods
- Vectorization methods
- Optimization methods
- Evaluation methods
- Other objection

According to the extraction technique applied**Low and mid level methods**

- Road tracking methods
- Morphology and filtrate
- Dynamic programming and snakes
- Segmentation and classification
- Multi-scale and multi-resolution
- Stereoscopic analysis
- Multi-temporal analysis
- Other techniques

Mid and high level methods

- Knowledge representation and fuzzy modeling
- Other methods of spatial reasoning

According to the type of sensor utilized

- Monochromatic imagery
 - Infrared band
 - Color imagery (RGB)
 - Multi- and hyper-spectral imagery
 - Synthetic aperture radar imagery
 - Laser imagery
 - Other type of sensor
-

Source: Mena (2003)

The low and mid level classification methods for road extraction were designed to performed in this research. The methods include the road tracking methods, dynamic programming and snakes, and segmentation and classification.

2.1.5.1 Road tracking methods

The road tracking methods was obtained to determine the road network. It was started on a manually and automatically selected of a set of seed points (Mena, 2003). Park and Kim (2001) presented the semi-automatic road extraction algorithm using the template matching of IKONOS image. In this work, the initial input points were manually used in a road centerline. The adaptive of least square matching algorithm for the initial seed point, was also used for road centerline extraction. Shukla, ChandraKanth, and Ramachandran (2002) presented the initial seed points which were manually selected for semi-automatic road extraction algorithm using high resolution images and path following approach. Zhao, Kumagai, Nakagawa, and Shibasaki (2002) proposed road seed points for semi-automatic road extraction using template matching for tracking a road line. The road seeds were traced by using the direction of linking edge pixel.

2.1.5.2 Dynamic programming and snakes

Dynamic programming and snakes were used for road extraction by Gruen and Li (1997). Dynamic programming was used to solve the optimization problems of linear feature extraction and road extraction. It was also able to be used with a multistage optimization processes. LSB-Snakes (Least-Squares *B*-spline Snakes) was used to improve the curve of road network. Zhang, Xiao, and Zhou (2008) presented the adaptive of using the LSB-Snakes for semi-automatically road extraction from high resolution remote sensing images, so called an auto-initial-

valued LSB-Snake model. This technique is used the self-adapt template matching method to provide the road character to LSB-Snake model, and add the seed points based on the initial points at the same time automatically.

Dal Poz, Gallis, and Silva (2002) proposed a novel road extraction methodology based on the dynamic programming algorithm. This method was to divide an initial seed point into three seed points in E, N, and H coordinates of road centerline segment. Road features were traced in the object space, which implied that a rigorous mathematical model was used.

2.1.5.3 Segmentation and classification

The methods were based on the supervised or unsupervised segmentation and classification of an image for extracting the road network. Frequently the segmentation process was based on texture analysis which could offer a binary image clean enough for serving an input of a posterior vectorization process (Mena, 2002). Segmentation is a powerful tool for the description of that image analysis, leads to meaningful objects only when the image is segmented in homogenous areas. Segmentation and classification were used for road extraction in Song and Civco (2004). The support vector machine (SVM) was used to classify the image into two groups including road and non-road groups. The road network has been using in a region growing technique for road segmentation. A simple threshold on the shape index and density features derived from these objects and that was performed to extract road features, which were further processed by thinning to obtain road centerlines.

Grote, Butenuth, and Heipke (2007) presented the segmentation using the normalized cut algorithm for the road extraction of high resolution image.

Normalized cuts is a graph-based method which is used to divide an undirected graph with weighted edges into segments of similar features.

2.1.6 Mathematical morphology

Mathematical morphology has been developed for binary image which can be represented mathematically as set. The corresponding morphological operators essentially use only four ingredients from set theory, namely set intersection, union, complementation and translation. But from the very beginning there was a need for a more general theory powerful enough to deal with object spaces such as the close subset of a topological space, the convex sets of a (topological) vector space, and gray scale images.

The basic concepts of Mathematical Morphology operation explained by Serra (1982) are erosion, dilation, opening and closing. Erosion and dilation are considered the primary morphological operations. Erosion shrinks or thins object in a binary image where as dilation grows or thickens objects. Erosion and dilation constitute the basis for more complex morphological operators and can be defined as follows:

Let A set be an image and B set be a structure element. The dilation of A by B is denoted by $(A \oplus B)$. This definition is also known as “Minkowski Addition” defined as:

$$(A \oplus B) = \left\{ x : \hat{B}_x \cap A \neq \emptyset \right\} \quad (2.9)$$

where $\emptyset =$ the empty set

The erosion is the opposite of dilation. This is defined as:

$$(A \ominus B) = \left\{ x : B_x \subseteq A \right\} \quad (2.10)$$

This definition is also known as ‘Minkowski Subtraction’.

The opening of A by B , denoted by $(A \circ B)$, is given by the erosion by B , followed by the dilation by B , that is

$$(A \circ B) = (A \ominus B) \oplus B \quad (2.11)$$

The opposite of opening is closing, denote by $(A \bullet B)$ which is defined by:

$$(A \bullet B) = (A \oplus B) \ominus B \quad (2.12)$$

Opening generally smooths a contour in an image. Closing tends to narrow smooth sections of contours, fusing narrow breaks and long thin gulfs, eliminating small holes, and filling gaps in contours.

2.1.7 Difference-of-Gaussians algorithm for edge detection

Edge detection is the most common use operation for image enhancement and image analysis. The challenges of the edge detection in high spatial resolution imagery were first indentified with line in order to extract the road network. There are many methods for the edge detection as: Sobel, Canny, Prewit, Laplacian-of-Gaussians and Difference-of-Gaussians operators.

Marr and Hildreth (1980) presented the theory of edge detection algorithm for detecting edges using the Laplacian-of-Gaussians (LoG) function on an

image and then looking for the zero crossing in the filtered result. The Difference-of-Gaussians (DoG) algorithm is similar to LoG algorithm , which works by performing two different Gaussian blurs on the image, with a different blurring radius for each, and subtraction to the results. The DoG algorithm and approximates LoG algorithm (Marr and Hildreth, 1980) can be approximated by the difference between two different Gaussian. The DoG algorithm is defined as:

$$DoG = G_{\sigma_1} - G_{\sigma_2} \quad (2.13)$$

When G_{σ_1} and G_{σ_2} are

$$G_{(x,y)} = \frac{1}{\sqrt{2\pi\sigma^2}} \exp\left(-\frac{(x+y)^2}{2\sigma^2}\right)$$

Where (x,y) = distance from center of mask

σ = standard derivation of Gaussian distribution

An example of the edge DoG detection can be as shown in Figure 2.3.

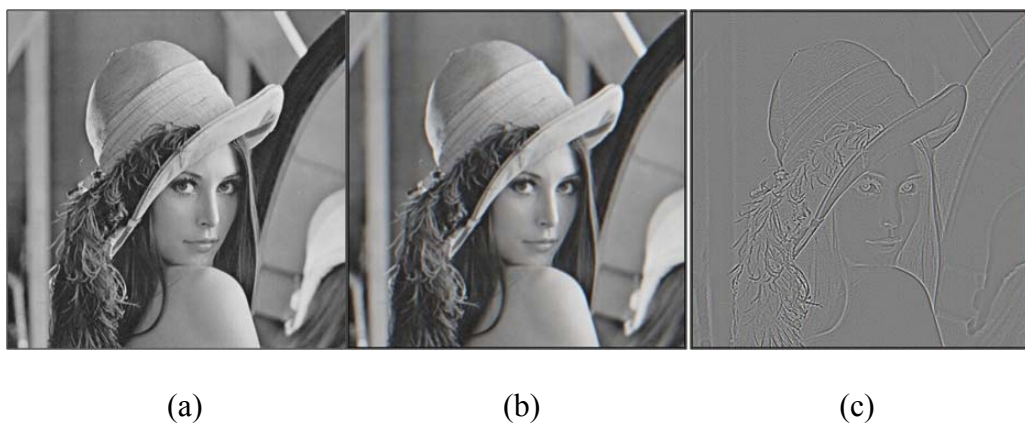


Figure 2.3 An example of the edge DoG detection (a) the Gaussian 1, (b) the Gaussian 2, and (c) The result of the edge DoG detection (Narasimhan, 2006).

2.2 Literature reviews

Three main related previous works of this study include pan-sharpening techniques, fuzzy clustering and mathematical morphology of road extraction.

2.2.1 Pan-sharpening model

A number of pan-sharpening techniques have been developed by many researches and can be found in many literatures. This section briefly explains previous works of the improve IHS transform techniques for pan-sharpening.

Tu et al. (2001) introduced a new look at IHS-like image fusion methods. The IHS fusion techniques convert a color image from red, green and blue space into the IHS color space. The intensity band (I) in the IHS space is replaced by the panchromatic image as follows:

$$\begin{bmatrix} R' \\ G' \\ B' \end{bmatrix} = \begin{bmatrix} R + (Pan - I) \\ G + (Pan - I) \\ B + (Pan - I) \end{bmatrix} \quad (2.14)$$

The problem with the IHS methods is that spectral distortion may occur during the merging process.

Gonzalez-Audicana et al. (2004) introduce the fusion technique. The improved IHS fusion technique and wavelet decomposition to execute the detail extraction phase, and followed by the IHS transform. The steps are to generate a new panchromatic image whose histogram matches that of the I and to apply decimated or undecimated wavelet decomposition to the I to the corresponding histogram match with Pan. The result of this methods is higher quality than IHS standard methods.

Li et al. (2005) introduced a new methods based on resolution degradation model is proposed to minimize the spectral distortion on the high

frequency detail of Pan. The degradation can be performed in frequency domain as follows:

$$Pan = Pan_{low} + Pan_{high} \quad (2.15)$$

Where Pan_{low} is the degraded Pan and Pan_{high} is the detail of the Pan image.

This technique can reduce the spectral distortion while keeping the same spatial resolution as the panchromatic images.

2.2.2 Fuzzy clustering model

Lizarazo and Barros (2008) presented general fuzzy approach for segmentation-based classification by focusing on partition imagery into image-objects with well-defined boundaries. The proposed methodology aims to produce and analyze fuzzy image-regions expressing degrees of membership to different target classes. This approach, called fuzzy image-regions method (FIRME), is suitable to deal with the spectrally and spatially complexity of urban landscapes. In the defuzzification stage, a SVM classification with radial basis kernel was applied to decision rules of the fuzzy regions from an assign full membership to the target land-cover classes. Fuzzy Image-Regions is a set of overlapping images representing degrees of memberships to computing land-cover classes. FIRME can be used for every target land-cover classes which are roads, rooftops, grass, trees, water and bare Soil.

Ameri et al. (2008) proposed road extraction system from multi-spectral and pan-sharpened IKONOS images of a city in Iran. It is spectral classification by use of FCM clustering technique and road class binary image is obtained by definition

of threshold value. This FCM technique tests different distance function types in performing FCM clustering and finds the most precise and fastest one.

Mohammadzadeh et al. (2006) developed a fuzzy method used to image segmentation from multispectral remote sensing image in two classes: road and non road. By sampling from road surface, mean value of the road in each band will be obtained. They have defined 5 membership functions with special means and standard deviations in each band. Then, a fuzzification step is applied for obtaining an estimation of the class contributions in each band assuming a Gaussian distribution of the classes. After a min and a max operation have been applied on these membership functions are inputs, it results to the fuzzy classification of the scene. Finally, they used mathematical morphology to automatic extraction of Iranian roads from pan-sharpened IKONOS images.

Madhan et al. (2005) presented fuzzy and mathematical morphology for the automatic extraction of road networks. In this article they proposed an explicit fuzzy classification methods for multi-spectral remote sensing image carried out in three steps. The first step is an explicit fuzzification for obtaining estimation of the class contributions in each band. The second step applied a fuzzy reasoning rule on these fuzzy inputs to obtain after a deduce in the fuzzy classification of the scene. Finally, a hard classification can be deduced in the defuzzification step in order to illustrate the whole of the cover classes in the same map. After fuzzy classification, they applied mathematical morphology operation to the automatic extraction of road networks.

2.2.3 Mathematical morphology of road extraction model

The most widely method for the road extraction is based on the linear analysis methods. Zhang et al. (1999) presented the road network extraction using mathematical morphology. The morphological trivial opening has been developed to preserve the whole road network and filter of the noises. Granulometry analysis was performed with trivial opening to provide the size of road network. This methods demonstrated for detecting a road network with the significant width on the high resolution images.

Mohammadzadeh et al. (2004) presented the morphological operation trivial opening, granulometry and skeleton for automatic removing of the small objects, narrow paths and noises. The morphological operation is processed after the using of the fuzzy classification and segmentation. The result of this research is shown the automatic linear feature extraction of Iranian roads from the pan-sharpened IKONOS images.

Madhan et al. (2005) presented the automatic road network extraction from high resolution multi-spectral images based on fuzzy and mathematical morphology. This research described an explicit fuzzy supervised classification methods applied for obtaining an estimated of the class contribution in each bands, assuming a Gaussian distribution of the class. The morphological operation trivial opening and closing operation are combined to the structure element for removing the small objects, narrow path and noises.

Ma et al. (2008) presented the road extraction from the high resolution remote sensing image using mathematical morphology. This work proposed the road extraction using the steps which are image clustering segmentation based on the

support vector machine for image classification and 30 classes were selected. The morphological operation openings, closing, erosion and dilation were applied in this research. Two structure elements were combined to the morphological operation, resulting in the long linear structure element for the noise removal.

Wang et al. (2009) presented the road extraction in remote sensing image based on the Pulse-Coupled Neural Network (PCNN) and the mathematical morphology. This research used the simplified PCNN for employing the image segmentation. The morphological operation erosion, dilation, opening and closing are used to purify the road information and the road centerline. This research is a successful experiment using the remote sensing in the urban areas.

Zeng et al. (2006) presented the design of TOPHAT morphological filter to apply to infrared target detection. This work proposed the TOPHAT morphological filters using the neural network and genetic algorithm for optimal training and applying in infrared images detection. The result of the TOPHAT morphological filters were optimized by using the genetic algorithm and that was better performing than using the neural network.

Hernandez and Marcotegul (2009) presented the method for filtering and segmentation of the 3D point clouds using the mobile LIDAR systems. The artifact detection based TOPHAT morphological operation as the filtering algorithm. The algorithm removed all of the minima without border by using the morphological reconstruction of erosion. The TOPHAT morphological was also applied to remove the noise surface.

2.3 Synthesis for the research approach

The final aim of this study is to extract the road centreline from the THEOS satellite imagery covering the downtown of Nakhon Ratchasima province. The Pan-sharpening process is the first process followed by the integrated fuzzy c-means and simulated annealing technique for image clustering. The result of fuzzy c-means and simulated annealing are then used as input for road extraction through the mathematical morphology and the edge detection processing. The steps are described as follows:

- (1) Pan-sharpening

The pan-sharpening process is the data combination of the high resolution and the multi-spectral resolution data. The IHS transform process was applied in the study and modified from the method of Tu et al. (2004) in order that the method can be fit to the THEOS images. In the Tu et al. (2004) method, IHS transformation was used to reduce the value of Blue and Green band for obtaining the parameter a and b ; in this study we proposed method to improve IHS transformation to decreased value of RED and NIR bands by using two weighting parameters. In other word, the study attempts to find the best parameters, a and b , that best fit to the IHS transformation technique for THEOS data. The CCs between the pan-sharpened and multi-spectral images was used to select the best pair of a and b so that the pan-sharpened images obtained can preserve the most original characteristics. The CCs between the pan-sharpened and panchromatic images was used to examine the image quality in order to prove that the pan-sharpened images obtained contain characteristics closest to the panchromatic.

(2) Clustering technique

The FCM and simulated annealing are selected for clustering image in this study. The clustering validity technique of Xie-Beni is used with the simulated annealing technique for the better cluster centre of membership.

(3) Road extraction

The mathematical morphology is the one of the mostly used for the road extraction. Mena (2003) presented the mathematical morphology for the road extraction using the low level, and hence the aforementioned mathematical morphology is used for filtering processing in this study. The method is using the suitable combination of the morphological operation and structure element for filtering non-road objects. Meanwhile, the adaption of edge detection technique is added for improving the data before input to the process of morphological operation and the Difference of Gaussian (DoG) for the road extraction.

CHAPTER III

DATA, EQUIPMENT, AND RESEARCH

METHODOLOGY

3.1 Equipment and data used for the study

3.1.1 Software

The MATLAB and the ENVI/IDL software were used to analyze the data and also used in the simulation process.

- MATLAB is the software with high-performance language features for technical computing. It integrates computation, visualization, and programming in an environment where problems and solutions are expressed in the familiar mathematical notation.

- ENVI/IDL is the software composing functions of visualization, analysis and presentation of all types of digital imagery, geometric correction, terrain analysis, radar analysis, raster and vector GIS capabilities, also including underlying language, IDL (the Interactive Data Language).

- IDL is a powerful programming language for visualizing and analyzing large data sets. For remote sensing applications, IDL can be coupled with a graphical user interface, called ENVI, which provides basic functionalities for the processing of multi-spectral, hyper-spectral and radar imagery. Since ENVI itself is written in IDL, it is highly extensible.

3.1.2 Data

The proposed of road extraction algorithm used tested on the high spatial resolution and multi-spectral resolution of THEOS images. The area of 82.10284 sq.km. of Nakhon Ratchasima province (Figure 3.1) is used in this study, which is located between latitude $14^{\circ} 52' 44''$ to $14^{\circ} 57' 42''$ North and longitude $101^{\circ} 59' 55''$ to $102^{\circ} 4' 58''$ East. THEOS data consisting of panchromatic image and multi-spectral images from the same date (February 19th, 2010).

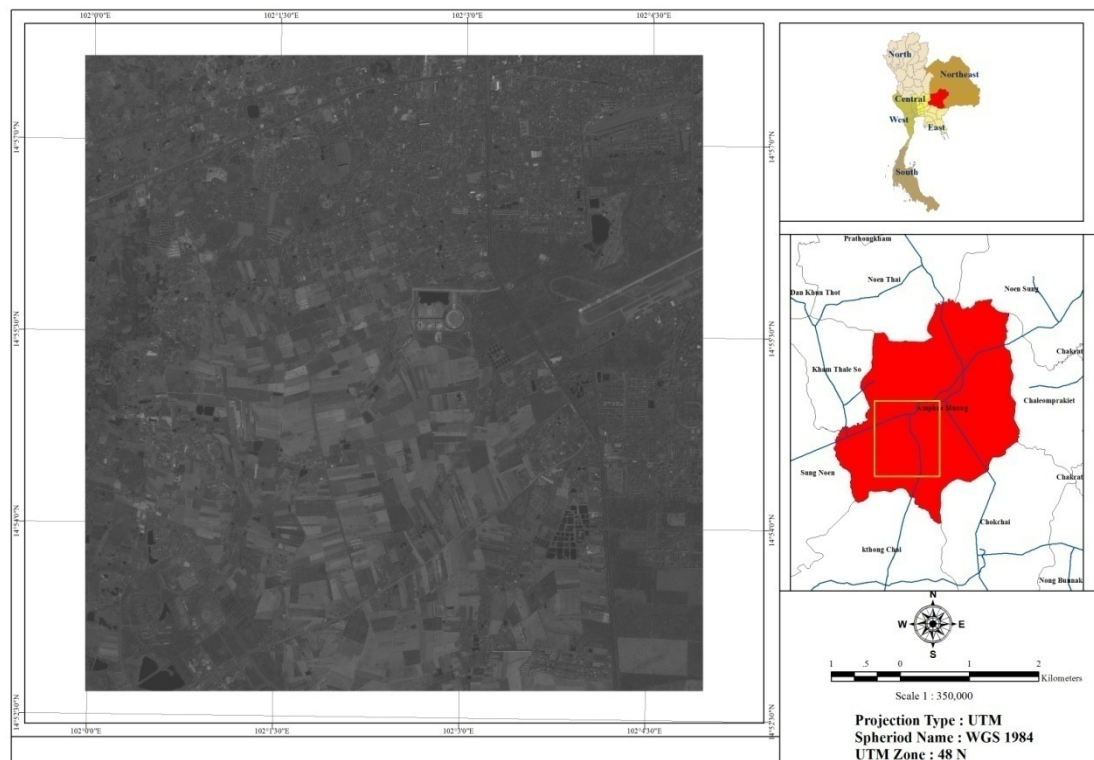


Figure 3.1 The study area is Nakhon Ratchasima city municipality and the vicinity.

3.2 Research methodology

The conceptual framework of study is composed of three steps including (1) the image fusion based on improved IHS transformation technique for image pan-sharpening, (2) the spectral reflectance clustering of pan-sharpened images for road network, (3) the automated road extraction and accuracy assessment. The framework or the procedure of the proposed approach is illustrated in Figure 3.2.

The Multi-spectral image (Blue, Green, Red, and NIR) and Panchromatic THEOS images are first fused into pan-sharpened images which contain both high spatial information from panchromatic image and multi-spectral information from the multi-spectral image. The clustering techniques are then applied to the pan-sharpened images to produce the cluster partition of candidate road image. Then, the morphological operation which uses for road network filtering is employed to eliminate those non-road objects. In the meantime the edge-aid segmentation stage, the binary image from panchromatic image is employed to edge detection for combination with morphological operation to remove the non-road objects. Finally, the morphological thinning operation is developed for extracting road centerlines. The individual processes of proposed approach are described in the following section.

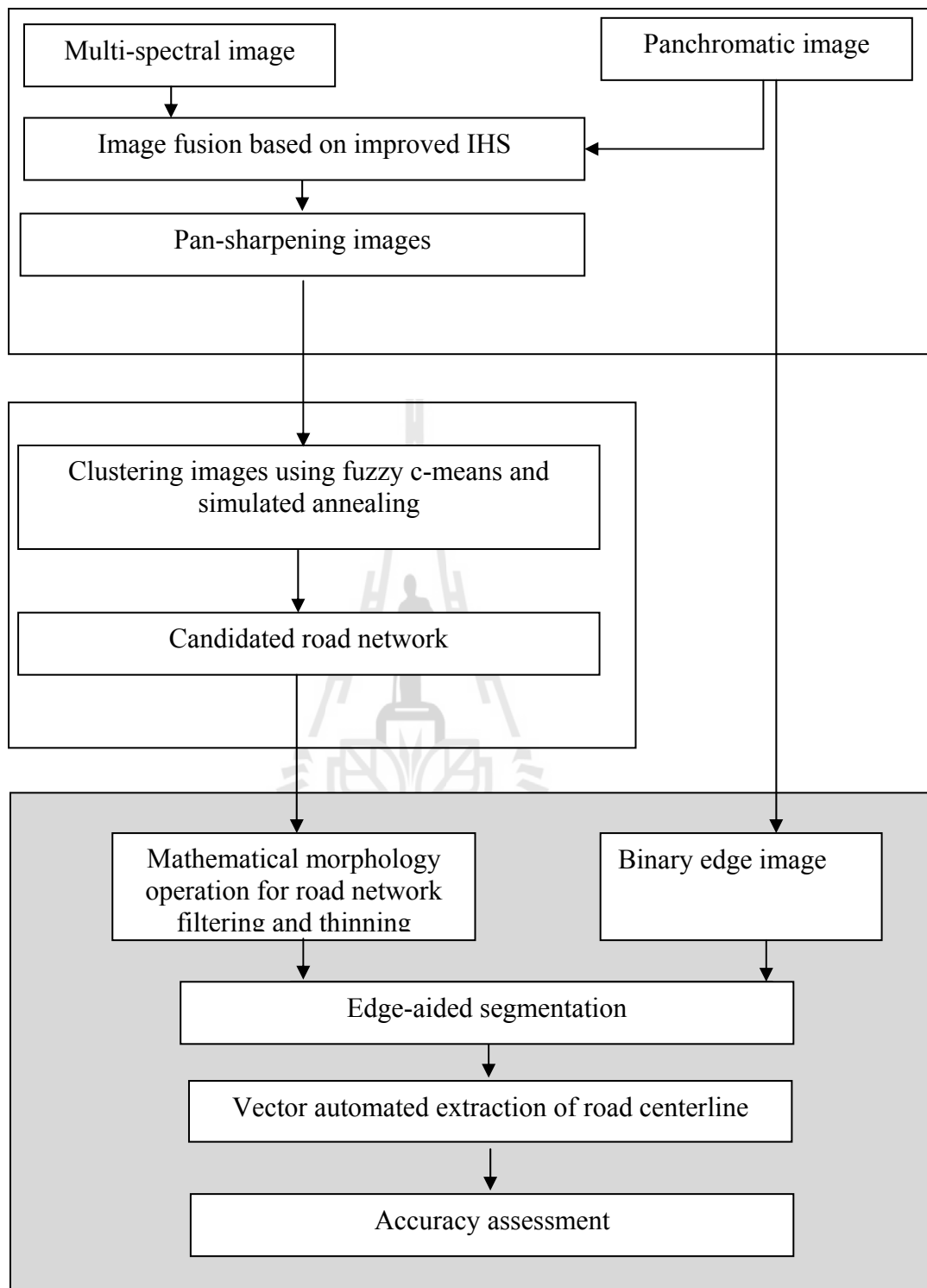


Figure 3.2 Conceptual framework of the study.

In practice, the trials and errors were operated from IHS pan-sharpening through fuzzy c-means and simulated annealing image clustering. The results were observed, if it not satisfied, the weighting parameters for IHS pan-sharpening were modified and adjusted. Then, the following clustering results were observed. The processes went on until the satisfied results were achieved. The result satisfaction is mainly based on 1) visual comparison of composite images from all trials, 2) the CCs of panchromatic images and pan-sharpened images band by band and the average, 3) consideration on clustering results of all trials. The flowchart of the comparison processes can be displayed as a diagram in Figure 3.3.

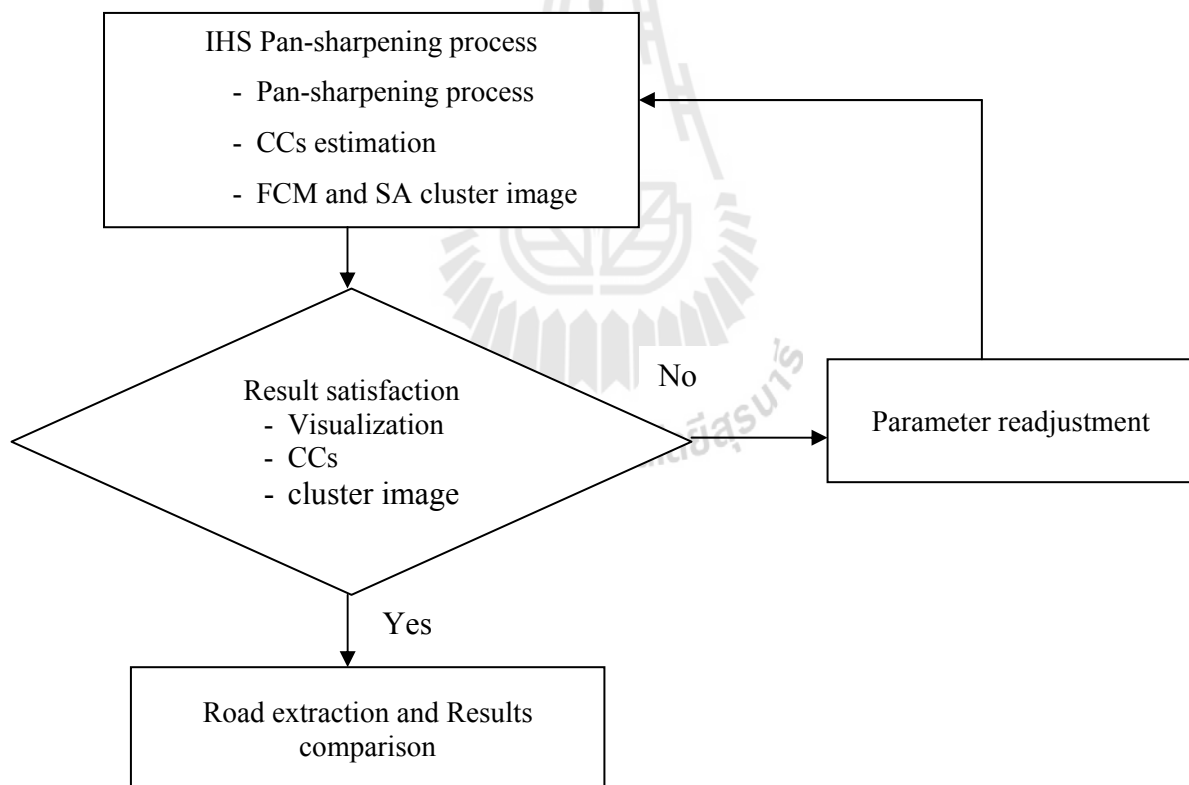


Figure 3.3 Trials and errors of pan-sharpening process.

3.2.1 Pan-sharpening

The Pan-sharpening process (as shown in Figure 3.4) of the high spatial resolution of panchromatic image and multi-spectral images was conducted based on the IHS transformation technique and its modification in 3 trials. Firstly (trial no.1), with modified FIHS method of Tu et al. (2004) the spectral adjustment is additionally applied to Red and NIR bands by assigning $a < b$ while a and b are the parameters of those 2 bands, respectively. Secondly (trial no.2), the modification is the same as the first one but $a > b$ is assigned. The weighting parameters adjustment was performed to obtain pan-sharpened images with the best spectral response between pan-sharpened images and original multi-spectral images. Thirdly (trial no.3), considering the relationship between the relative spectral response of multi-spectral and panchromatic sensors of the THEOS data, the new weighting parameters specifically for them were determined to adjust pan-sharpened images which express closer relationship to the original multi-spectral images.

In order to obtain the best a and b from each trial, 10 sets of THEOS data (1500×1500 pixels for each set) were selected from the study area and used for pan-sharpening process. The highest average correlation coefficient of 10 sets will indicate the best a and b values.

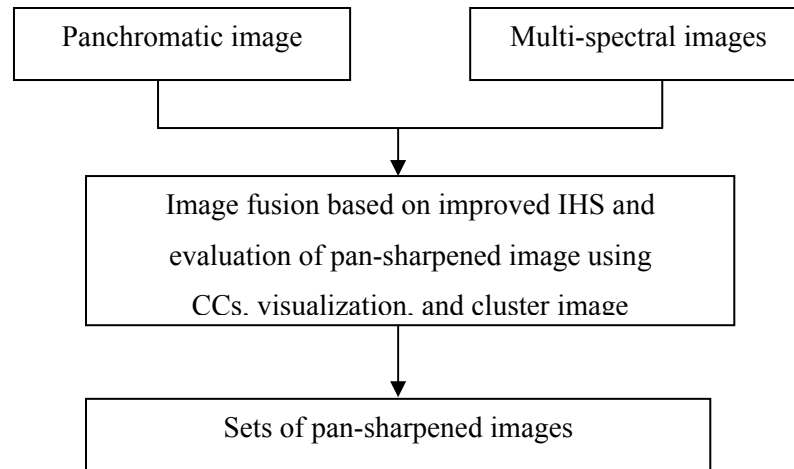


Figure 3.4 Pan-sharpening of high spatial resolution and multi-spectral image based on improved IHS transformation.

Therefore, a new intensity component can be determined by the following this equation.

$$I'' = \frac{\sum_i w_i MS_i}{3} \quad (3.1)$$

where MS_i is the corresponding multi-spectral images.

w_i is the weight of band i .

For THEOS , MS_i represent Blue, Green, Red and NIR infrared bands.

The proposed method is expressed as follows:

$$\begin{bmatrix} R' \\ G' \\ B' \\ NIR' \end{bmatrix} = \begin{bmatrix} R + \delta''' \\ G + \delta''' \\ B + \delta''' \\ NIR + \delta''' \end{bmatrix}$$

where

$$\delta''' = Pan - I''' = Pan - \frac{\sum_i w_i MS_i}{3}$$

First (trial no.1), the proposed methods used the same parameter weights as those of the FIHS of Tu et al. (2004) for the Green and Blue bands (as 0.75 and 0.25), while weighting parameter of Red and NIR bands were assigned to be a and b with the condition of $a + b = 1$ and $a < b$. Then, the pan-sharpening can be expressed in the (3.2) and (3.3).

$$I''' = \frac{a * R + 0.75 * G + 0.25 * B + b * NIR}{3} \quad (3.2)$$

Then

$$\delta''' = Pan - I''' = Pan - \frac{a * R + 0.75 * G + 0.25 * B + b * NIR}{3} \quad (3.3)$$

For the second trial, the parameter weighting for the Red and NIR bands is similar to the first trial is assumed that $a > b$ and the correlation coefficients between the original MS images and the fused images were used as an index to determine the values of a and b .

Third (trial no.3), the spectral response image of THEOS (as displayed in Figure 2.1) is unlike the spectral response image of IKONOS. Therefore, this study

proposes the modified IHS method of THEOS images by adding the parameter weights to only the Red and NIR bands which show lower spectral response than the panchromatic image while the response of Green and Blue bands were kept the same as the origin images. The proposed method can be expressed as follows:

$$\begin{bmatrix} R' \\ G' \\ B' \\ NIR' \end{bmatrix} = \begin{bmatrix} R + \delta''' \\ G + \delta''' \\ B + \delta''' \\ NIR + \delta''' \end{bmatrix}$$

where

$$\delta''' = Pan - I'''$$

$$I''' = \frac{a * R + G + B + b * NIR}{3} \quad (3.4)$$

In this proposed approach, the parameter weighting for the Red and NIR bands was assumed that $a+b = 2.5$. From the THEOS spectral responses (Figure 2.1) the response of Red and NIR bands can be close to the panchromatic response when they are multiplied by a value ranging from 1 to 1.5, which becomes a value of a or b . To increase the response of Red and NIR bands, a value of a or b should not be less than 1. The correlation coefficients between the original multi-spectral images and the fused images were also used as an index to determine the values of a and b . The better of weighting parameters for a and b between the trials no.1 and no.2 were selected to process pan-sharpening images for further clustering and road extraction processes. Then, its extraction result was compared to the result extracted from the fused images of the trial no.3.

Additionally, the quality of the pan-sharpened images from all trials is examined based on the CCs of the original MS and the pan-sharpened images band by band and the average, visual comparison of composite images, the CCs of panchromatic images and pan-sharpened images band by band and the average, and clustering results.

3.2.2 Image clustering approach

The image clustering tool was developed as a module using IDL environment. The module steps can be displayed as the flowchart in Figure 3.5.

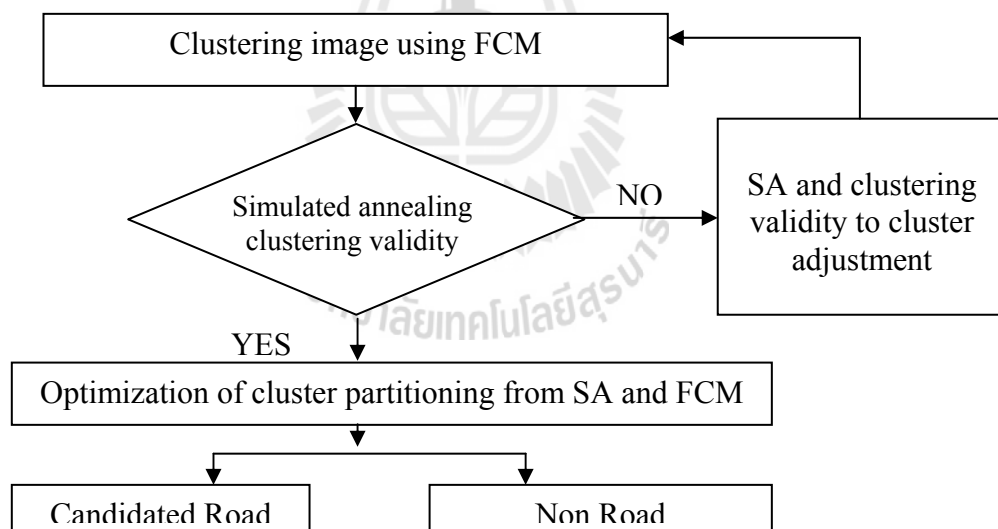


Figure 3.5 Image clustering approaches.

The process of image clustering is performed using fuzzy c-means and simulated annealing algorithms as displayed in the Figure 3.6.

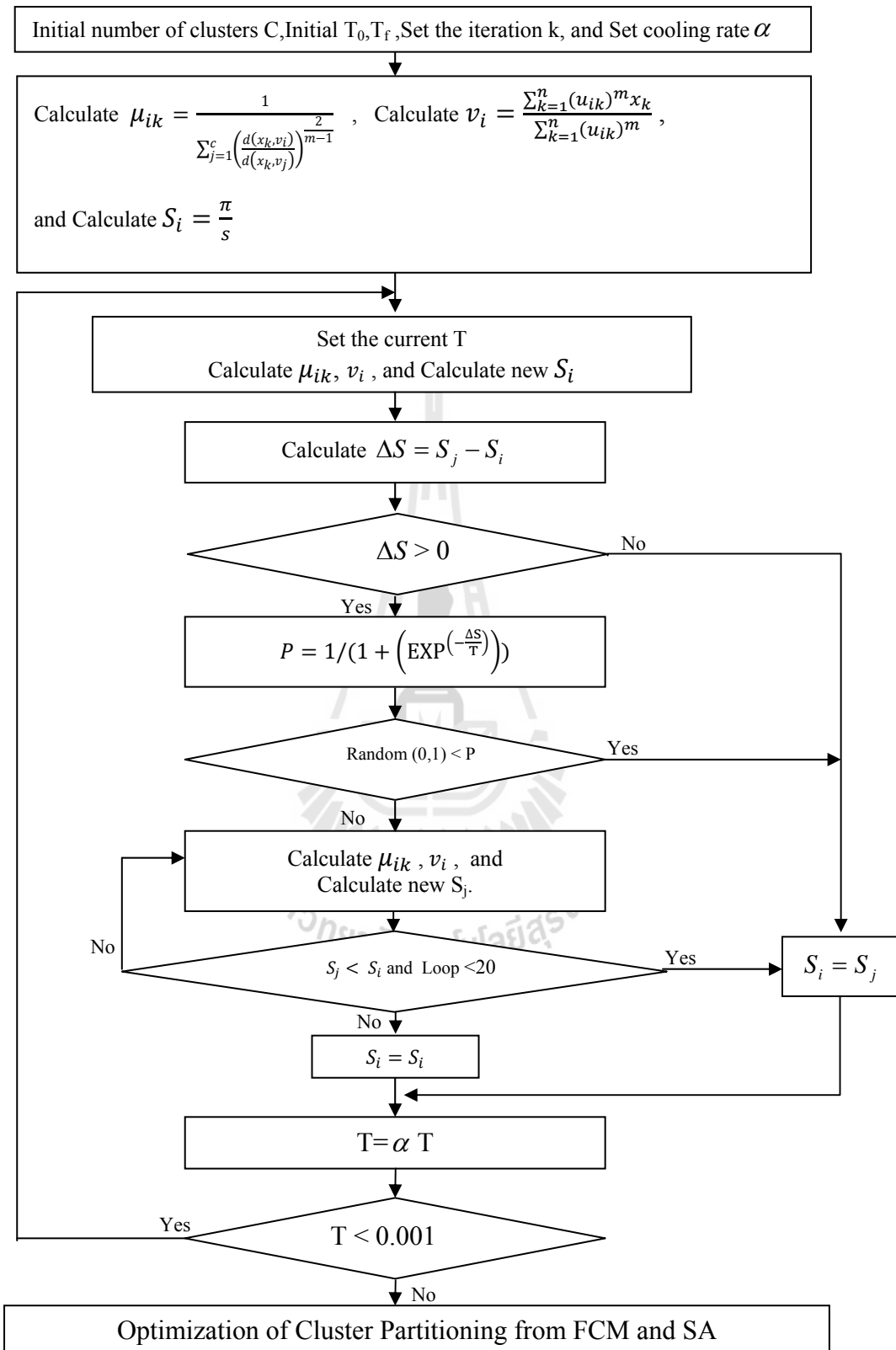


Figure 3.6 Optimization of clustering methods.

3.2.3 Road extraction

One of the research objectives is the module development for automated road extraction from segmented image. An automated road network extraction can be displayed as a flow diagram in Figure 3.7. An unsupervised classification was applied to the pan-sharpened images to obtain certain clusters which were performed as candidates of road network extraction. The road centerline networks were extracted using the combination of mathematical morphology technique and binary edge detection from the panchromatic image. Finally, extracted road networks will be converted to be vector road centerlines. These road centerlines in form of vector data model can be directly imported into GIS for future non-spatial data updating.

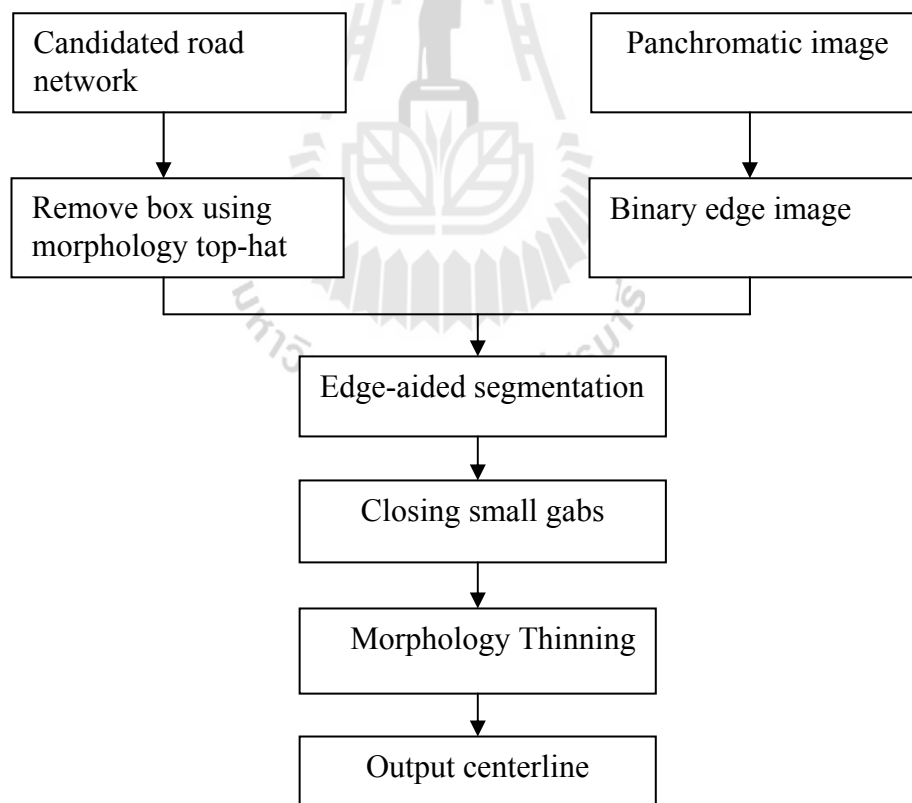


Figure 3.7 Automated road extraction using mathematical morphology and edge-aided segmentation.

In Figure 3.7, the small region and large region of non-road objects in the candidate road network were filtered using the morphological top-hat operation with optimum structure elements. Then, the edge-aided segmentation process was additionally used to remove the rest of non-road object. After that, the morphology thinning was applied to obtain the road centerline from binary image. The processes of the proposed approach can be described as follows:

3.2.3.1 Appropriate structure element acquiring

When morphology was first introduced for road network filtering and thinning, it was based on set theory. In practice, for road filtering and thinning after classification using fuzzy c-mean and simulated annealing it was convert color to binary image. The morphological operations used in this thesis include: opening, closing, top-hat and thinning operation. In order to remove small area, the appropriate structure element must be selected. The structure element has similar function as filter's window or reference template with regarding to image processing; both shape and size of structuring element have important effect on morphological filtering. The attributes of the structure element is controlled by its shape, width and height images. Larger structuring elements preserve larger features while smaller elements preserve the finer details of image features. In this study determination of appropriate structuring element in terms of shape and sizes in order to remove small and large area for road network filtering are described in the followings:

By a set of tests through morphology top-hat operations, the appropriate structure elements were squares of 3 by 3 and 8 by 8 for removing the small and large regions of non-road objects respectively. The appropriate structure elements are shown in Figure 3.8.

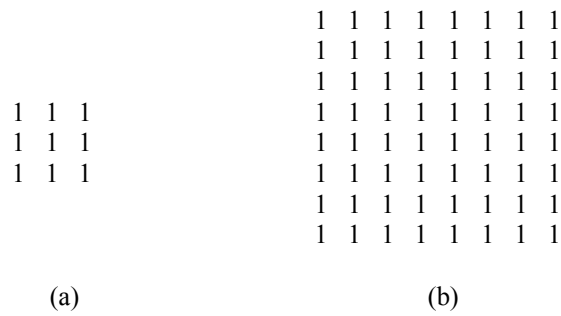


Figure 3.8 Structure elements with (a) 3 by 3 square and (b) 8 by 8 square.

The using of the morphology top-hat operation with the structure element bigger than 8 by 8 resulted in the unacceptable error on road extraction in the road centerline processes.

3.2.3.2 Morphological opening and closing

The morphological opening and closing were applied to a binary image of road network. The morphological opening operation is simply an erosion operation followed by a dilation operation denoted by Eq. (2.12). In this study the opening operation has effect on smoothing image by removing small object. The morphological opening operation with structure element of a 3 by 3 square applied to the original image can be shown in Figure 3.9.

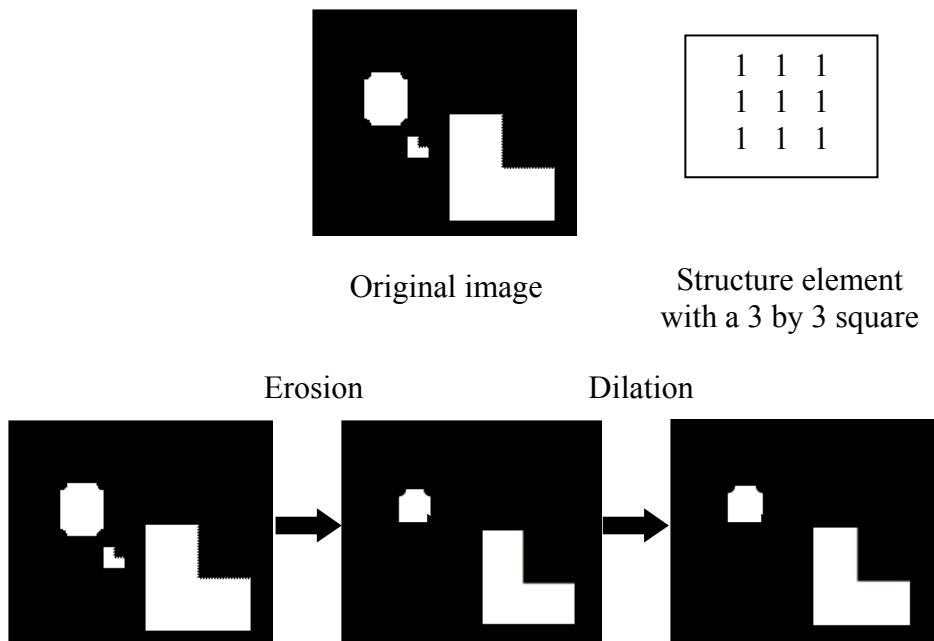


Figure 3.9 The morphological opening operation with a 3 by 3 square.

The morphological closing operation or call the holes filtering is simply a dilation operation followed by an erosion operation denoted by Eq. (2.13). In this study the closing operation have effect of smoothing image, with the closing operation to adding object. The morphological closing operation with structure element with a 3 by 3 square applied to the original image can be shown in Figure 3.10.

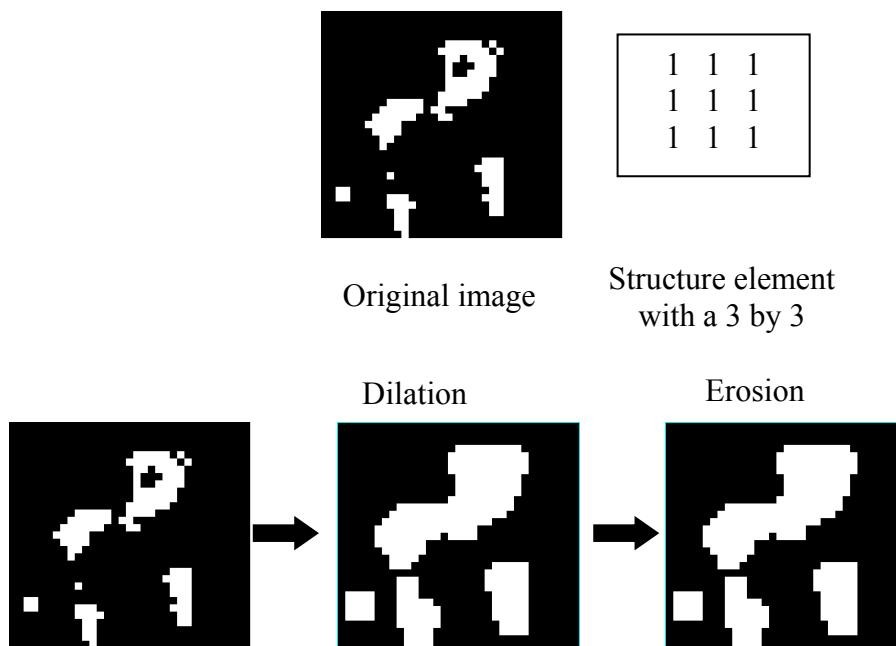


Figure 3.10 The morphological closing operation with a 3 by 3 square.

3.2.3.3 Morphological top-hat

In this study, the morphological top-hat operation aims at removing small and large objects from the road network. The process is a simple subtraction between the original image and the top-hat operation image. For small object removal the structure element with a 3 by 3 square was applied and a 8 by 8 square for large object removal. The morphological top-hat operation is implemented by first applying the opening operation to the original image defined as:

$$TopHat_{AB} = (A - (A \circ B)) \quad (3.5)$$

The original image and the result of morphological top-hat operation with structure element of a 3 by 3 square are shown in Figure 3.11.

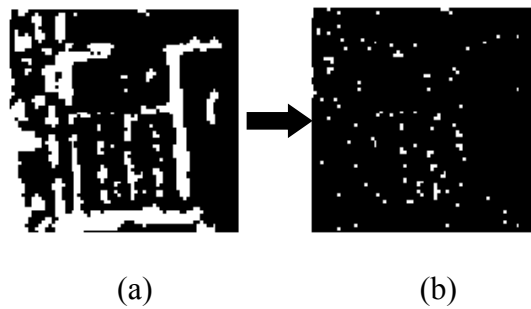


Figure 3.11 The original image (a) and the result of morphological top-hat operation of a 3 by 3 square (b).

The result of morphological top-hat operation with structure element of a 8 by 8 square compare to the original image can be shown in Figure 3.12.

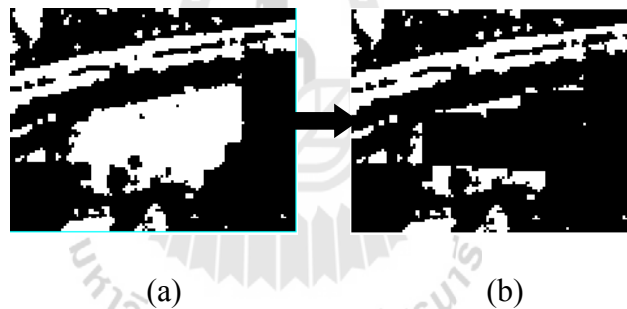


Figure 3.12 The original image (a) and the result of morphological top-hat operation of a 8 by 8 square (b).

The using of morphology top-hat operation with 3x3 structure elements was to remove non-road objects in form of small areas. The using of morphology top-hat operation with 8x8 structure elements was to remove the larger areas of non-road objects. Hence the road object could be existed using 3x3 and 8x8 structures because the length of the road are normally longer than 3 pixels and no wider than 8 pixels.

3.2.3.4 Edge-aid segmentation

Edge-aided segmentation approach was applied to extract road networks extraction from a classified road image with the help of edge information from the corresponding panchromatic image. Wang and Zhang (2003) presented the edge-aided segmentation for extraction of urban road network from QUICKBIRD imagery. The processes perform as edge detector to generate of appropriate edge information. Robert edge detector was used to perform edge-aided segmentation (Wang and Zhang, 2003). Wang, Hu, and Zhang (2005) used Canny edge detector using the following rule:

$$C = \begin{cases} \text{road} & \text{if } A \text{ is candidated road and } B \text{ is not road of edge detection} \\ \text{non-road} & \text{Otherwise} \end{cases} \quad (3.6)$$

In this study, the proposed methods used the edge detector called the difference of Gaussians. The rule of the proposed method can be displayed as the following:

$$C = \begin{cases} \text{road} & \text{if } A \text{ is candidated road and } B \text{ is not road of edge detection} \\ \text{non-road} & \text{Otherwise} \end{cases} \quad (3.7)$$

3.2.3.5 Morphological thinning

The morphological thinning operation is applied to road centerline extraction from binary images after the mathematical morphology operations for road network filtering. The morphological thinning operation removes pixel from binary image into single pixel or center line. The morphological thinning operates using

strings of template with varying iteration. The morphological thinning uses a sequence of the structure elements as follows:

$$B = \{B^1, B^2, \dots, B^n\}$$

The morphological thinning operation defines by as:

$$\text{Thinning}_{AB} = A \cap (A \otimes B)^c \quad (3.8)$$

3.2.4 Accuracy assessment

The methods used to evaluate the data quality of road centerline extraction were proposed by Heipke, Mayer, and Wiedemann (1996). The matching process is an important part of the evaluation process. The matching length of road centerline and the reference data was used to compute the completeness and correctness measures (Heipke et al., 1996), the following section describes the two basic quality measurements.

3.2.4.1 Completeness

The completeness is the percentage of the reference data which is explained by the extracted data (Heipke et al., 1996), i.e. the percentage of the reference network which lies within the buffer around the extracted data (Figure 3.13). It can be defined by:

$$\text{completeness} = \frac{\text{length of matched reference roads}}{\text{length of all reference road}} \times 100 \quad (3.9)$$

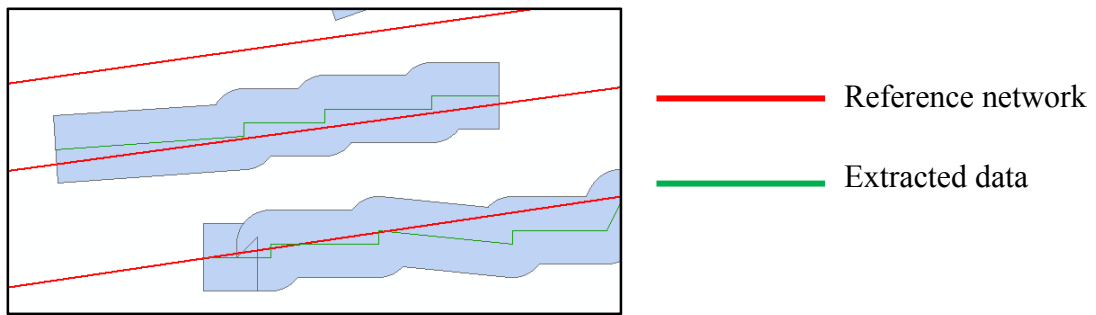


Figure 3.13 The length matched reference road is the length of reference network falling in the buffer area of extracted data.

3.2.4.2 Correctness

The correctness represents the percentage of correctly extracted road data (Heipke et al., 1996), i.e. the percentage of the extracted data which lies within the buffer around the reference network (Figure 3.14). It can be defined by:

$$correctness = \frac{\text{length of matched extraction}}{\text{length of extraction}} \times 100 \quad (3.10)$$

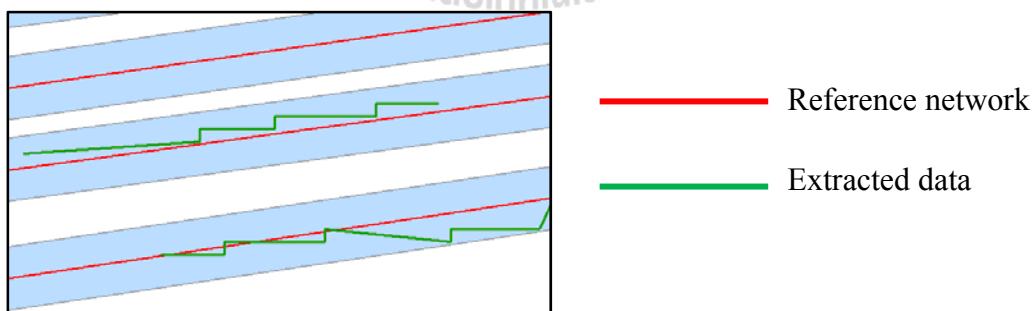
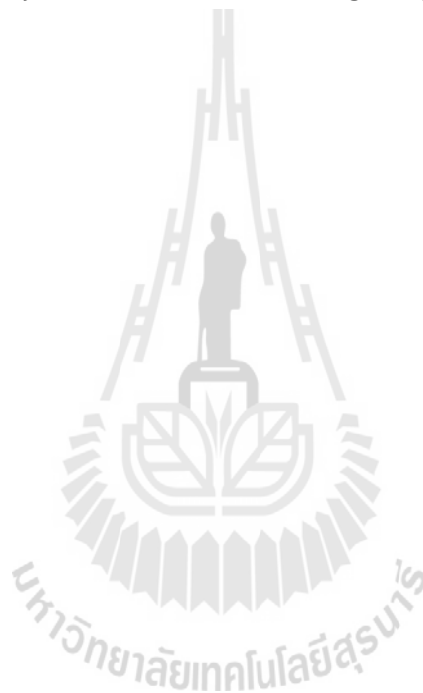


Figure 3.14 The length of matched extraction is the length of extracted data falling in the buffer zone of the reference network.

3.2.4.3 Quality

The quality is a measure of the goodness of the final result. It takes into account the completeness of the extracted data as well as its correctness (Heipke et al., 1996). It can be defined by as:

$$quality = \frac{\text{length of matched extraction}}{\text{length of extracted data} + \text{length of unmatched reference}}$$



CHAPTER IV

RESULT AND DISCUSSION

Main results are here explained to response the main objectives which include pan-sharpening, image clustering using fuzzy c-means and simulated annealing and road centerline extraction.

According to the aforementioned description in Section 3.2.1, the result of 3 trials for pan-sharpening can be discussed as follows:

4.1 Pan-sharpening, fuzzy c-means simulated annealing of trial no.1

4.1.1 Pan-sharpening

The best weighting parameters (a and b) for the band Red and band NIR were investigated from 10 sets (1500x1500 pixels for each set) of the THEOS pan-sharpened images. One set is represented one area (all of 10 data sets can be seen in Appendix A). The Matlab software was used to implement the pan-sharpening methods and to determine the values of a and b through the correlation coefficients (CCs) between the original multi-spectral images (including R,G,B and NIR bands) and the pan-sharpened images. The varying a and b were set to be 9 pairs (Table 4.1). The average 10-sets correlation coefficients of all pairs were compared and a pair which had the highest average coefficient was selected to be the best pair of weighting parameters a and b .

In trial no.1, it was assumed that $a+b = 1$ and $a < b$. Therefore, a was set to increase 0.05 at a time from 0.05 to 0.45 and b was set to decrease 0.05 at a time from 0.95 to 0.55. This resulted in 9 pairs of weighting parameters (a and b) for the experiment. Every pair of a and b was applied to 10 sets of images (1500x1500 pixels) and the average CCs was calculated. The average CCs of 10 sets of THEOS images of all pairs of a and b were listed in Table 4.1. According the result of trial no.1, the best weighting parameters for the Red and NIR bands were 0.05 for a and 0.95 for b .

Table 4.1 Average correlation coefficients (CCs) between resembled original and pan-sharpened images of 10 sets of THEOS images of the trial no.1, with varying spectral weights.

Pairs of weighting parameters									
a	0.05	0.1	0.15	0.2	0.25	0.3	0.35	0.4	0.45
b	0.95	0.9	0.85	0.8	0.75	0.7	0.65	0.6	0.55
(CCs)	0.8018	0.8006	0.7987	0.7947	0.7926	0.7883	0.7830	0.7768	0.7695

The 2 sets of pan-chromatic image, multispectral images in form of a composite image, pan-sharpened images using the best a and b from the trial no.1 and their zoom-in ones were shown as examples in Figures 4.1 to 4.4. The data set 1 was selected to represent area of local road while the date set 2 was represent the area of main road.

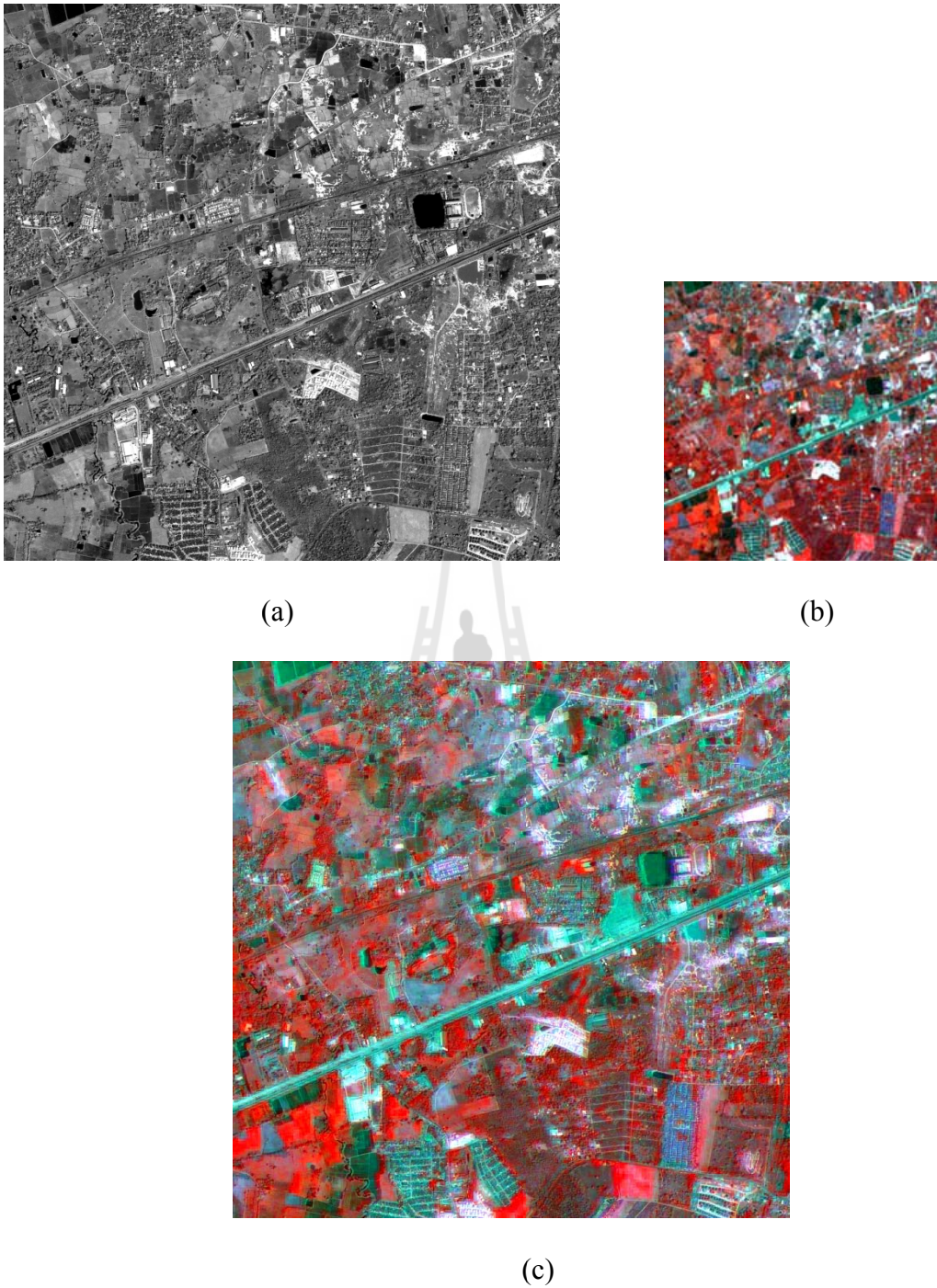
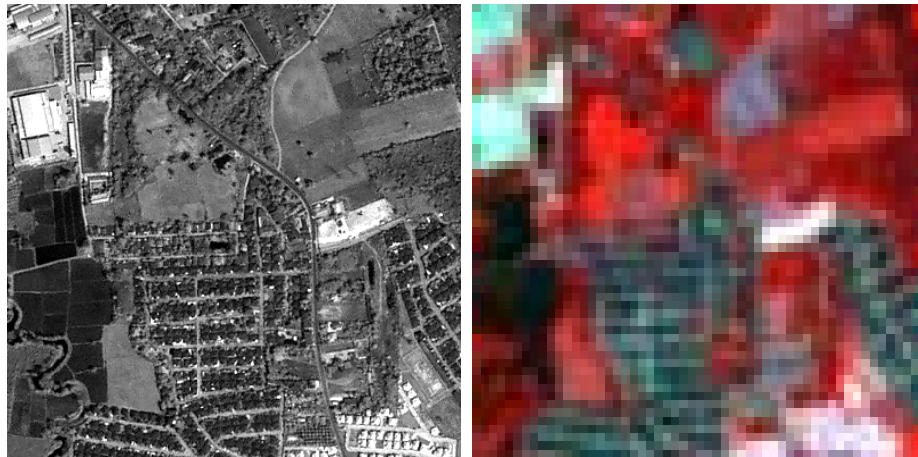
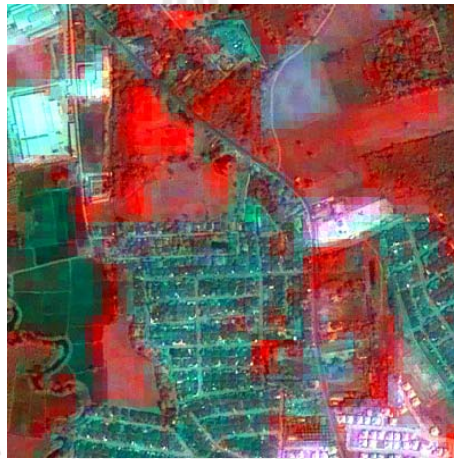


Figure 4.1 The image dataset 1 (a) Panchromatic image (b) Multi spectral images (c) pan-sharpened images from the trial no.1 using parameters 0.05 for a and 0.95 for b .



(a)

(b)



(c)

Figure 4.2 The zoom-in image dataset 1 (a) Panchromatic image (b) Multi spectral images (c) pan-sharpened images from trial no.1 using parameters 0.05 for a and 0.95 for b .

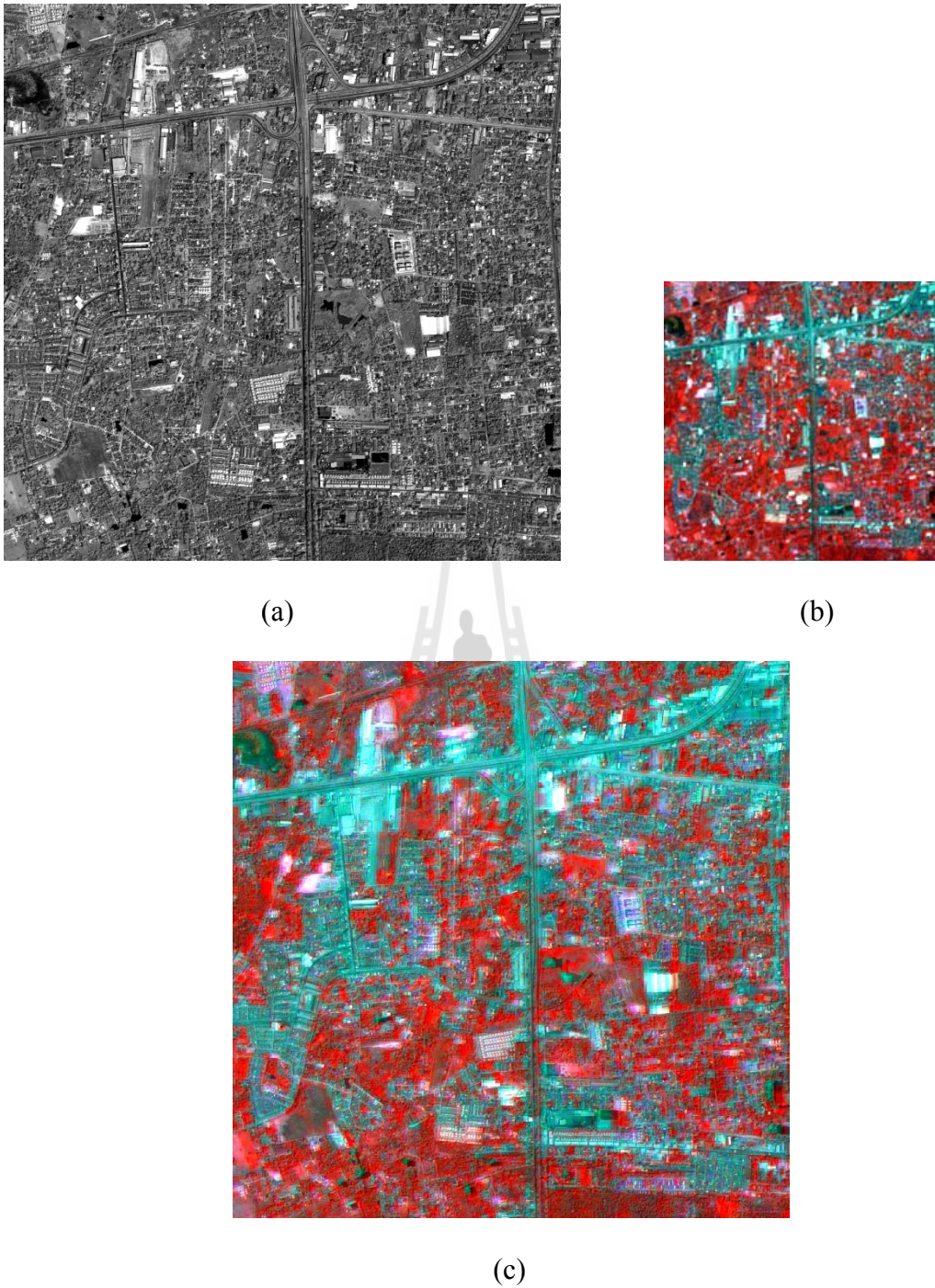


Figure 4.3 The image dataset 2 (a) Panchromatic image (b) Multi spectral images (c) pan-sharpened images from the trial no.1 using parameters 0.05 for a and 0.95 for b .

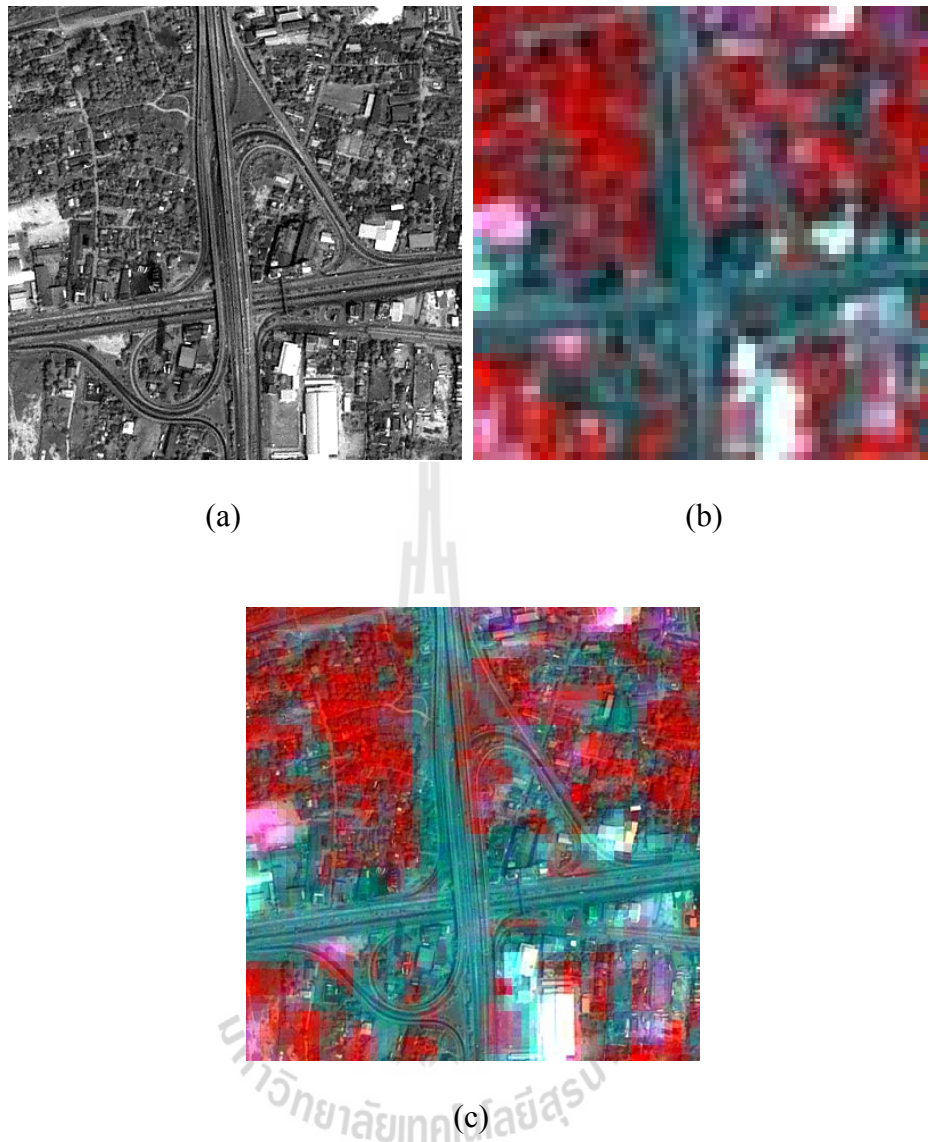


Figure 4.4 The zoom-in image dataset 2 (a) Panchromatic image (b) Multi spectral images (c) pan-sharpened images from the trial no.1 using parameters 0.05 for a and 0.95 for b .

4.1.2 The evaluation of image pan-sharpening

The evaluation of image pan-sharpening was based on the average correlation coefficients (CCs) between resembled original and pan-sharpened images. The highest CC of the pair of certain values a and b was selected to be input

for further road extraction processes. To evaluate the proposed pan-sharpening method, the average CC is estimated when apply each pair of weights to 10 sets of 1500×1500 pixels data in the study area. As examples, the CCs of the FIHS method of Tu et al. (2004) and trial no.1 (using parameters 0.05 for a and 0.95 for b) from 2 data sets are shown in Table 4.2. All CCs of 10 data sets can be seen in Appendix B.1. The CCs between trial no.1 and the FIHS from the Table 4.2 show that the pan-sharpened images resulted from the trial no.1 is better than the ones from the FIHS method. The transformed images resulted from the FIHS methods of Tu et al. (2004) and the trial no.1 were compared. Two image sets in form of composite images (R:G:B 4:2:1) of the trial no.1 and their corresponding images from the FIHS are shown in Figures 4.5 and 4.6.

Table 4.2 The comparison of the CCs resulted from the trial no.1 and the FIHS method of Tu et al. (2004).

CCs	Data set 1		Data set 2	
	FIHS	Trial no.1	FIHS	Trial no.1
Band 1	0.1440	0.5600	0.2297	0.6682
Band 2	0.3874	0.7412	0.4536	0.7998
Band 3	0.7278	0.8989	0.7310	0.9085
Band 4	0.7564	0.8991	0.7313	0.8855
Average	0.5039	0.7748	0.5364	0.8155



Figure 4.5 The comparison of pan-sharpened images data set 1 (a) pan-sharpened images from FIHS (b) pan-sharpened images from the trial no.1 using parameters 0.05 for a and 0.95 for b .

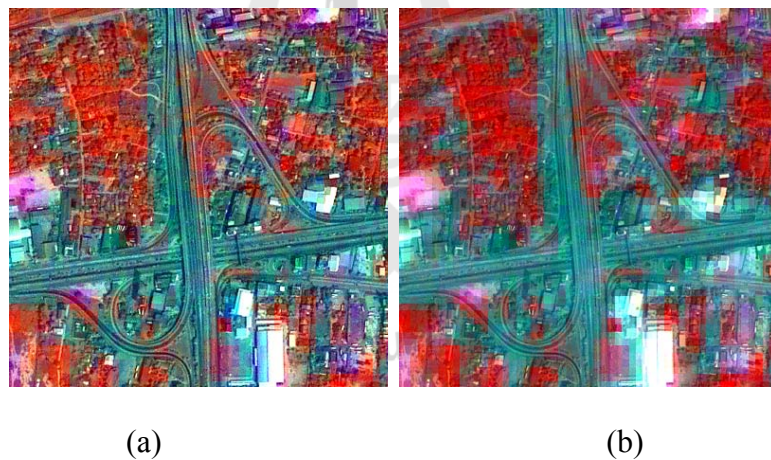


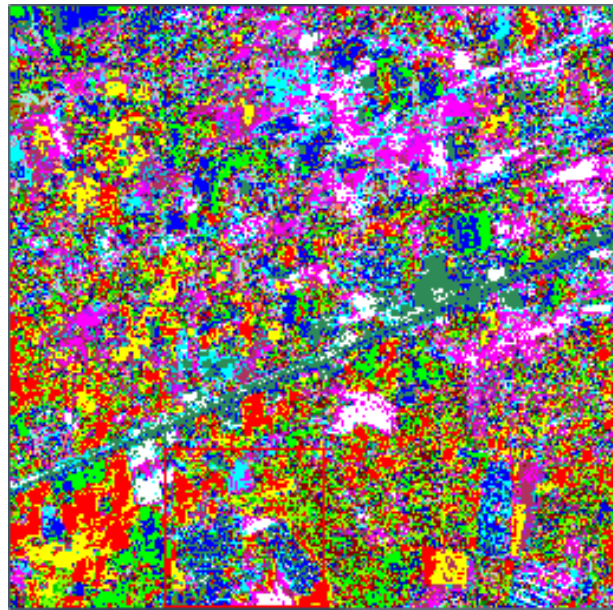
Figure 4.6 The comparison of pan-sharpened images data set 2 (a) pan-sharpened images from FIHS (b) pan-sharpened images from the trial no.1 using parameters 0.05 for a and 0.95 for b .

From the Table 4.2, the CCs of each band and the average one from the trial no.1 were higher than the ones from the FIHS. By visual consideration of the images resulted from both methods (as shown as examples in Figures 4.5 and 4.6), it

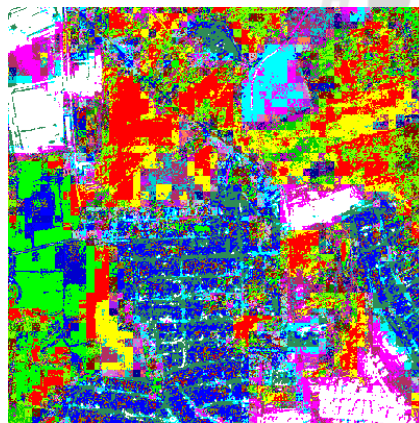
reveals that the quality of composite image resulted from the trial no.1 was poorer than the one resulted from the FIHS in term of the crispiness of the feature appearance.

4.1.3 Fuzzy c-means clustering and simulated annealing

The selected pan-sharpened images were classified using the unsupervised FCM and SA processes. The FCM and SA algorithm process was summarized in Section 3.2.2. For this trial, 30 classes of the unsupervised classification using these processes were performed for pan-sharpened images resulted from both the FIHS and the trial no.1. The results of unsupervised classification using the FCM and SA of both of them were shown in Figures 4.7 and 4.8, respectively.



(a)

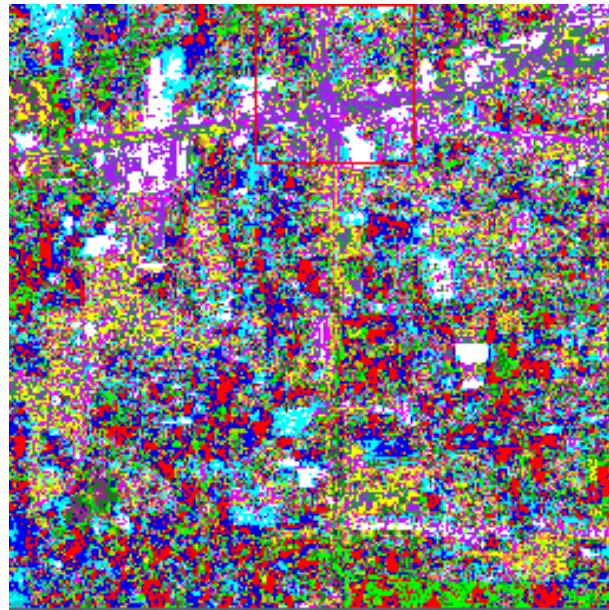


(b)

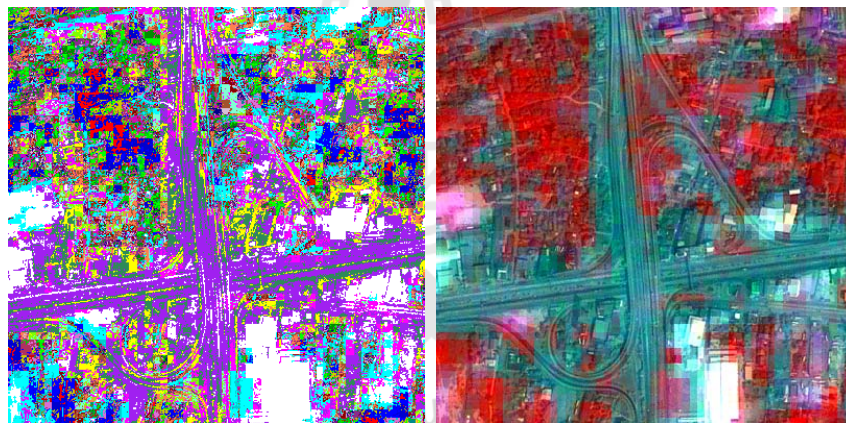


(c)

Figure 4.7 The result of unsupervised classification with 30 classes operated on pan-sharpened images resulted from the trial no.1 using FCM and SA (a), the zoom-in classified image (b), the zoom-in pan-sharpened images (c).



(a)



(b)

(c)

Figure 4.8 The result of unsupervised classification with 30 classes operated on pan-sharpened images resulted from the trial no.1 using FCM and SA (a), the zoom-in classified image (b), the zoom-in pan-sharpened images (c).

4.2 Pan-sharpening, fuzzy c-means and simulated annealing of trial no.2

4.2.1 Pan-sharpening

For this trial, the pan-sharpening process was performed for the sets of images as same as it is for the trial no.1 but the assumption of weighting parameters was changed to be $a+b = 1$ and $a > b$. Every pair of a and b was applied to 10 sets of images (1500x1500 pixels) and the average CCs is calculated. The average CCs of 10 sets of THEOS images of all pairs of a and b were listed in Table 4.3. According to experimental results in Table 4.3, the best weighting parameters for the Red and NIR bands of the trial no.2 were 0.55 for a and 0.45 for b .

Table 4.3 Average correlation coefficients (CCs) between resembled original and pan-sharpened images of 10 sets of THEOS images of the trial no.2, with varying spectral weights.

Pairs of weighting parameters									
a	0.95	0.9	0.85	0.8	0.75	0.7	0.65	0.6	0.55
b	0.05	0.1	0.15	0.2	0.25	0.3	0.35	0.4	0.45
(CCs)	0.6519	0.6657	0.6794	0.6928	0.7059	0.7185	0.7304	0.7416	0.7519

The 2 sets of pan-chromatic image, multispectral images inform of a composite image, pan-sharpened images processed using the best a and b of trial no.2 and their zoom-in ones are shown as examples in Figures 4.9 to 4.12. The data set 1 was selected to represent area of local road while the date set 2 was represent the area of main road.

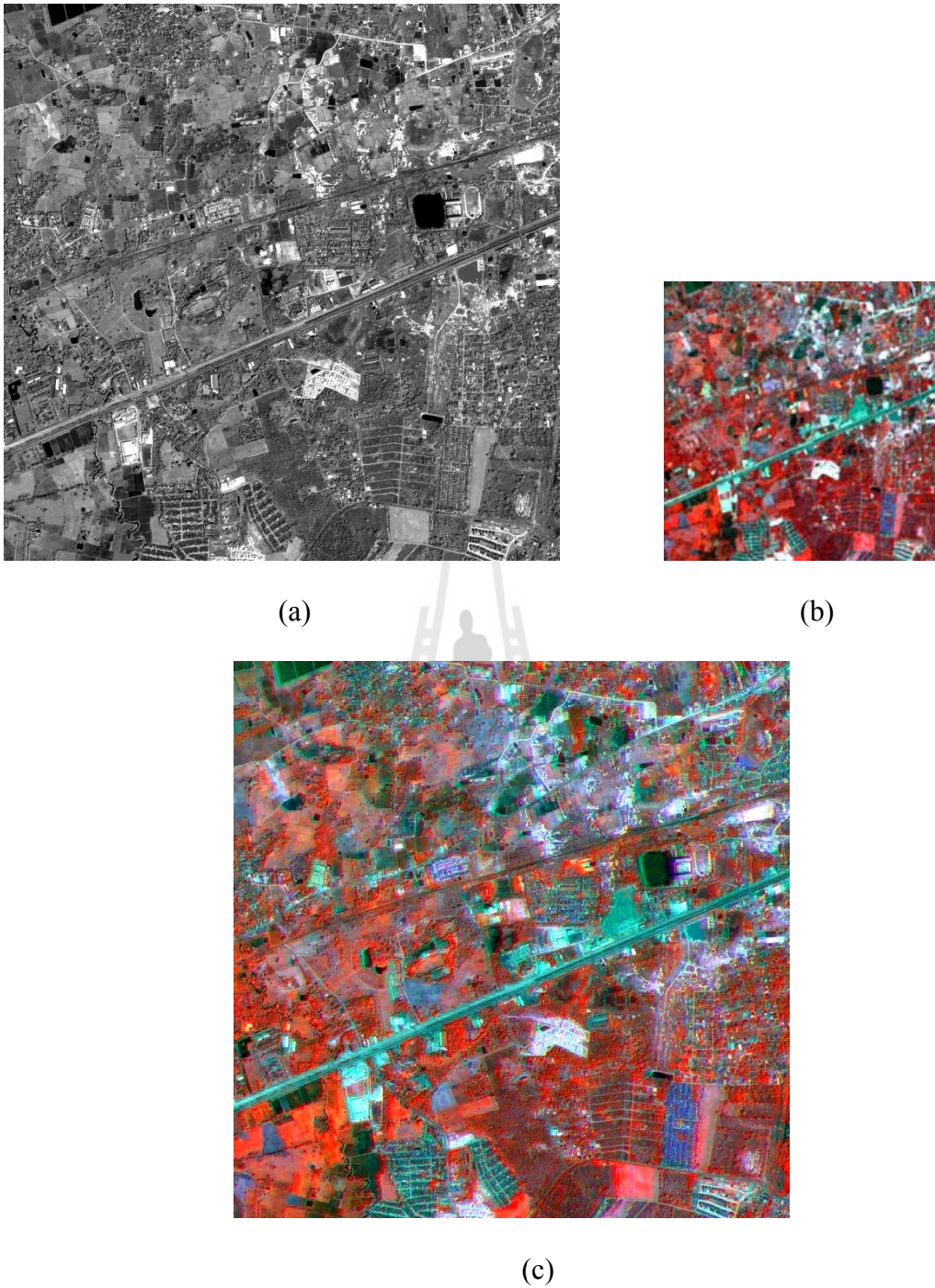
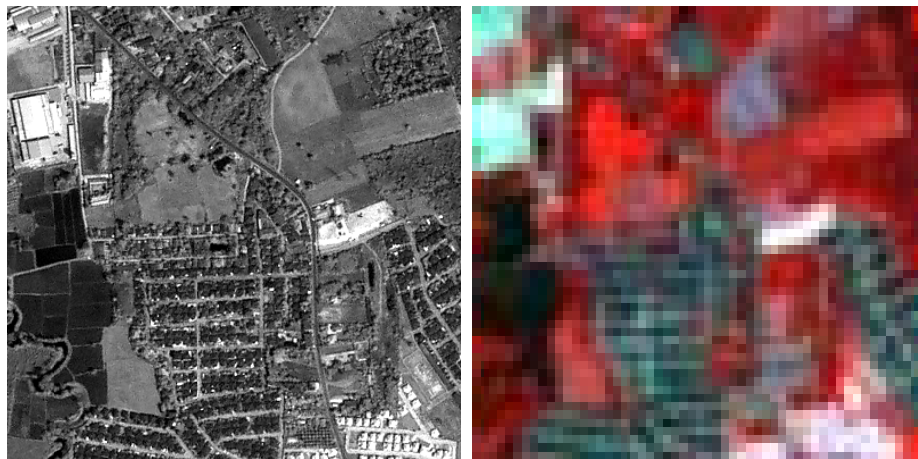


Figure 4.9 The image dataset 1 (a) Panchromatic image (b) Multi spectral images (c) pan-sharpened images from the trial no.2 using parameters 0.55 for a and 0.45 for b .



(a)

(b)



(c)

Figure 4.10 The zoom-in image dataset 1 (a) Panchromatic image (b) Multi spectral images (c) pan-sharpened images from trial no.2 using parameters 0.55 for a and 0.45 for b .

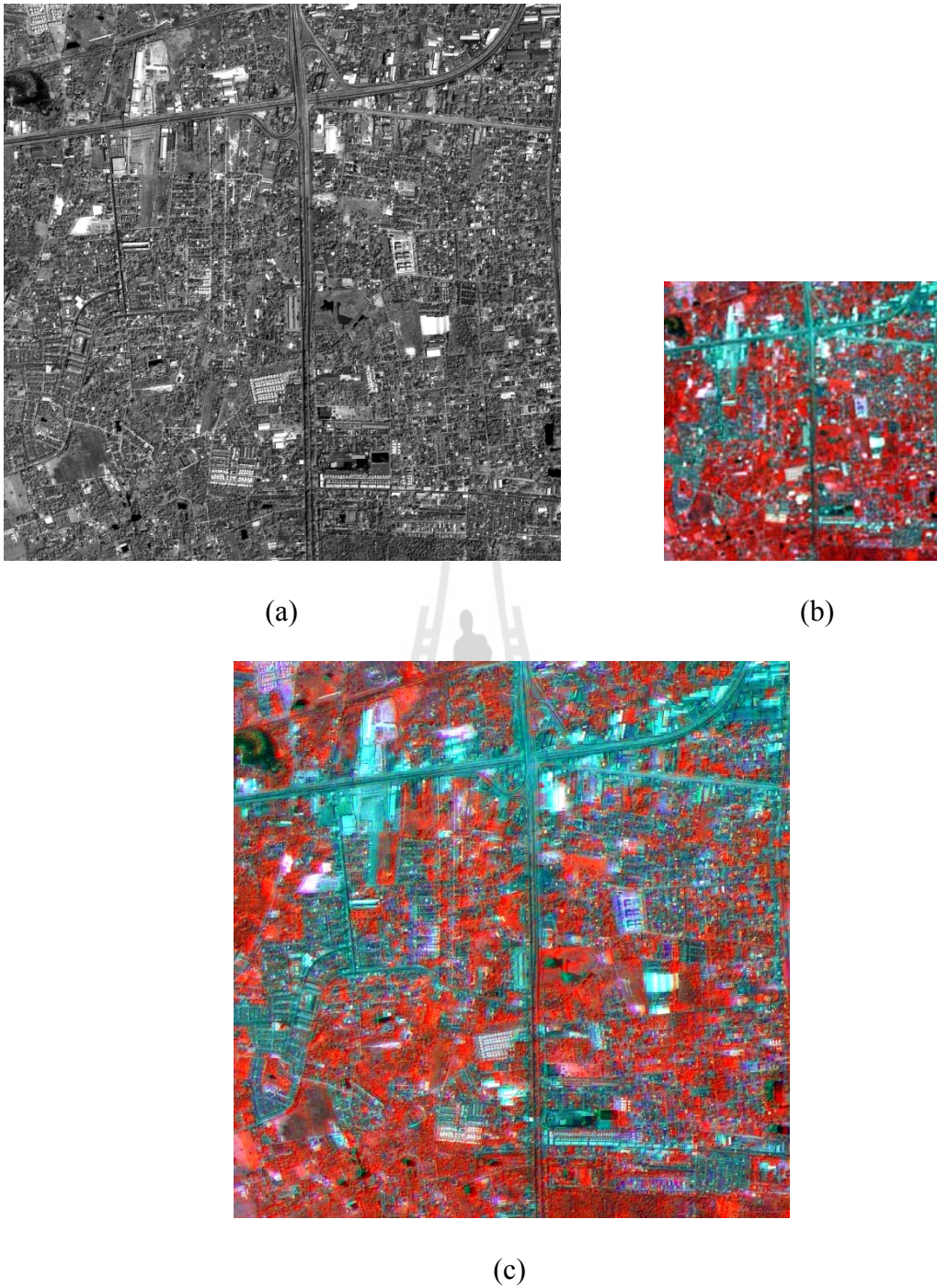


Figure 4.11 The image dataset 2 (a) Panchromatic image (b) Multi spectral images (c) pan-sharpened images from the trial no.2 using parameters 0.55 for a and 0.45 for b .

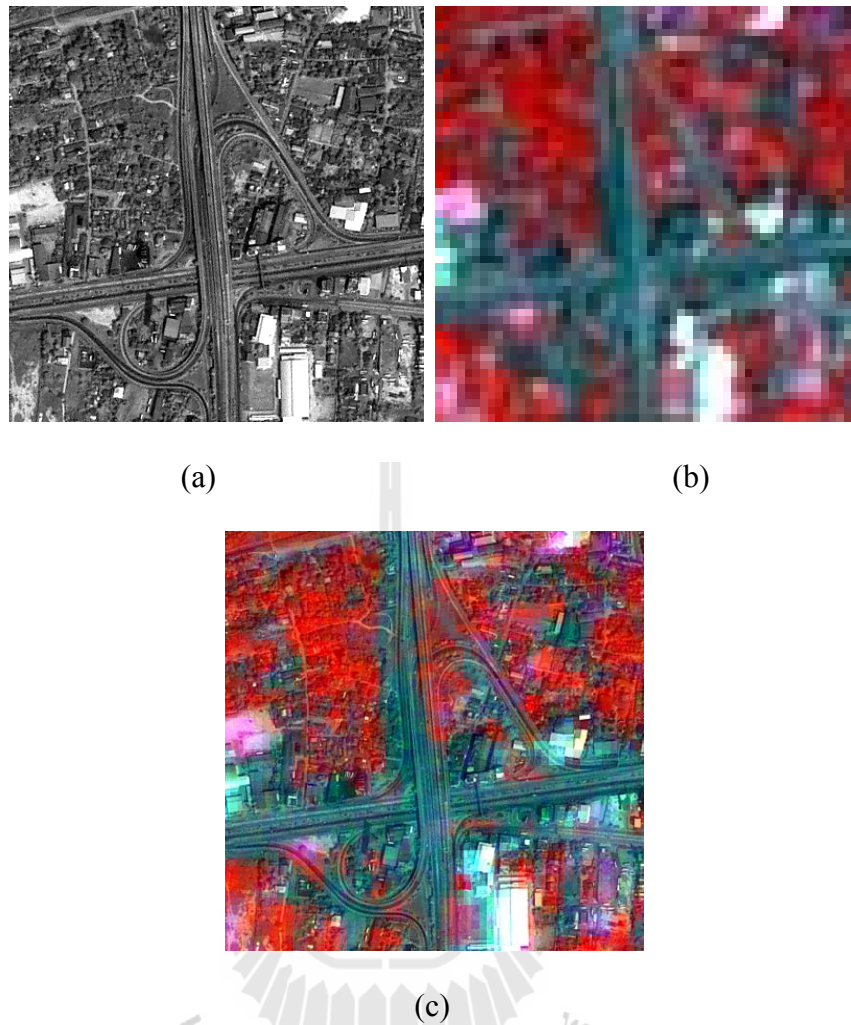


Figure 4.12 The zoom-in image dataset 2 (a) Panchromatic image (b) Multi spectral images (c) pan-sharpened images from trial no.2 using parameters 0.55 for a and 0.45 for b .

4.2.2 The evaluation of image pan-sharpening

To evaluate the proposed pan-sharpening method of the trial no.2, the average CC was estimated when apply each pair of weights to 10 sets of 1500×1500 pixels data in the study area. As examples, the CCs of the FIHS method of Tu et al. (2004) and trial no.2 (using weighting parameters 0.55 for a and 0.45 for b) from 2 data sets were shown in Table 4.4. All CCs of 10 data sets can be seen in Appendix

B.2. The CCs between trial no.2 and the FIHS from the Table 4.4 show that the pan-sharpened images resulted from the trial no.2 was better than the ones from the FIHS method. The transformed images resulted from the FIHS methods of Tu et al. (2004) and the trial no.2 was compared. Two image sets in form of composite image (R,G,B 4:2:1) of the trial no.2 and their corresponding images from the FIHS were shown as examples in Figures 4.13 and 4.14.

Table 4.4 The comparison of the CCs resulted from the trial no.2 and the FIHS method of Tu et al. (2004).

CCs	Dataset 1		Dataset 2	
	FIHS	Trial no.2	FIHS	Trial no.2
Band 1	0.1440	0.1703	0.2297	0.1945
Band 2	0.3874	0.5239	0.4536	0.5013
Band 3	0.7278	0.8297	0.7310	0.7827
Band 4	0.7564	0.8839	0.7313	0.8517
Average	0.5039	0.6019	0.5364	0.5826

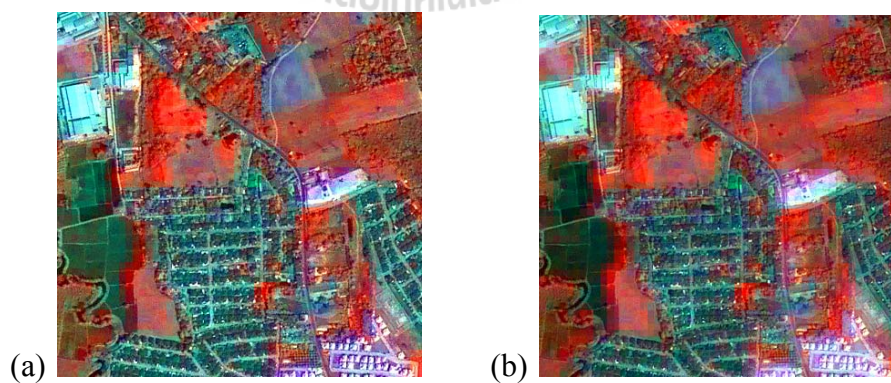


Figure 4.13 The comparison of pan-sharpened images data set 1 (a) pan-sharpened images from FIHS (b) pan-sharpened images from the trial no.2 using parameters 0.55 for *a* and 0.45 for *b*.

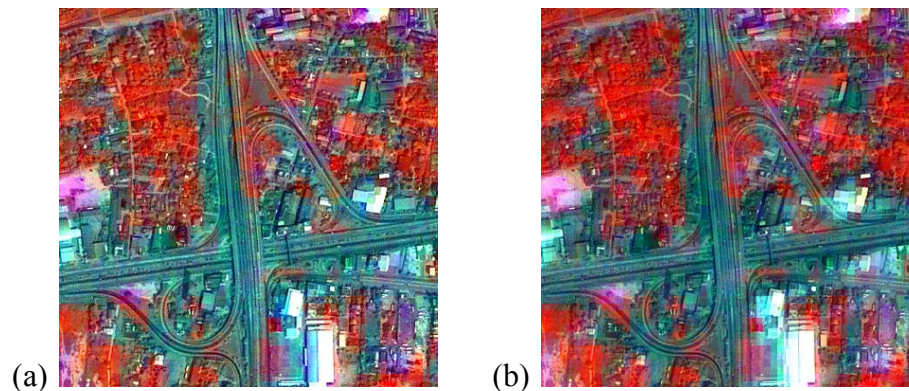
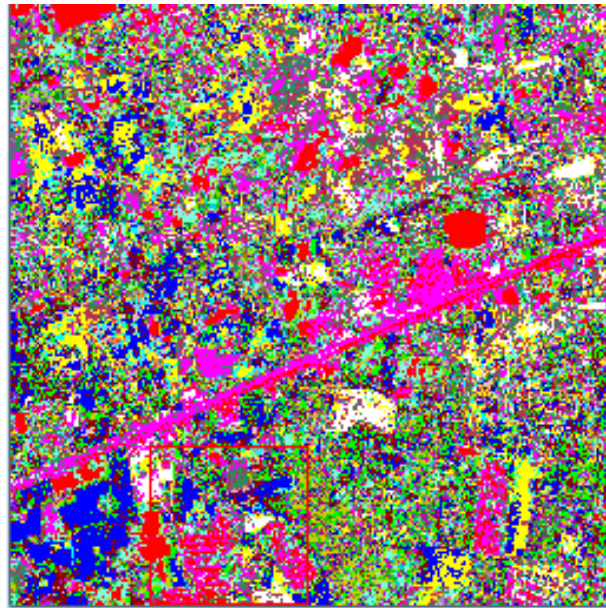


Figure 4.14 The comparison of pan-sharpened images data set 2 (a) pan-sharpened images from FIHS (b) pan-sharpened images from the trial no.2 using parameters 0.55 for a and 0.45 for b .

From the Table 4.4, the CCs of each band and the average one from the trial no.2 were higher than the ones from the FIHS. By visual consideration of the images resulted from both methods (as shown in Figures 4.13 and 4.14), it reveals that the crispiness of the feature appearance in the composite images resulted from both methods is about the same.

4.2.3 Fuzzy c-means clustering and simulated annealing

For this trial, 30 classes of the unsupervised classification, as same as the trial no.1, using these processes were performed for pan-sharpened images resulted from both the FIHS and the trial no.2. The results of unsupervised classification using the FCM and SA of both of them were shown in Figures 4.15 and 4.16, respectively.



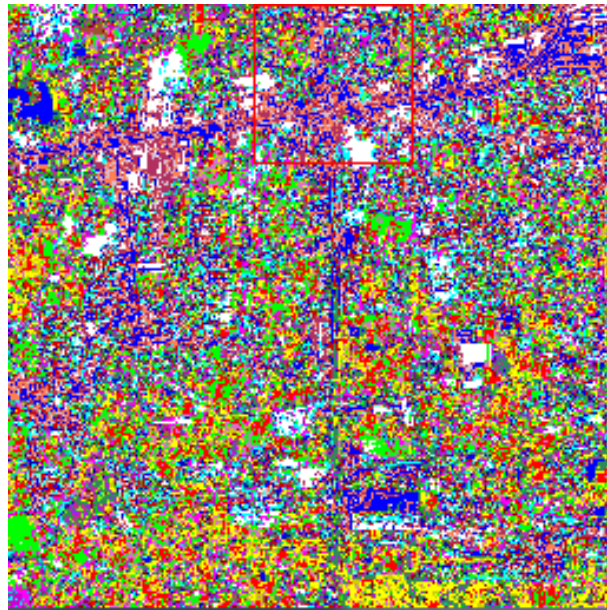
(a)



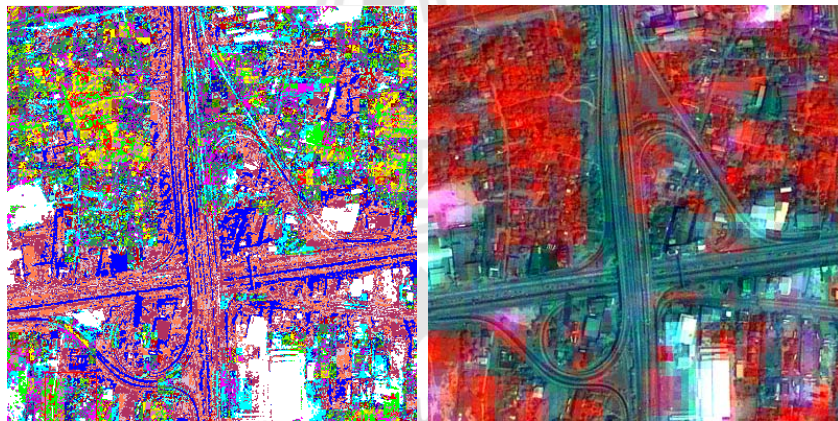
(b)

(c)

Figure 4.15 The result of unsupervised classification with 30 classes operated on pan-sharpened images resulted from the trial no.2 using FCM and SA (a), the zoom-in classified image (b), the zoom-in pan-sharpened images (c).



(a)



(b)

(c)

Figure 4.16 The result of unsupervised classification with 30 classes operated on pan-sharpened images resulted from the trial no.2 using FCM and SA (a), the zoom-in classified image (b), the zoom-in pan-sharpened images (c).

4.3 Pan-sharpening, fuzzy c-means simulated annealing of trial no.3

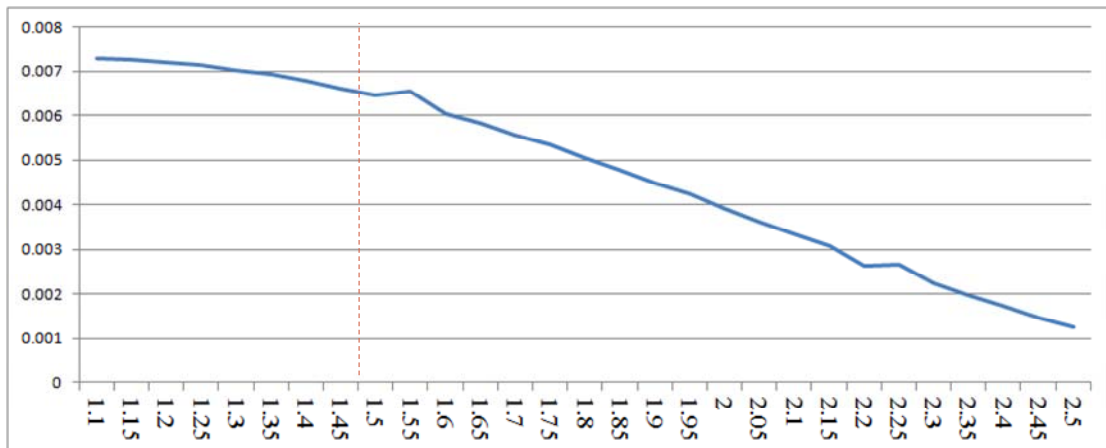
4.3.1 Pan-sharpening

For this trial, the pan-sharpening process was performed for the sets of images as same as it is for the trial no.1 and no.2 but the assumption of weighting parameters was changed to be $a+b = 2.5$, a or $b \geq 1.05$ and no weights were applied to the Green and Blue bands as expressed in Eq.(3.4). Every pair of a and b was applied to 10 sets of images (1500x1500 pixels) and the average CCs was calculated. The average CCs for 10 sets of THEOS images of all pairs of a and b are listed in Table 4.5.

Table 4.5 Average correlation coefficients (CCs) between resembled original and pan-sharpened images of 10 sets of THEOS images of the trial no.3, with varying spectral weights.

		Pairs of weighting parameters										
a		1.45	1.40	1.35	1.30	1.25	1.20	1.15	1.10	1.05	1.00	0.95
b		1.05	1.10	1.15	1.20	1.25	1.30	1.35	1.40	1.45	1.50	1.55
(CCs)		0.3687	0.3760	0.3833	0.3905	0.3976	0.4046	0.4116	0.4183	0.4249	0.4314	0.4379

According to experimental results in Table 4.5, the best weighting parameters for the Red and NIR bands (a and b) of the trial no.3 are 1.05 for a and 1.45 for b . As displayed in Figure 4.17, the rate of increment of the difference distance of average CCs was dropped and became constant when b was between 1.45 to 1.55. The optimum b at 1.45 was selected because it was located at the turning point of increment before a was lower than 1.



x-axis: weighting parameter for NIR band (b)

y-axis: different distance of average CCs according to varying pair

Figure 4.17 The plot between different distance of average CCs and varying b . When a is bigger than 1 and b is less than 1.5, the turning point of the rate of increment of the different distance appeared at $b=1.45$.

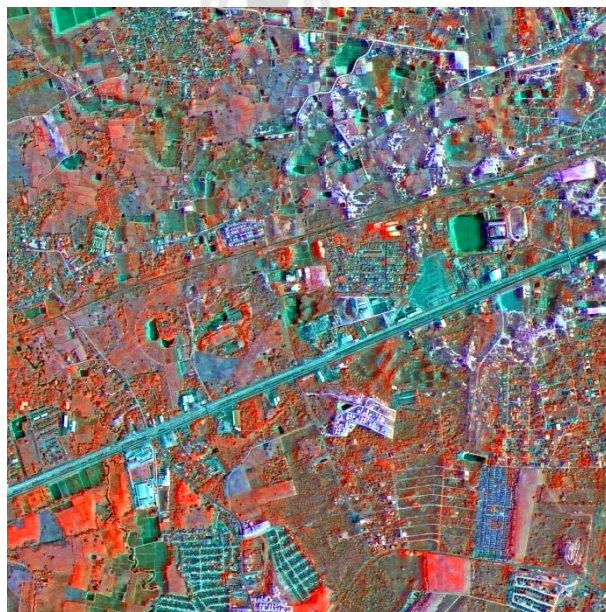
The 2 set of panchromatic image, multispectral images in form of a composite image, pan-sharpened images using the best a and b from the trial no.3 and their zoom-in ones are shown as examples in Figures 18 to 21. The data set 1 was selected to represent area of local road while the date set 2 was represent the area of main road.



(a)



(b)



(c)

Figure 4.18 The image dataset 1 (a) Panchromatic image (b) Multi spectral images (c) pan-sharpened images from the trial no.3 using parameter 1.05 for a and 1.45 for b .



(a)

(b)



(c)

Figure 4.19 The zoom in of image dataset 1 (a) Panchromatic image (b) Multi spectral images (c) pan-sharpened images from the trial no.3 using parameter 1.05 for a and 1.45 for b .

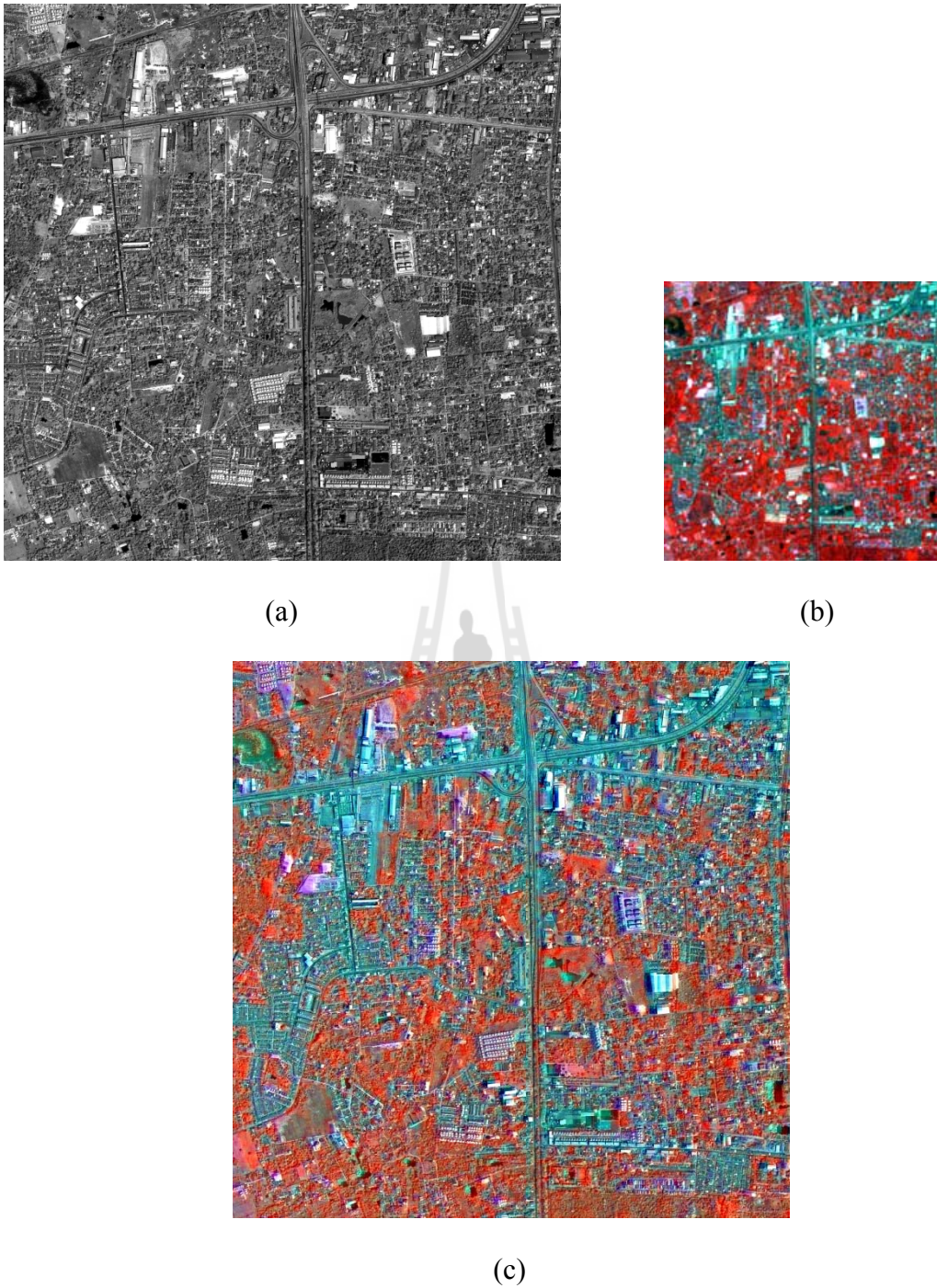


Figure 4.20 The image dataset 2 (a) Panchromatic image (b) Multi spectral images (c) pan-sharpened images from the trial no.3 using parameter 1.05 for a and 1.45 for b .

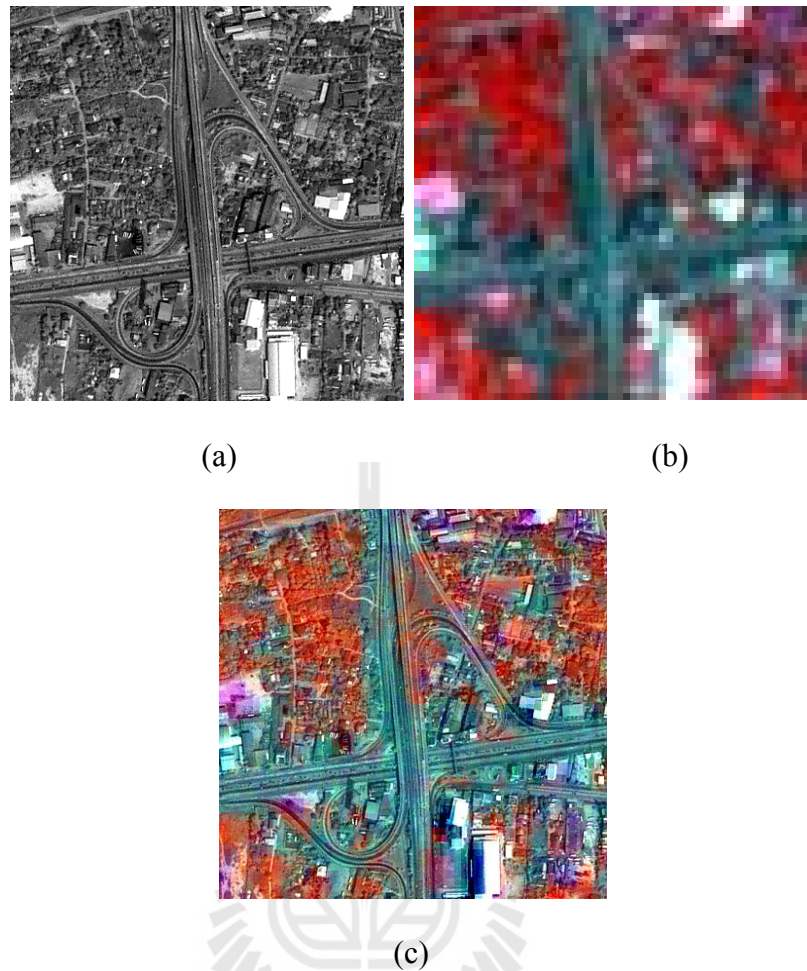


Figure 4.21 The zoom in of image dataset 2 (a) Panchromatic image (b) Multi spectral images (c) pan-sharpened images from the trial no.3 using parameter 1.05 for a and 1.45 for b .

4.3.2 The evaluation of image pan-sharpening

To evaluate the proposed pan-sharpening method of the trial no.3, the average CC was estimated when apply each pair of weights to 10 sets of 1500×1500 pixels data in the study area. As examples, the CCs of the FIHS method of Tu et al. (2004) and trial no.3 (using weighting parameters 1.05 for a and 1.45 for b) from 2 data sets were shown in Table 4.6. All CCs of 10 data sets can be seen in Appendix

B.3. The CCs between trial no.3 and the FIHS from the Table 4.6 show that the pan-sharpened images resulted from the trial no.3 is lower than the ones from the FIHS method. The transformed images resulted from the FIHS methods of Tu et al. (2004) and the trial no.3 were compared. Two image sets in form of composite images (R:G:B 4:2:1) of the trial no.3 and their corresponding images from the FIHS were shown as examples in Figures 4.21 and 4.22.

Table 4.6 The comparison of the CCs resulted from the trial no.3 and the FIHS method of Tu et al. (2004).

CCs	Dataset 1		Dataset 2	
	FIHS	Trial no.3	FIHS	Trial no.3
Band 1	0.1440	-0.0043	0.2297	0.0373
Band 2	0.3874	0.1832	0.4536	0.2201
Band 3	0.7278	0.5552	0.7310	0.5448
Band 4	0.7564	0.5960	0.7313	0.5704
Average	0.5039	0.3325	0.5364	0.3431

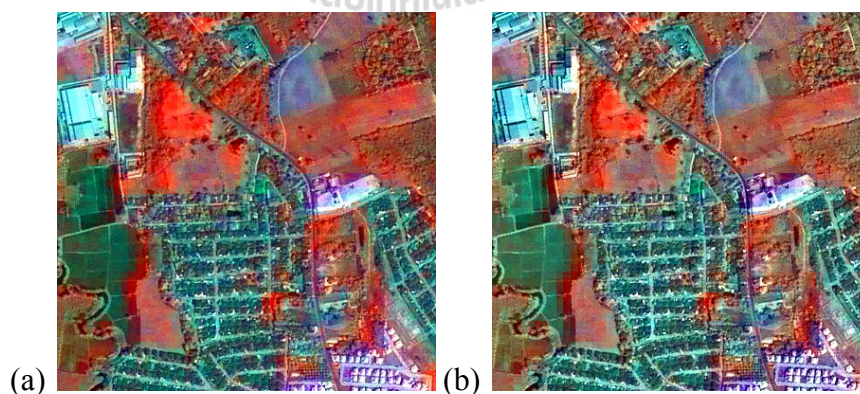


Figure 4.22 The comparison of pan-sharpened images data set 1 (a) pan-sharpened images from FIHS (b) pan-sharpened images from the trial no.3 using parameter 1.05 for *a* and 1.45 for *b*.

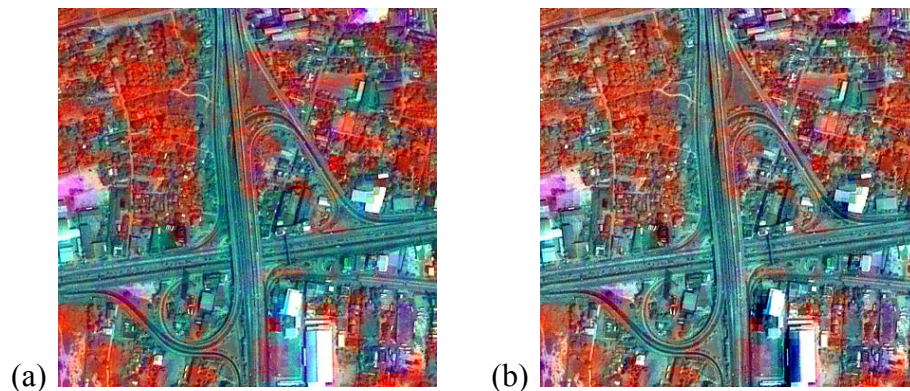
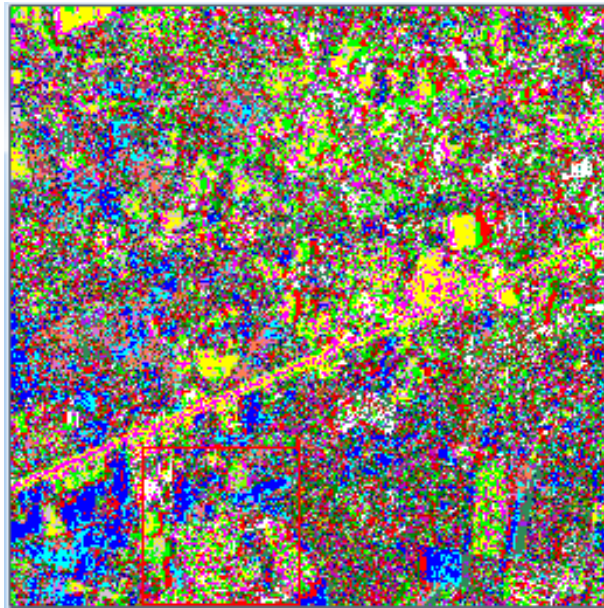


Figure 4.23 The comparison of pan-sharpened images data set 2 (a) pan-sharpened images from FIHS (b) pan-sharpened images from the trial no.3 using parameter 1.05 for a and 1.45 for b .

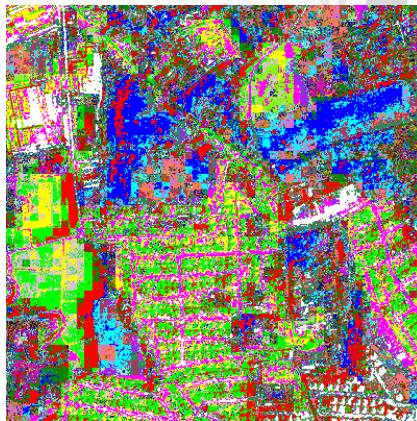
From the Table 4.6, the CCs of each band and the average one from the trial no.3 were lower than the ones from the FIHS. By visual consideration of the images resulted from both methods (as shown in Figures 4.22 and 4.23), it reveals that the crispiness of the feature appearance in the composite images resulted from the trial no.3 is better than the ones from the FIHS.

4.3.3 Fuzzy c-means clustering and simulated annealing

For this trial, 30 classes of the unsupervised classification, as same as the trial no.1 and no.2, using these processes were performed for pan-sharpened images resulted from both the FIHS and the trial no.3. The results of unsupervised classification using the FCM and SA of both of them are shown in Figures 4.24 and 4.25, respectively.



(a)

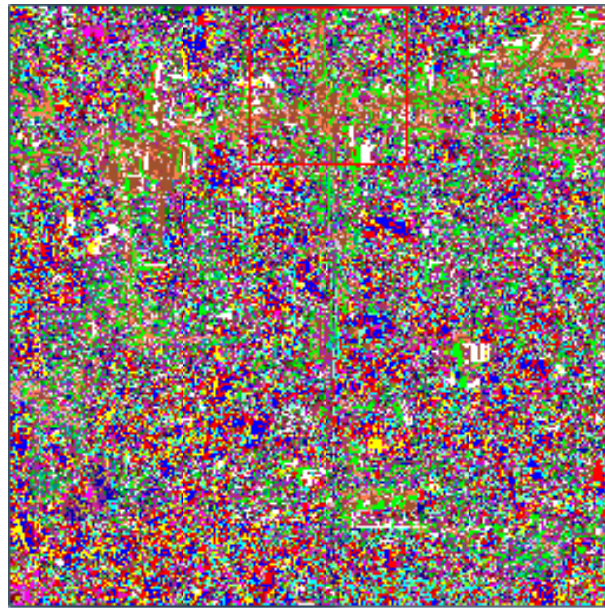


(b)

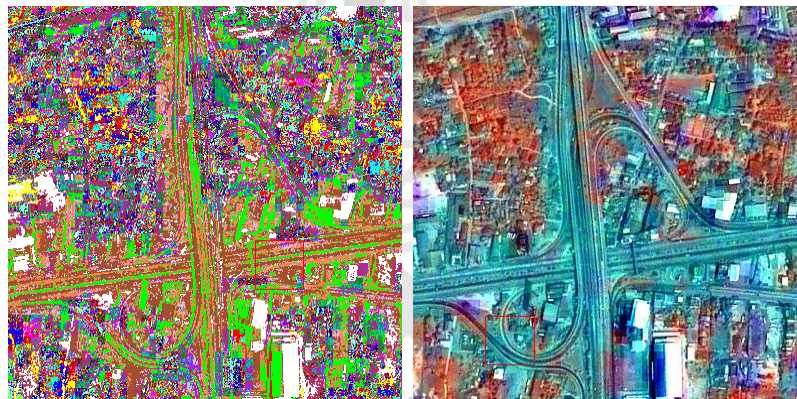


(c)

Figure 4.24 The result of unsupervised classification with 30 classes operated on pan-sharpened images resulted from the trial no.3 using FCM and SA (a), the zoom-in classified image (b), the zoom-in color composite of the pan-sharpened images (c).



(a)



(b)

(c)

Figure 4.25 The result of unsupervised classification with 30 classes operated on pan-sharpened images resulted from the trial no.3 using FCM and SA (a), the zoom-in classified image (b), the zoom-in color composite of the pan-sharpened images (c).

4.4 The comparison of image quality of all trials

In this study, the improved IHS transformation methods for image pan-sharpening was developed and applied to the trial no.1 to no.3. The quality of the pan-sharpened images from all trials was compared and assessed mainly based on

- visual comparison of composite images from all trials.
- the CCs of panchromatic images and pan-sharpened images band by band and the average.
- consideration on clustering results of all trials.

4.4.1 Visual comparison of composite images from all trials

The comparison of the spectral and spatial quality using visual analysis was operated among composite images from all trials as shown as examples in Figure 4.26 and 4.27. The former represents the local road network while the later represents the area having main highway network. From the Figures, it reveals that the crispiness of the feature appearance of image resulted from the trial no.3 was the best while the image resulted from the trial no.1 shows the highest color distortion.

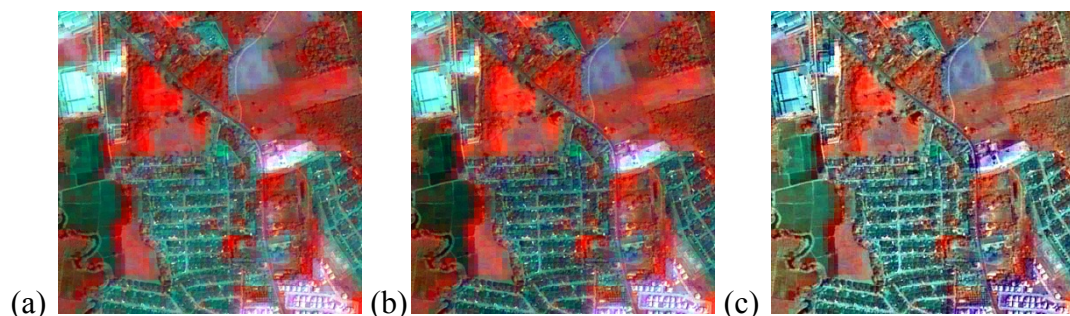


Figure 4.26 The pan-sharpened images in the area representing local road network resulted from (a) the trial no.1, (b) the trial no.2, and (c) the trial no.3.

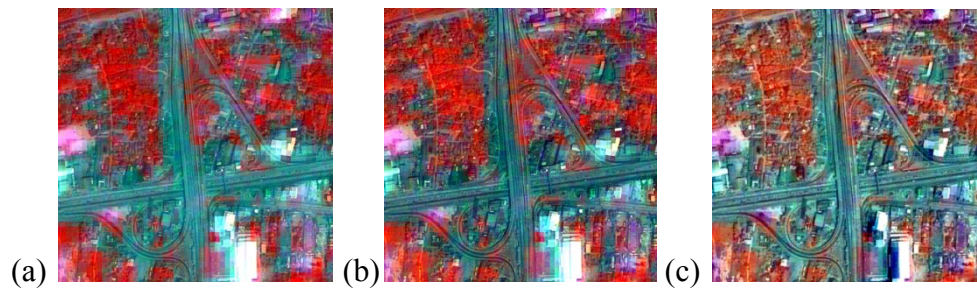


Figure 4.27 The pan-sharpened images in the area representing main highway network resulted from (a) the trial no.1, (b) the trial no.2, and (c) the trial no.3.

4.4.2 The CCs of the pan-sharpened and panchromatic images

Table 4.7 shows the CCs between the pan-sharpened images resulted from all trials and the panchromatic images.

It reveals that the CCs of the Red and NIR bands and the average of the trial no.3 were the best. They indicate that the readjusted Red and NIR bands of the pan-sharpened images of this trial for all data sets show closer spectral relation to the panchromatic images which cover wave length of these bands. This leads to better crispiness of feature appearance in the images. This is obviously observable when the pan-sharpened images of Red and NIR bands from all trials were compared to the panchromatic image as shown in the Figures 4.28.and 4.29, respectively. It is obvious that, from both bands, the crispiness of the images resulted from the trial no.3 were much better than the ones resulted from the trials no.1 and 2 and their quality was very close to the panchromatic images. This will benefit to further clustering process for extracting the candidate road network. This should be confirmed by comparing the color composite images of all trials and the panchromatic image as displayed in Figure 4.30. The crispiness of features in the image from the trial no.3 was the best and closest to the panchromatic image.

Table 4.7 The comparison CCs between pan-sharpened images of all trials and the panchromatic images.

CCs	Data set 1			Data set 2			Data set 3			Data set 4			Data set 5		
	Trial no.1	Trial no.2	Trial no.3	Trial no.1	Trial no.2	Trial no.3	Trial no.1	Trial no.2	Trial no.3	Trial no.1	Trial no.2	Trial no.3	Trial no.1	Trial no.2	Trial no.3
1&Pan	0.7854	0.9059	0.8228	0.7509	0.9085	0.8696	0.6585	0.8363	0.7511	0.8096	0.8990	0.7930	0.7695	0.8753	0.7544
2&Pan	0.7854	0.9092	0.8944	0.7183	0.8780	0.9182	0.6606	0.8377	0.8480	0.8496	0.9450	0.8883	0.8253	0.9336	0.8779
3&Pan	0.6740	0.7638	0.8957	0.6064	0.7325	0.8919	0.5602	0.6691	0.8379	0.7762	0.8380	0.9154	0.7628	0.8319	0.9105
4&Pan	0.6953	0.6008	0.8153	0.5925	0.5146	0.7461	0.5367	0.4450	0.6708	0.8168	0.7380	0.8935	0.8076	0.7313	0.8706
Average	0.7350	0.7949	0.8570	0.6670	0.7584	0.8564	0.6040	0.6970	0.7770	0.8130	0.8550	0.8726	0.7913	0.8430	0.8534

CCs	Data set 6			Data set 7			Data set 8			Data set 9			Data set10		
	Trial no.1	Trial no.2	Trial no.3	Trial no.1	Trial no.2	Trial no.3	Trial no.1	Trial no.2	Trial no.3	Trial no.1	Trial no.2	Trial no.3	Trial no.1	Trial no.2	Trial no.3
1&Pan	0.7107	0.8242	0.6485	0.7468	0.8651	0.7165	0.7468	0.8651	0.7165	0.6685	0.8102	0.6538	0.7833	0.8921	0.7679
2&Pan	0.7959	0.9133	0.8345	0.8090	0.9357	0.8678	0.8090	0.9357	0.8678	0.7682	0.9054	0.8123	0.8176	0.9242	0.8622
3&Pan	0.7322	0.8028	0.8893	0.7417	0.8182	0.8907	0.7417	0.8182	0.8907	0.7272	0.8043	0.8653	0.7362	0.8073	0.8901
4&Pan	0.7421	0.6537	0.7963	0.7658	0.6758	0.8112	0.7658	0.6758	0.8112	0.7892	0.7032	0.8359	0.7817	0.6951	0.8584
Average	0.7452	0.7985	0.7921	0.7658	0.8237	0.8216	0.7658	0.8237	0.8216	0.7383	0.8058	0.7919	0.7797	0.8297	0.8446

1, 2, 3, and 4: bands of pan-sharpened images.

Pan: Panchromatic image.

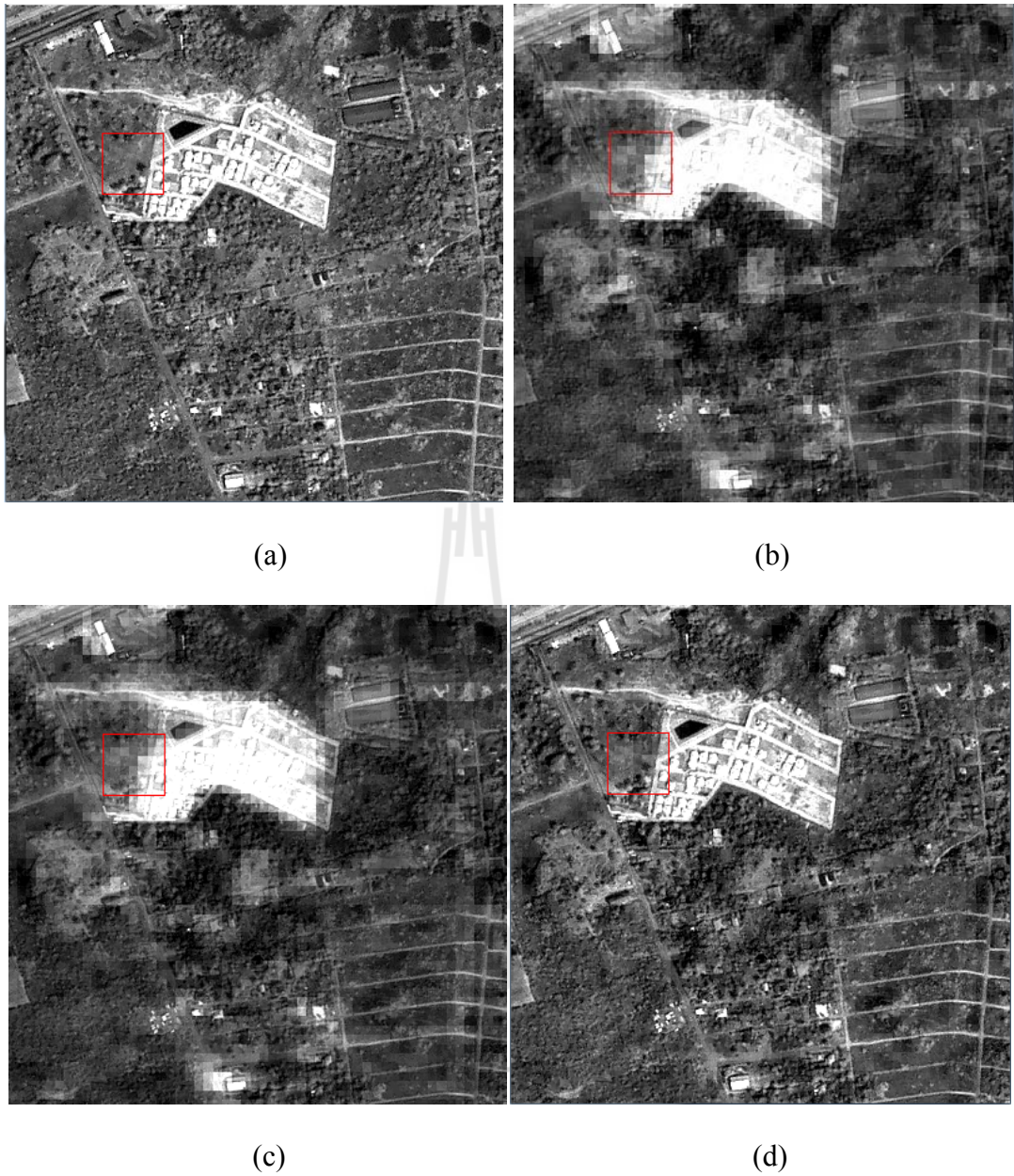


Figure 4.28 The comparison of panchromatic image (a) and the pan-sharpened images data set 1 of Red band from the trial no.1 (b), the trial no.2 (c), and the trial no.3 (d).

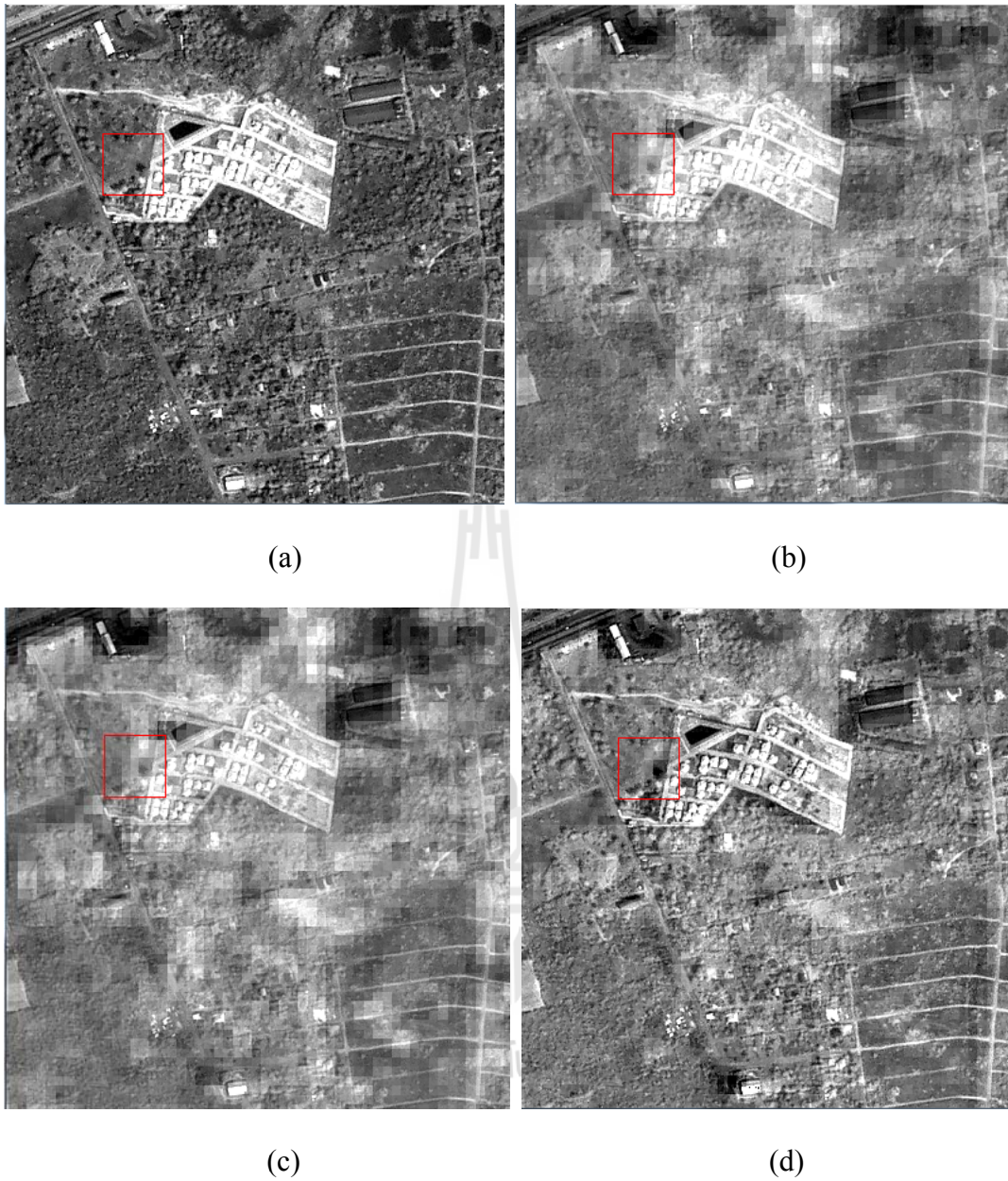


Figure 4.29 The comparison of panchromatic image (a) and the pan-sharpened images data set 1 of NIR band from the trial no.1 (b), the trial no.2 (c), and the trial no.3 (d).

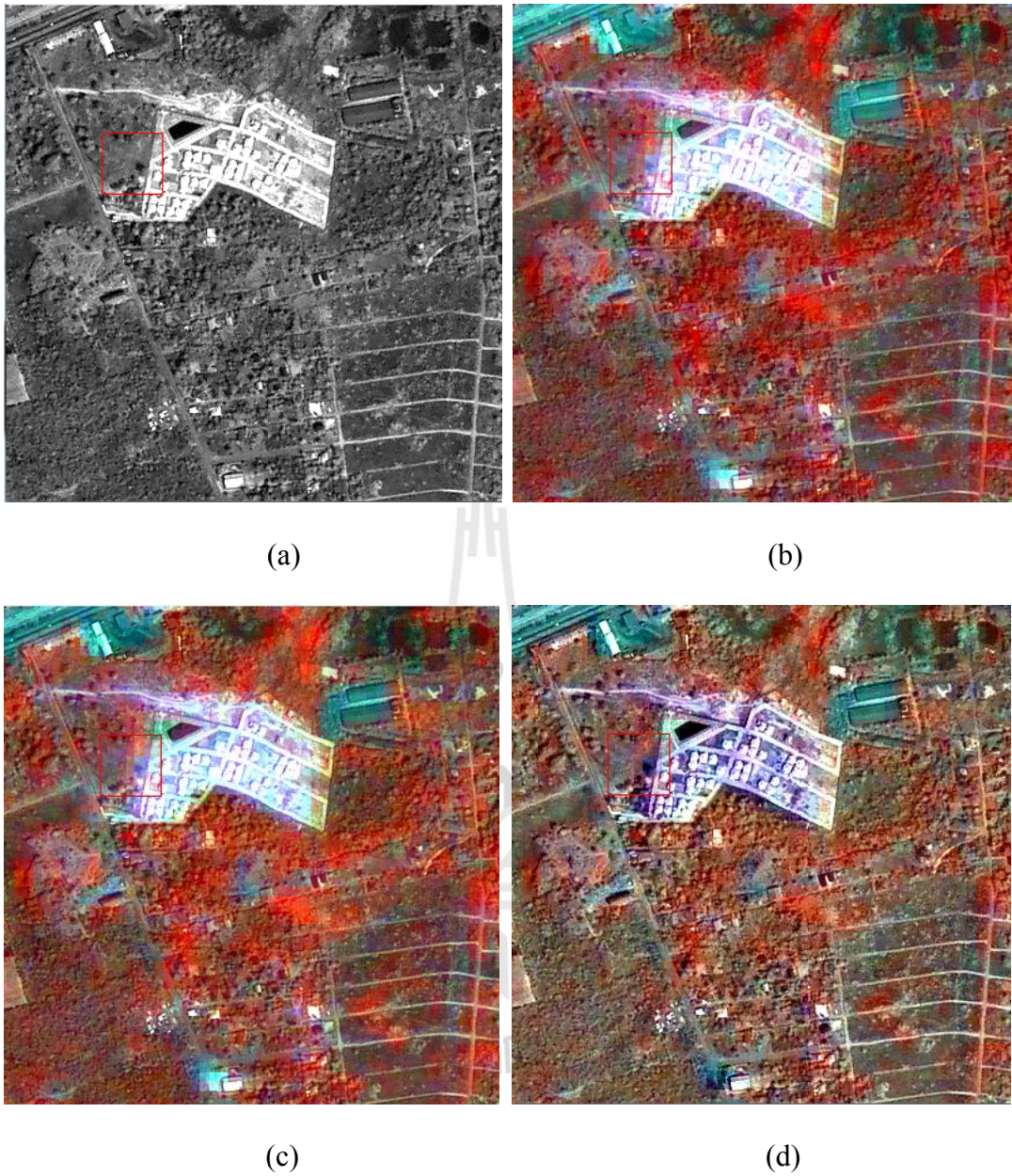


Figure 4.30 The comparison the panchromatic image data set 1 (a) and the color composite images (R:G:B 4:2:1) of pan-sharpened images resulted from the trial no.1 (b), trial no.2 (c), and trial no.3 (d).

4.4.3 Consideration on clustering results of all trials

The 30-classes of clustering process using the FCM and SA is performed on the pan-sharpened images of all trials. The results comparison for examples expresses that, for the data set represents the local road network, the cluster continuity of the candidate road network of the trial no.3 is obviously better than the ones of the trial no.1 and no.2. For the data set represents the main highway network, the candidate road network of the trial no.3 obviously falls into only 2 clusters with less non-road candidate included. The candidate road network of the trial no.1 falls into 2 clusters as well but obviously with more non-road candidate included. For the trial no.2, the candidate road network falls into 3 clusters.

By visual comparison of color composite images from each trial, it reveals that the one from the trial no.3 is the best in terms of crispiness of feature appearance. Trial no.1 shows the highest color distortion. By comparing CCs of pan-sharpened and panchromatic images, the trial no.3 shows the highest average CCs followed by the trial no.2. Considering pan-sharpen images of Red, NIR bands and color composite image (R:G:B 4:2:1) of all trials, the trial no.3 is the best quality and their crispiness is very close to the panchromatic image. By clustering comparison, the result from the trial no.3 shows that a smaller number of clusters can cover candidate road network and its connectivity is better than other trials.

Based on the quality of pan-sharpened images of trials no.1 and no.2, the images from the trial no.2 were better than the trial no.1 whereas the one from the trial no.3 were the best. Resulting images from the trial no.2 were the representative of the method of Tu et al. (2002) while resulting images from the trial no.3 were the representative of this research method attempted to design the modified pan-

sharpening fit to the THEOS data. Then pan-sharpened images from the trial no.2 and no.3 were selected for further road extraction processes so that their results can be compared.

4.5 Image clustering

The FCM and SA processes clustering are developed as an extension and implemented under the environment of ENVI/IDL software. The extension interface of the FCM and SA is shown in Figure 4.31.

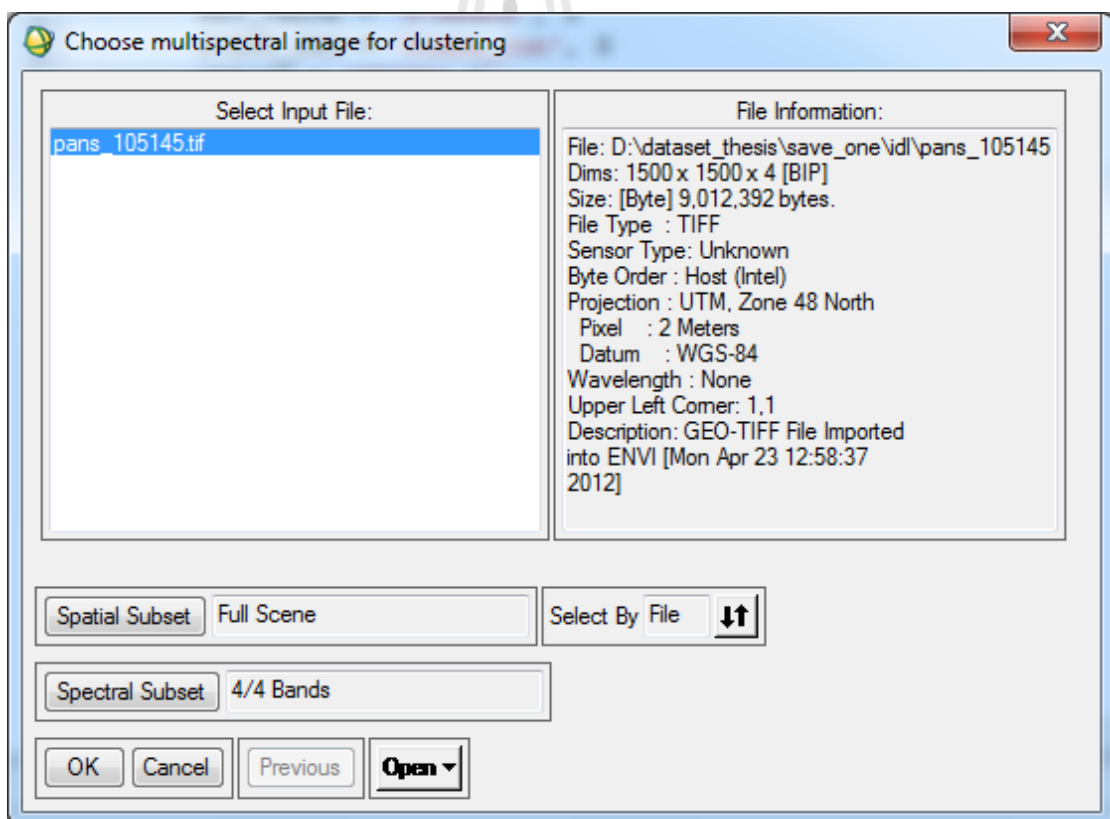


Figure 4.31 The extension interface of FCM and SA processes.

The experimental image clustering using the FCM and SA was tested on the pan-sharpened images of the trial no.3 to examine the effectiveness of the algorithm. The result was compared to the results using ISODATA and K-means techniques. The images were classified to be 7 classes for all techniques. The number of classes was obtained by providing 5 to 10 classes to ISODATA technique, optimum 7 classes was returned from the ISODATA process. After processes, classes 1-7 could be identified as: (1) water body, (2) dense vegetation, (3) horticultural area, (4) shrub paddy field, (5) built-up area, (6) miscellaneous land, and (7) grass field/bare soil.

In this study, the comparison of classification resulted from ISODATA, K-means, and FCM and SA was carried out and assessed mainly based on:

- the descriptive statistics (histograms, mean, and standard derivation).
- visual comparison of the clustering results.
- the accuracy assessment based on overall accuracy and the kappa statistics.

4.5.1 Comparison based on descriptive statistics

The clustering results by using ISODATA, K-means, and FCM and SA techniques were shown in Figure 4.32.

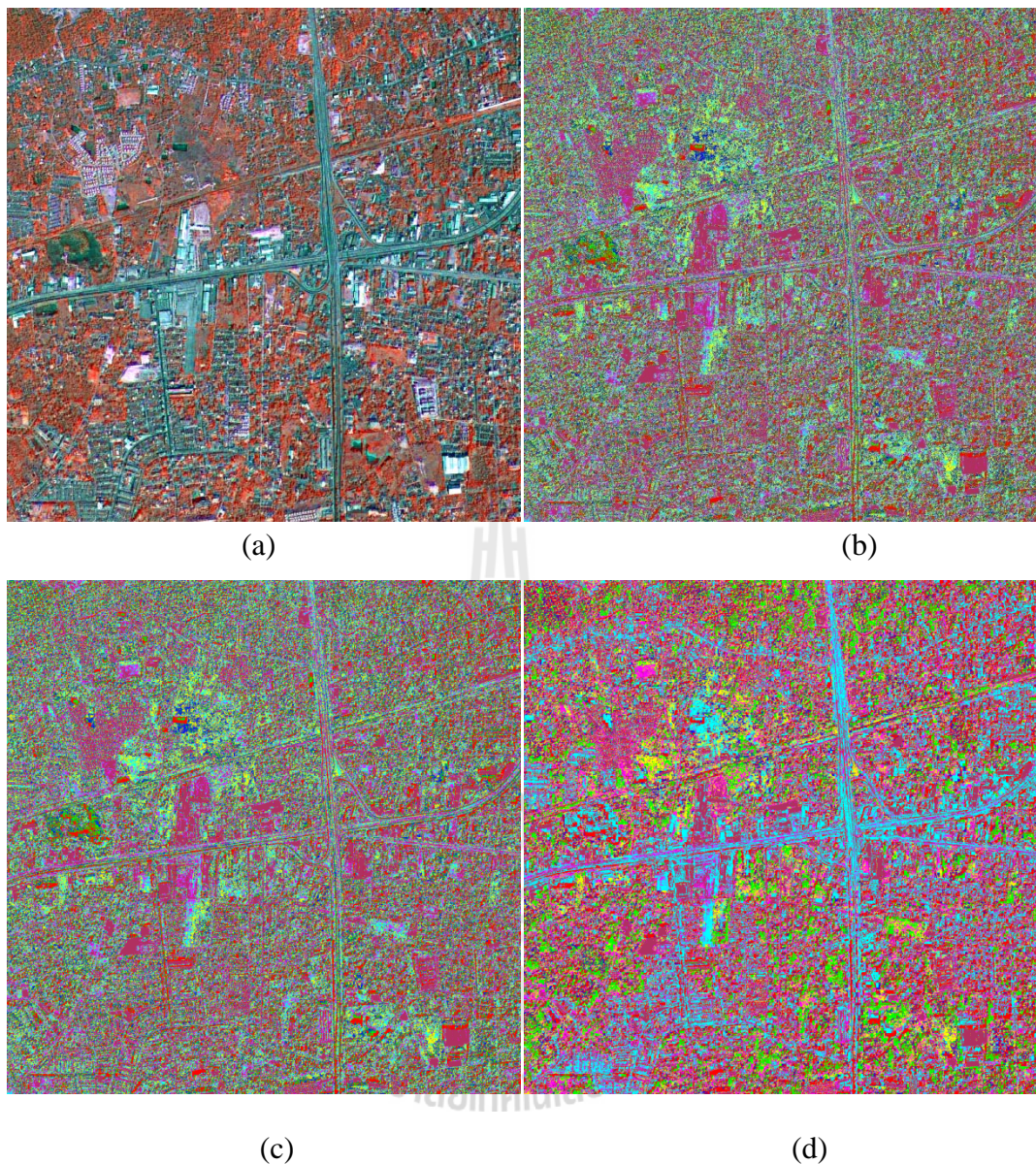


Figure 4.32 (a) The color composite of the pan-sharpened images from the trial no.3, the results of clustering using (b) ISODATA, (c) K-means, and (d) FCM and SA.

The histograms of 7 classes resulted from each technique were displayed band by band in Figures 4.33-4.36. It is obvious that band NIR of FCM and SA technique shows the isolated clusters of built-up area and water, which represent built-up area and water quite clear while other bands of techniques show unclear separation among classes.

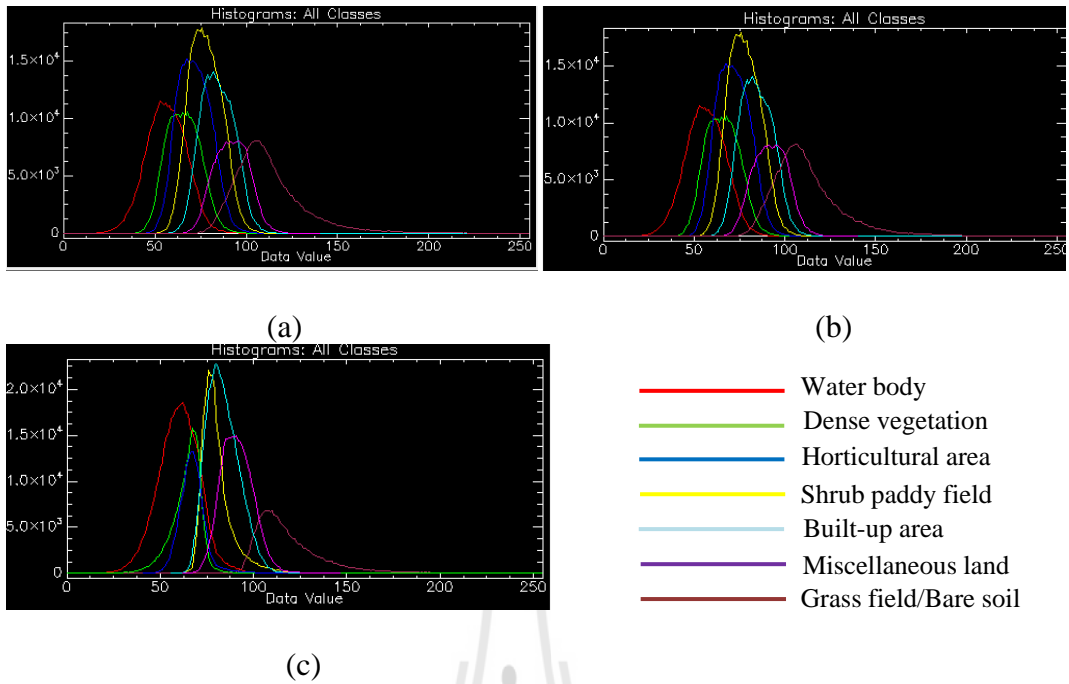


Figure 4.33 The comparison of the descriptive statistics measurement on clustering results on the Red band using (a) ISODATA, (b) K-means, and (c) FCM and SA.

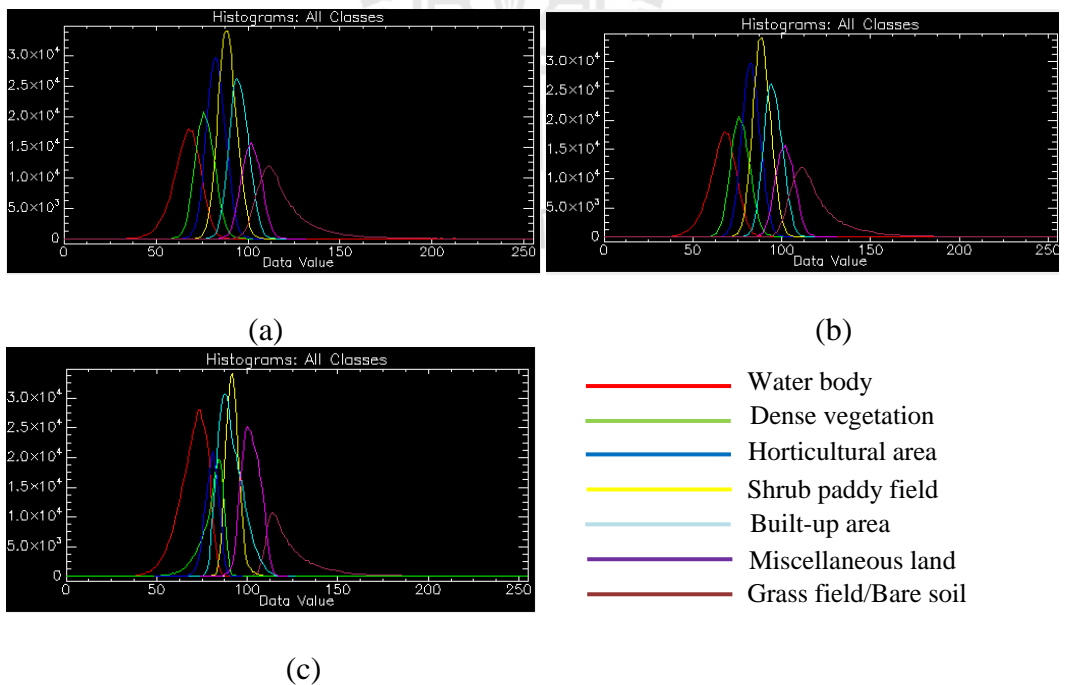


Figure 4.34 The comparison of the descriptive statistics measurement on clustering results on the Green band using (a) ISODATA, (b) K-means, and (c) FCM and SA.

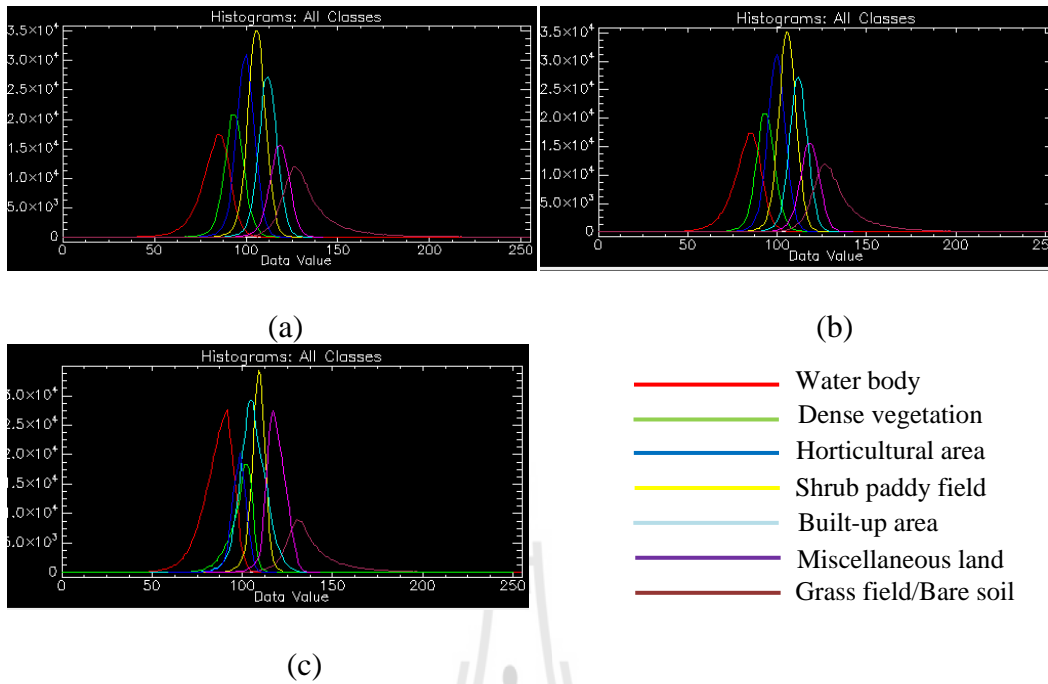


Figure 4.35 The comparison of the descriptive statistics measurement on clustering results on the BLUE band using (a) ISODATA, (b) K-means, and (c) FCM and SA.

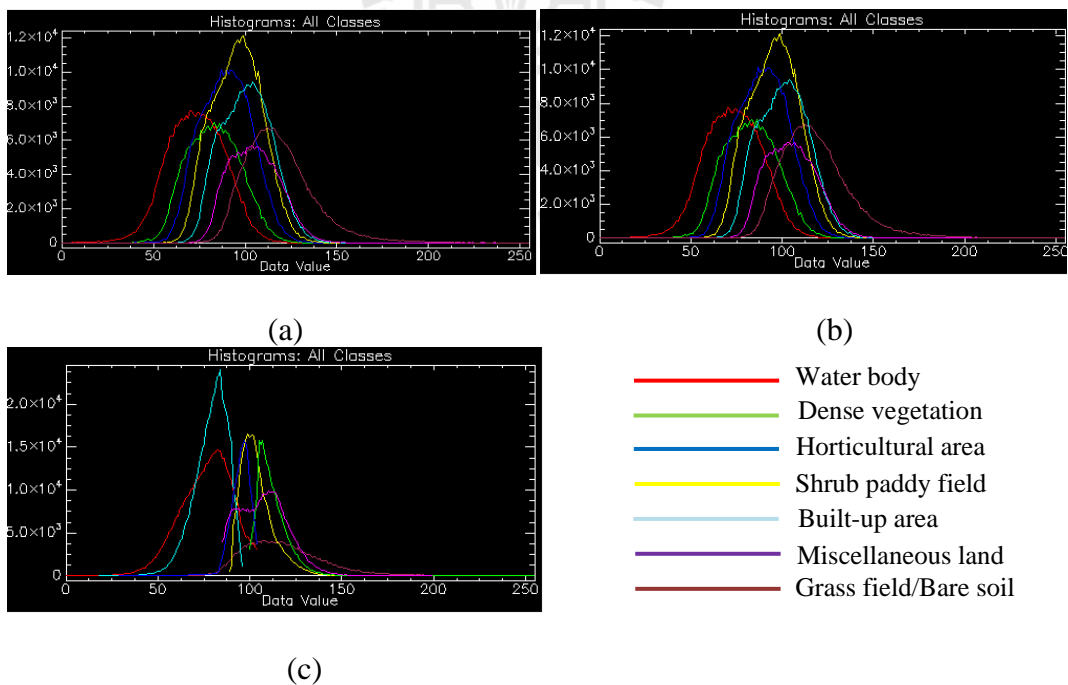


Figure 4.36 The comparison of the descriptive statistics measurement on clustering results on the NIR band using (a) ISODATA, (b) K-means, and (c) FCM and SA.

Descriptive statistics i.e. minimum, maximum, mean, and standard derivations of clusters from each technique were tabulated band by band in Tables 4.8-4.11. From the Red band (Table 4.8), class 6 of all techniques and class 3-5 of FCM-SA show higher ability for clustering due to their narrow min-max range.

Table 4.8 The comparison of the descriptive statistics measurement on clustering results on the Red band using ISODATA, K-means, and FCM and SA.

Class	Min-Max			Mean			standard derivation		
	ISODATA	K-means	FCM-SA	ISODATA	K-means	FCM-SA	ISODATA	K-means	FCM-SA
1	0-242	0-242	0-255	56.24	56.24	60.03	10.90	10.90	11.13
2	2-251	2-251	0-255	65.69	65.69	64.25	9.24	9.24	9.04
3	24-251	24-251	41-118	71.60	71.60	67.23	9.02	9.02	6.96
4	21-251	21-251	58-143	77.71	77.71	80.17	8.82	8.82	8.10
5	43-255	43-255	56-136	84.37	84.37	83.55	8.98	8.98	8.63
6	37-140	37-140	62-146	92.05	92.05	91.20	9.29	9.29	8.65
7	0-255	0-255	0-255	112.85	112.85	119.38	20.52	20.52	19.74

Note: 1 = Water body, 2 = Dense vegetation, 3 = Horticultural area, 4 = Shrub paddy field, 5 = Built-up area, 6 = Miscellaneous land, and 7= Grass field/Bare soil

From the Green band (Table 4.9), classes 3-6 of all techniques and class 2 of ISODATA and K-means show higher ability for clustering due to their narrow min-max range. However, classes 3-6 of FCM and SA show narrower ranges.

Table 4.9 The comparison of the descriptive statistics measurement on clustering results on the Green band using ISODATA, K-means, and FCM and SA.

Class	Min-Max			Mean			standard derivation		
	ISODATA	K-means	FCM-SA	ISODATA	K-means	FCM-SA	ISODATA	K-means	FCM-SA
1	1-254	1-254	0-254	66.51	66.51	69.89	7.90	7.90	7.95
2	0-105	0-105	0-255	76.74	76.74	80.37	5.39	5.39	6.96
3	1-111	1-111	49-97	82.77	82.77	80.35	5.18	5.18	3.84
4	10-120	10-120	76-116	88.89	88.89	91.91	5.08	5.08	3.69
5	15-126	15-126	68-126	95.23	95.23	91.00	5.20	5.20	6.83
6	50-131	50-131	74-122	101.92	101.92	102.14	5.33	5.33	4.7
7	0-255	0-255	96-255	119.76	119.76	125.32	17.79	17.79	17.84

Note: 1 = Water body, 2 = Dense vegetation, 3 = Horticultural area, 4 = Shrub paddy field, 5 = Built-up area, 6 = Miscellaneous land, and 7= Grass field/Bare soil

From the Blue band (Table 4.10), class 3-6 of all techniques and class 2 of ISODATA and K-means show higher ability for clustering due to their narrow min-max range. However, classes 3-6 of FCM and SA show narrower ranges.

Table 4.10 The comparison of the descriptive statistics measurement on clustering results on the Blue band using ISODATA, K-means, and FCM and SA.

Class	Min-Max			Mean			standard derivation		
	ISODATA	K-means	FCM-SA	ISODATA	K-means	FCM-SA	ISODATA	K-means	FCM-SA
1	0-254	0-254	0-254	82.39	82.39	85.97	9.03	9.03	9.07
2	2-118	2-118	0-250	93.38	93.38	98.83	5.81	5.81	7.16
3	6-124	6-124	59-119	99.49	99.49	98.03	5.38	5.38	4.47
4	10-130	10-130	67-137	105.63	105.63	108.83	5.19	5.19	4.07
5	29-136	29-136	49-139	111.77	111.77	105.97	5.33	5.33	7.52
6	44-142	44-142	80-143	117.95	117.95	118.80	5.78	5.78	5.33
7	0-255	0-255	0-255	133.72	133.72	138.38	17.33	17.33	19.91

Note: 1 = Water body, 2 = Dense vegetation, 3 = Horticultural area, 4 = Shrub paddy field, 5 = Built-up area, 6 = Miscellaneous land, and 7= Grass field/Bare soil

From the NIR band (Table 4.11), only classes 3-6 of FCM and SA show higher ability for clustering due to their narrow min-max range. Among these classes, class 5 shows the narrowest range. That means the FCM and SA technique can classify the built-up area quite clear.

Table 4.11 The comparison of the descriptive statistics measurement on clustering results on the NIR band using ISODATA, K-means, and FCM and SA.

Cla SS	Min-Max			Mean			standard derivation		
	ISODATA	K-means	FCM-SA	ISODATA	K-means	FCM-SA	ISODATA	K-means	FCM-SA
1	0-247	0-247	0-104	73.08	73.08	76.47	15.76	15.76	14.20
2	13-253	13-253	100-255	82.91	82.91	112.13	14.34	14.34	8.66
3	28-255	28-255	29-104	89.66	89.66	94.89	13.77	13.77	5.07
4	46-255	46-255	89-184	95.67	95.67	103.87	13.50	13.50	8.93
5	52-254	52-254	18-96	100.84	100.84	79.03	13.55	13.55	9.09
6	56-255	56-255	85-199	105.03	105.03	107.54	13.52	13.52	13.09
7	0-255	0-255	0-255	118.87	118.87	118.57	19.72	19.72	22.33

Note: 1 = Water body, 2 = Dense vegetation, 3 = Horticultural area, 4 = Shrub paddy field, 5 = Built-up area, 6 = Miscellaneous land, and 7= Grass field/Bare soil

4.5.2 Visual comparison of clustering results

The comparison reveals that the image classified using the FCM and SA can provide higher crispy and distinct clusters than other 2 techniques. This statement is strongly confirmed when considering the results of those techniques in Figures 4.37-4.39 which displays the zoom-in results of clustering. Again, it is obviously observable from those Figures that the images classified using the FCM and SA provide higher crispy and distinct clusters than other 2 techniques, particularly for the clusters of road network, urban, and vegetation cover.

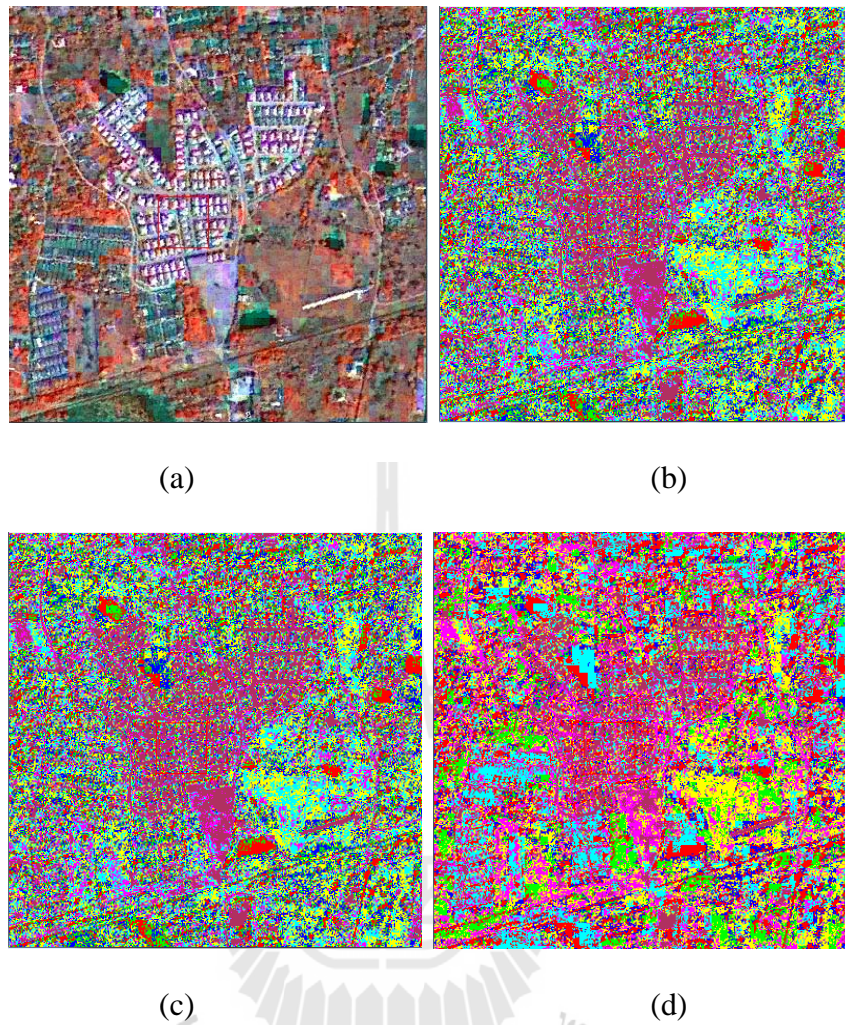


Figure 4.37 The zoom-in images of (a) the color composite of the pan-sharpened images, the results of clustering using (b) ISODATA, (c) K-means, and (d) FCM and SA.

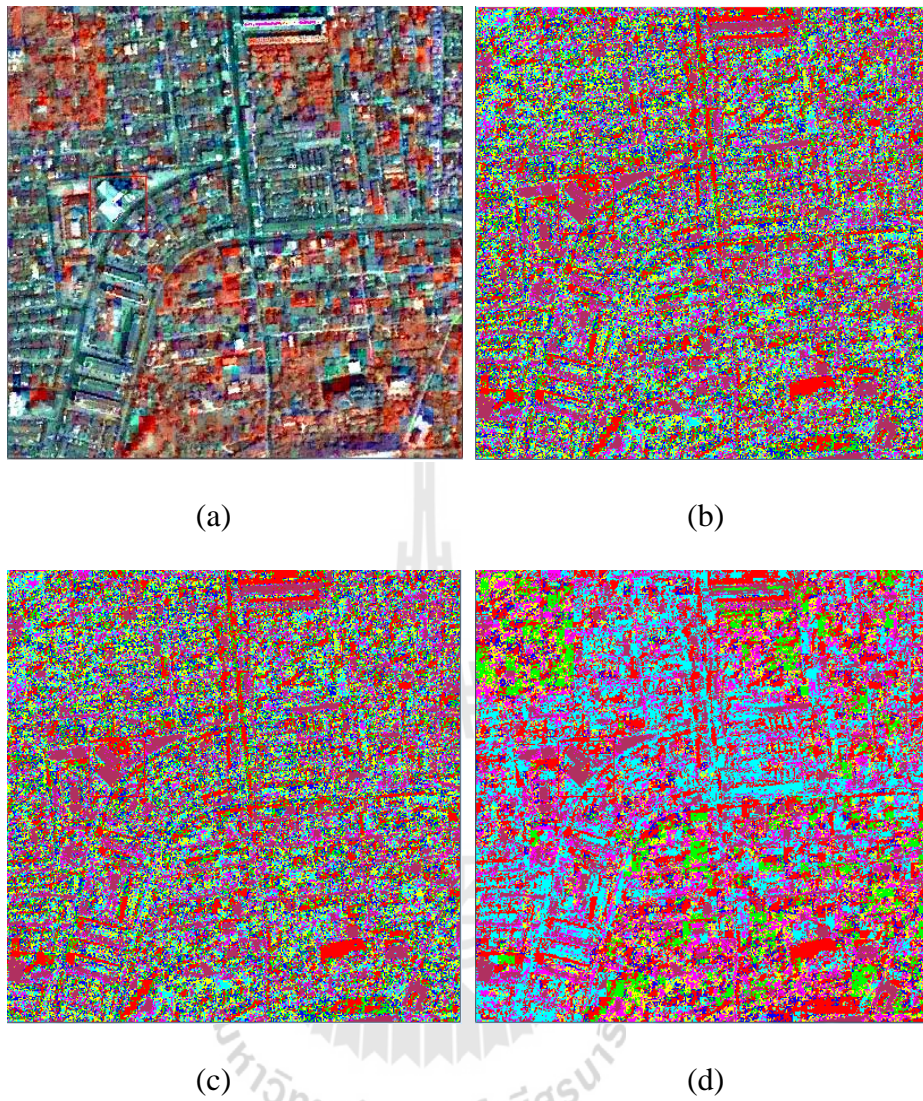


Figure 4.38 The zoom-in images of (a) the color composite of the pan-sharpened images, the results of clustering using (b) ISODATA, (c) K-means, and (d) FCM and SA.

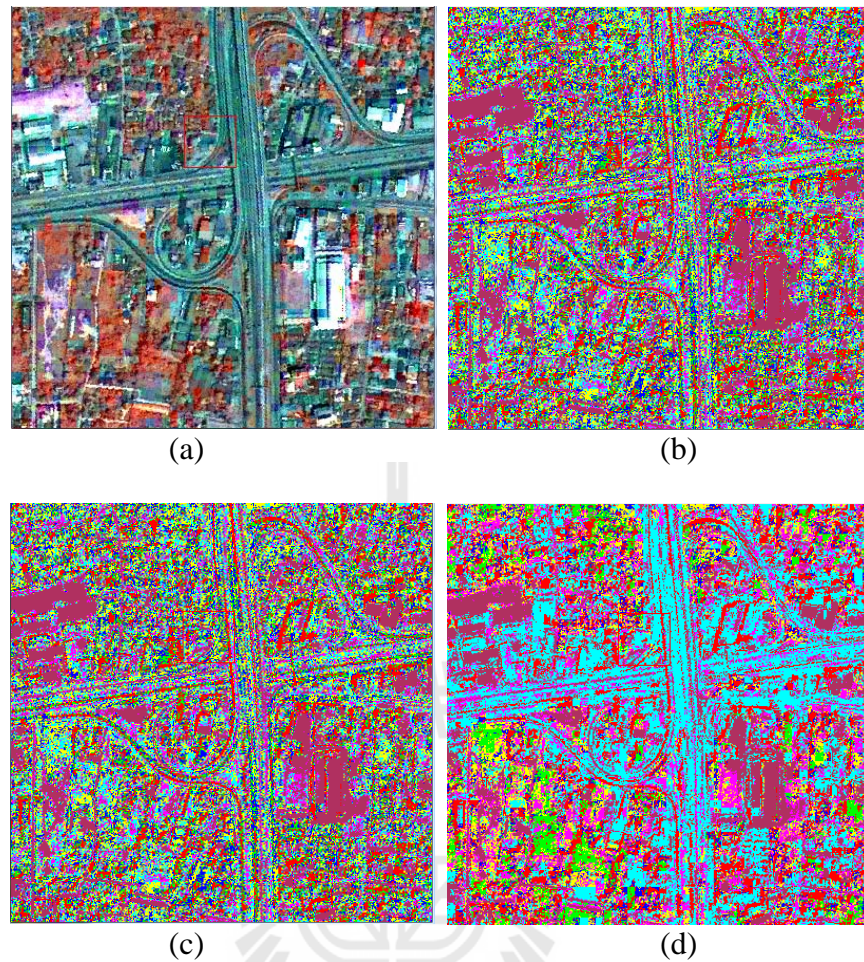


Figure 4.39 The zoom-in images of (a) the color composite of the pan-sharpened images, the results of clustering using (b) ISODATA, (c) K-means, and (d) FCM and SA.

4.5.3 Comparison of the clustering results with the accuracy assessment

Accuracy of images classified by the ISODATA, K-means, and FCM and SA techniques was assessed using the error matrix which was relied on the overall accuracy and the kappa statistics shown in the Tables 4.12 to 4.14. According based on binomial probability theory with desired level of confident 85 percent. The matrixes were performed on 203 samples. The reference data types using visual identified from the pan-sharpened images.

Table 4.12 Error matrixes and accuracy assessment of the result of clustering image using ISODATA technique.

Classified Data	Reference Data								User's Accuracy (%)
	W	DV	H	SP	B	M	GB	Total	
W	5	5	2	8	18	1	1	45	11.11
DV		18	1	2	1			21	85.71
H	2	1	4	11	1			17	23.52
SP		5	3	13	7	5	1	27	48.14
B				1	38	1		44	86.36
M		1		3	7	18	4	31	58.06
GB				1	7	2	5	18	27.78
Total	7	30	10	39	79	27	11	203	
Producer's Accuracy (%)	71.42	60	40	33	48.1	66.67	45.45		
Overall Accuracy (%)	= 49.75 %								
Kappa Coefficient	= 0.40 %								

Note: W = Water body, DV = Dense vegetation, H = Horticultural area, SP = Shrub paddy field, B = Built-up area, M = Miscellaneous land, and GB= Grass field/Bare soil

Table 4.13 Error matrixes and accuracy assessment of the result of clustering image using K-means technique.

Classified Data	Reference Data								User's Accuracy (%)
	W	DV	H	SP	B	M	GB	Total	
W	5	5	2	8	18	1	1	45	11.11
DV		18	1	2	1			21	85.71
H	2	1	4	11	1			17	23.52
SP		5	3	13	7	5	1	27	48.14
B				1	38	1		44	86.36
M		1		3	7	18	4	31	58.06
GB				1	7	2	5	18	27.78
Total	7	30	10	39	79	27	11	203	
Producer's Accuracy (%)	71.42	60	40	33	48.1	66.67	45.45		
Overall Accuracy (%)	= 49.75 %								
Kappa Coefficient	= 0.40 %								

Note: 1 = Water body, 2 = Dense vegetation, 3 = Horticultural area, 4 = Shrub paddy field, 5 = Built-up area, 6 = Miscellaneous land, and 7= Grass field/Bare soil

Table 4.14 Error matrixes and accuracy assessment of the result of clustering image using FCM and SA technique.

Classified Data	Reference Data								User's Accuracy (%)
	W	DV	H	SP	B	M	GB	Total	
W	7	3		13	20	1	1	45	15.55
DV		21						21	100.00
H			10	6			1	17	58.82
SP		5		18	4			27	66.67
B					44			44	100.00
M		1		1	3	26		31	83.87
GB				1	8		9	18	50
Total	7	30	10	39	79	27	11	203	
Producer's Accuracy (%)	100.00	70.00	100.00	46.15	55.69	96.29	81.81		
Overall Accuracy (%)	= 66.50 %								
Kappa Coefficient	= 0.60 %								

Note: W = Water body, DV = Dense vegetation, H = Horticultural area, SP = Shrub paddy field, B = Built-up area, M = Miscellaneous land, and GB= Grass field/Bare soil.

The overall accuracy, kappa statistics, and producer's and user's accuracies of error matrixes from each technique can be summarized in Tables 4.15 and 4.16. From these Tables, it reveals that FCM and SA technique shows the highest overall accuracy, kappa statistics, and producer's and user's accuracies.

Table 4.15 Summarized overall accuracy and kappa statistics of clustering image using ISODATA, K-means, and FCM and SA techniques.

Clustering technique	Overall accuracy	Kappa statistics
ISODATA	49.75%	0.40
K-means	49.75%	0.40%
FCM and SA	66.50%	0.60%

Table 4.16 Summarized producer's and user's accuracies of clustering image using ISODATA, K-means, and FCM and SA techniques.

Classified Data	Producer's accuracy (%)			User's accuracy (%)		
	ISODATA	K-means	FCM and SA	ISODATA	K-means	FCM and SA
w	71.42	71.42	100.00	11.11	11.11	15.55
DV	60.00	60.00	70.00	85.71	85.71	100.00
H	40.00	40.00	100.00	23.52	23.52	58.82
SP	33.00	33.00	46.15	48.14	48.14	66.67
B	48.10	48.10	55.69	86.36	86.36	100.00
M	66.67	66.67	96.29	58.06	58.06	83.87
GB	45.45	45.45	81.81	27.78	27.78	50.00

Note: W = Water body, DV = Dense vegetation, H = Horticultural area, SP = Shrub paddy field, B = Built-up area, M = Miscellaneous land, and GB= Grass field/Bare soil

In conclusion, based on histograms and descriptive statistics, almost all of classes from each technique show overlapping ranges of DN values but built-up area and water from FCM and SA technique show quite clear isolation. Considering the clustering ability, more classes from FCM and SA technique depict higher potential being clustered evidenced by their narrower min-max ranges.

By visual comparison the images classified using the FCM and SA provided higher crispy and distinct clusters than other 2 techniques, particularly for the clusters of road network, urban, and vegetation cover.

By accuracy assessment using error matrixes, FCM and SA is the best technique compared to others. It provides the highest overall accuracy, kappa statistics, and producer's and user's accuracies.

4.6 Road extraction

To understand the process of the road extraction from THEOS images, the pre-processing of THEOS images was introduced. First, pan-sharpened images were generated through improving FIHS technique using the Matlab software to obtain the proper weighting parameters of Red and NIR bands. After the readjustment and evaluation processes of parameters a and b , the candidate road network and non-road features are further clustered in the next step.

Second, the FCM and SA was used to cluster of the candidate road network and non-road features. The best pan-sharpened images from the trials no.2 and no.3 as shown in Figure 4.40 were classified using FCM and SA to be 15 clusters.

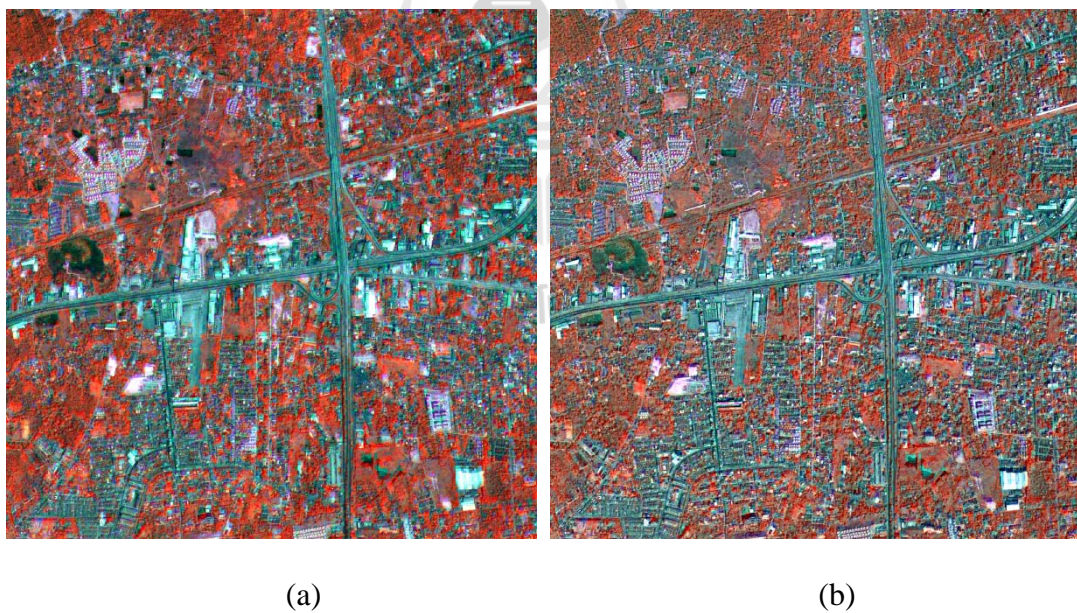
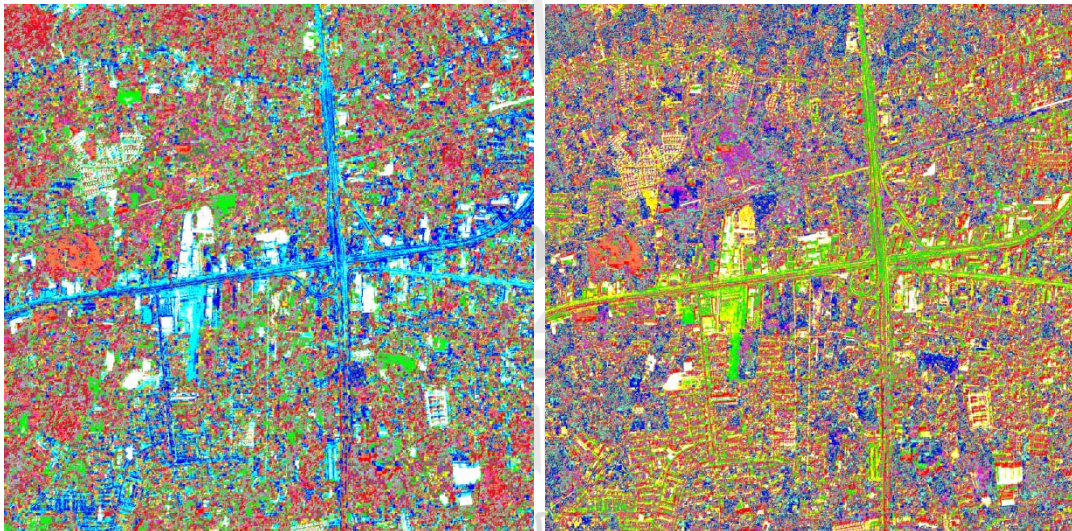


Figure 4.40 The color composite of pan-sharpened images from (a) the trial no.2 and (b) the trial no.3.

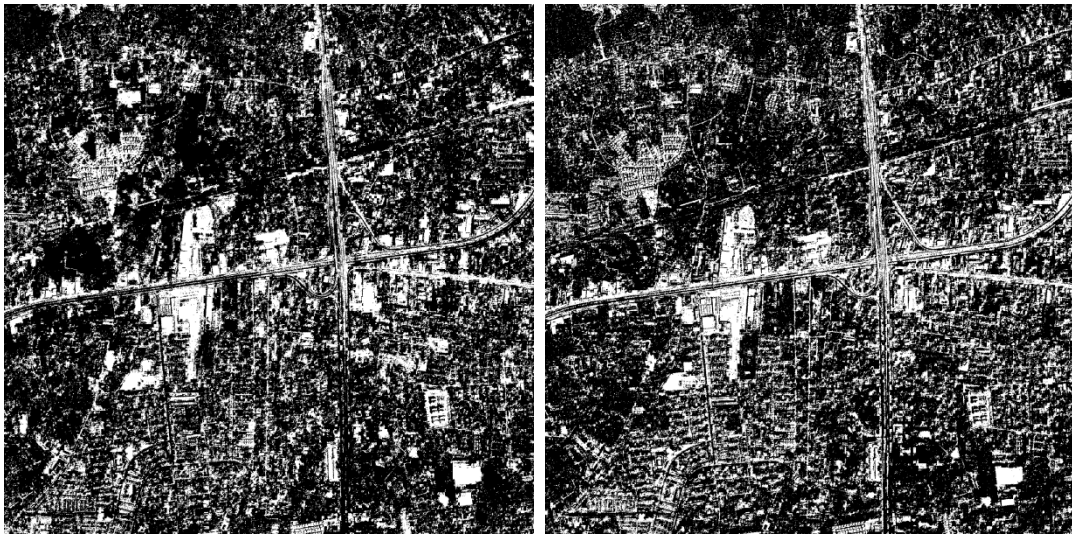
The results of classification from the trial no.2 and no.3 were shown in Figure 4.41. Then, all the possible road clusters and non-road features were manually selected and converted to be binary images shown in Figure 4.42. The black color (0) was used to represent the non-road feature while the white (1) was for the candidate road network. However, a lot of misclassification was noted among the road, building, and bare land. This misclassification would be reduced in further steps using mathematical top-hat operation and edge-aid segmentation.



(a)

(b)

Figure 4.41 The results of 15 clusters classified using FCM and SA operated on pan-sharpened images from (a) the trial no.2 and (b) the trial no.3.



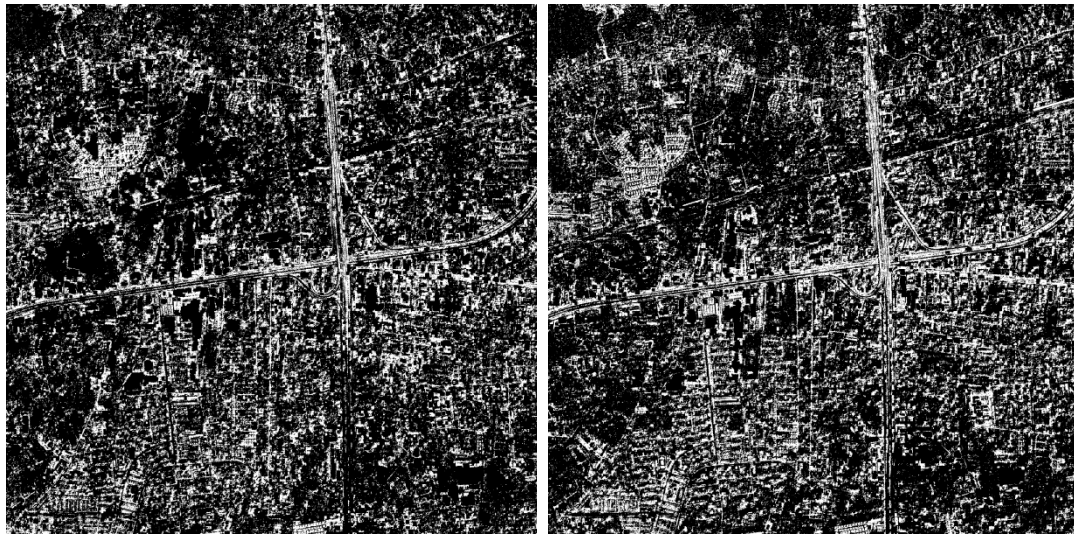
(a)

(b)

Figure 4.42 The binary images of candidate road network (white) and non-road features (black) from (a) the trial no.2 (b) the trial no.3.

4.6.1 Mathematical morphology operation for candidate road network

The morphological operation algorithm was applied to remove some of buildings, water, and bare lands, as shown in Figure 4.42. The morphological top-hat operation with 8 by 8 structure elements was used for filtering out the large white regions which should not be the candidate road network. For filtering the small white region, the morphological top-hat operation with a 3 by 3 structure elements was employed. The processes were operated on binary images of the trial no.2 and no.3 and the results were shown in Figure 4.43.



(a)

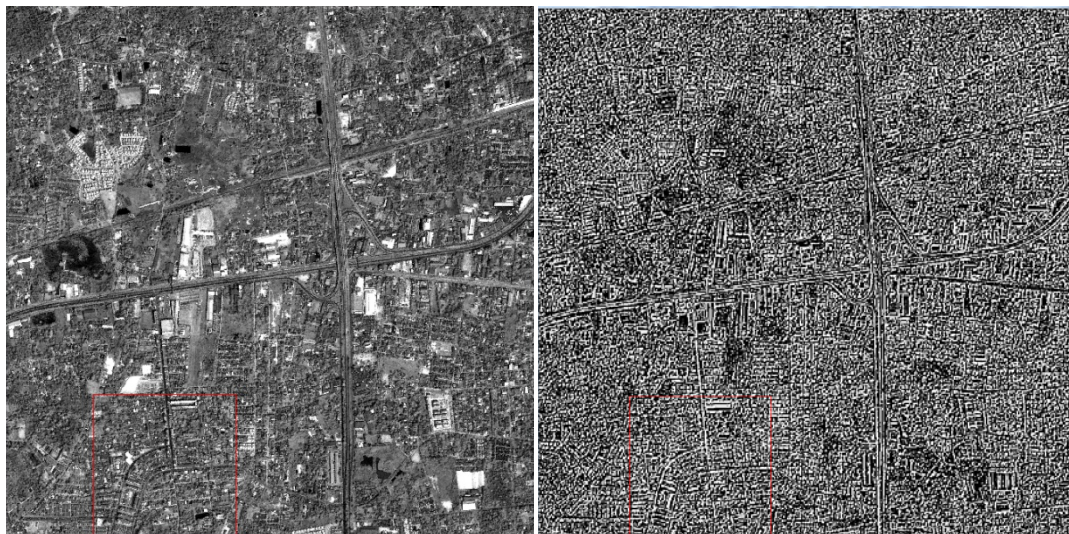
(b)

Figure 4.43 The result of morphology top-hat operation for binary images from (a) the trial no.2 and (b) the trial no.3.

The morphology top-hat operation was preserved the major roads. However, since many non-road objects has similar as roads, the error of misclassifying non-road objects as roads was also large. Many small object and house roofs were wrongly included in the road class, and other objects on a road can not to remove by morphology top-hat operation.

4.6.2 Edge-aid segmentation

To be able to perform more accurate road extraction in this research, the edge DoG for detecting the road edge in the panchromatic image was used, as shown in Figure 4.44.



(a)

(b)

Figure 4.44 The panchromatic image of the study area (a) and the edge image using edge DoG (b). The edge was displayed in white.

The results of binary edge DoG from the panchromatic image with black pixel for the road and white pixel for non-road. The binary edge DoG was denoted as B in the Eq. (3.7). Figure 4.45 shows the zoom-in images resulted from the binary edge DoG.



Figure 4.45 The zoom-in images resulted from edge DoG detection.

To extract the candidate road network from the binary images, the edge-aid segmentation was used to perform on the images obtained from the morphological top-hat filtering and edge DoG processes. The processes are as the following:

- Read the binary images from the morphology top-hat operation (A) and edge DoG detection (B).
- On the basis of pixel by pixel comparison of A and B under the conditions:
 - If A was candidate road (white pixel) and B was not road (black pixel), then a pixel was the road.
 - Else a pixel was non-road.

Then, the processed of the morphology top-hat operation and edge-aid segmentation should be removed the non-road and the other object from the classified road image. The results of the morphology top-hat operation and edge-aid segmentation were shown in Figure 4.46. In addition, the comparison of image quality based on the considered on the extracted candidate road network of images from the trials no.2 and no.3 were compared in Figure 4.46. From visual examination, the result from the trial no.3 shows more candidate road with better connectivity than from the trial no.2.



(a) (b)

Figure 4.46 The candidate road network (in white) resulted from morphology Top-Hat operation and edge-aid segmentation of images from (a) the trial no.2 and (b) the trial no.3.

4.6.3 Automated extraction of road centerline

The candidate road network resulted from morphology top-hat operation and edge-aid segmentation of images from (a) the trial no.2 and (b) the trial no.3 as shown in Figure 4.46 are input to the process of automated road centerline extraction. The thinning operation of the mathematical morphology was used as the extraction process. The process uses 3x3 with 8 structure elements as the following:

Structure1 = [0, 0, 0]
 [0, 1, 0]
 [1, 1, 1]
 Structure2 = [0, 0, 0]
 [1, 1, 0]
 [1, 1, 0]
 Structure3 = [1, 0, 0]
 [1, 1, 0]
 [1, 0, 0]
 Structure4 = [1, 1, 0]
 [1, 1, 0]
 [0, 0, 0]

Structure5 = [1, 1, 1]
 [0, 1, 0]
 [0, 0, 0]
 Structure6 = [0, 1, 1]
 [0, 1, 1]
 [0, 0, 0]
 Structure7 = [0, 0, 1]
 [0, 1, 1]
 [0, 0, 1]
 Structure8 = [0, 0, 0]
 [0, 1, 1]
 [0, 1, 1]

The results of the thinning operation were shown in Figure 4.47.

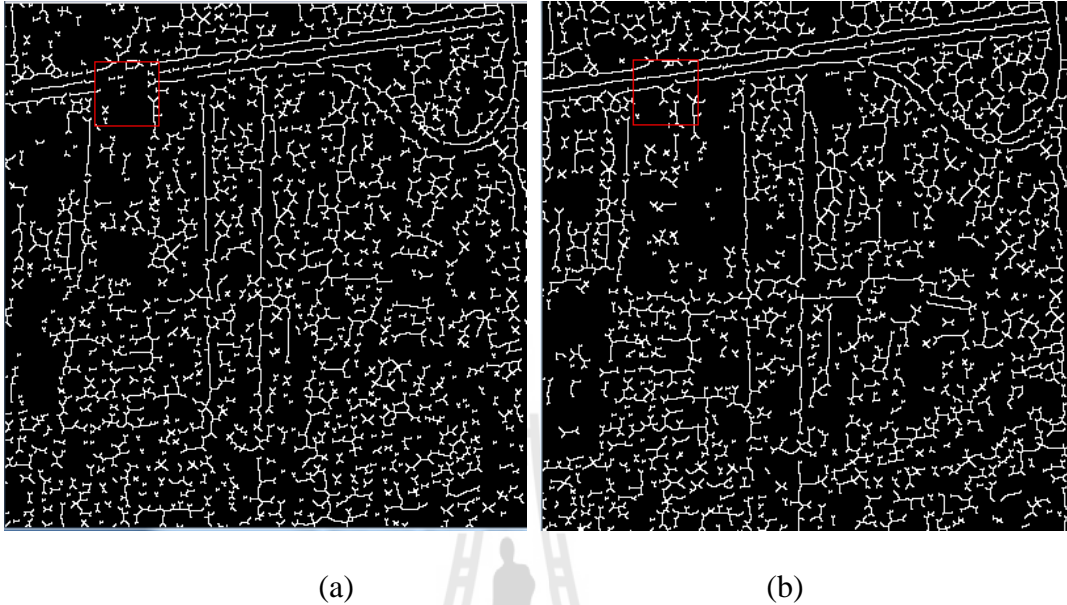


Figure 4.47 The extraction results of centerline road network using the morphological thinning operation on images (a) from the trial no.2 and (b) the trial no.3.

The road center line resulted from images of both trials were overlaid on the panchromatic image as shown in Figures 4.48 and 4.49. By visual examination, both results cannot be clearly detected which of them can express better road centerline in terms of actual being road network and its connectivity. Therefore, completeness and correctness using statistics of the length matched extraction and reference data were further applied to accuracy assessment.

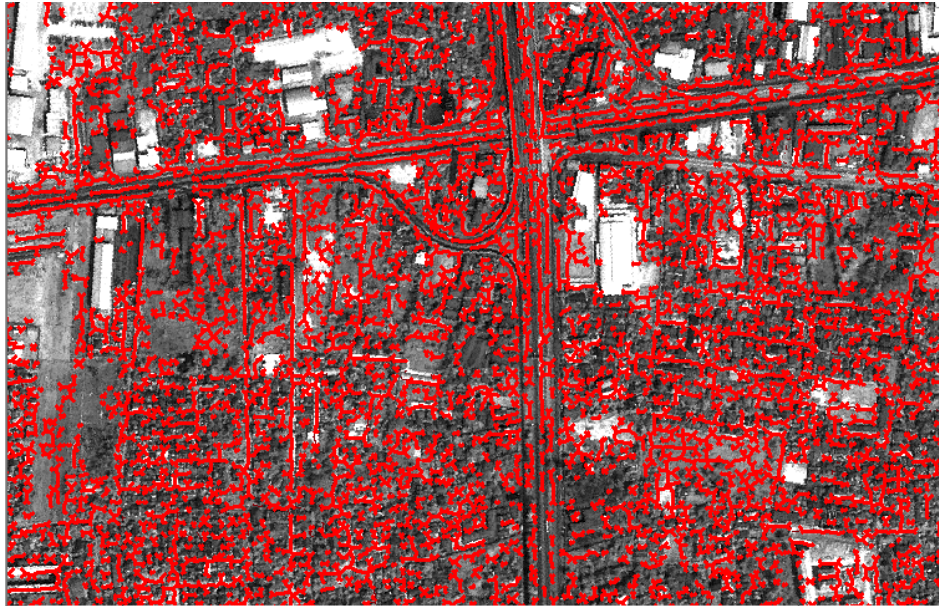


Figure 4.48 The overlay of road centerline network from the trial no.2 on the panchromatic image.

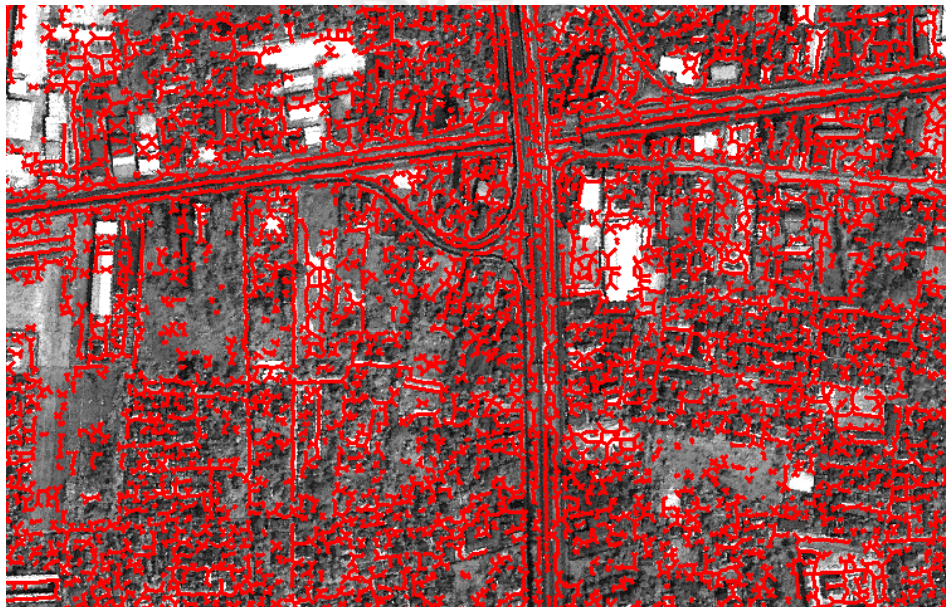


Figure 4.49 The overlay of road centerline network from the trial no.3 on the panchromatic image.

4.6.4 Accuracy assessment

The accuracy assessment was to measure the performance of the proposed road extraction algorithm. The length of extracted road centerline which was matched to the reference data were used to compute the completeness, correctness, and quality of the extraction as discussed in section 3.2.4. The 5-meter buffering was used to match the extracted data and reference network in terms of completeness and correctness. The reference data of road centerline extraction in the area correspond to the images shown in Figure 4.50. Table 4.17 shows the result of the accuracy assessment of the road centerline extraction which is performed on the testing images of both trials and the reference data (shown in Figures 4.51 and 4.52).



Figure 4.50 The reference data of road centerline network.



Figure 4.51 The result of the accuracy assessment of the road centerline extraction which is performed on the testing images of trial no.2 and the reference data.



Figure 4.52 The result of the accuracy assessment of the road centerline extraction which is performed on the testing images of trial no.3 and the reference data.

Table 4.17 The comparison of accuracy assessment of the road centerline extraction between the trials no.2 and no.3.

Accuracy assessment	Trial no.2		Trial no.3	
	Main highway	Local road	Main highway	Local road
Completeness	0.62	0.56	0.72	0.61
Correctness	0.69	0.19	0.70	0.20
Quality	0.52	0.17	0.56	0.19

From Table 4.17, the results of accuracy assessment are listed in terms of the quality measurement based on the completeness, the correctness, and the quality of the extracted centerline of the main highway and the local road. The assessment reported that the completeness, the correctness, and the quality of the extracted centerline of both types of road from the trial no.3 are better than the ones from the trial no.2.

For the trial no.3, the completeness for main highway and the local road is 0.72 and 0.61, respectively. It means that the length of matched reference network to the extracted one of main highway is 72% of the total length of the reference network while of the local road is 61%.

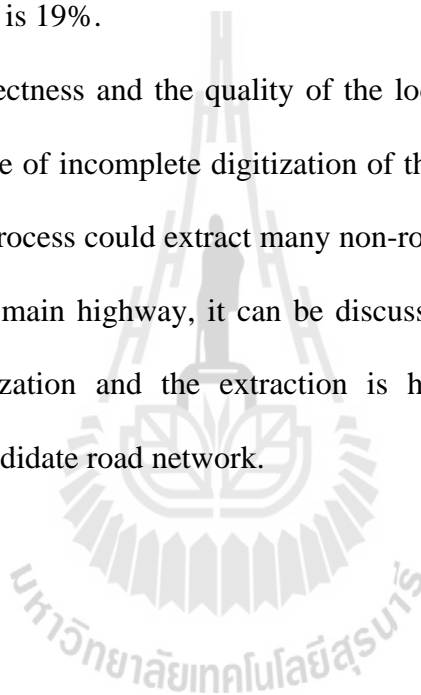
The mismatching could be due to under-extraction of the process together with the quality of the candidate road network.

Considering the correctness of the trial no.3 which is better than the one of the trial no.2, the correctness for main highway and the local road is 0.70 and 0.20, respectively. It means that the length of matched or successful extraction network to

the reference one of main highway is 70% of the total length of the extraction network while of the local road is 20%.

Considering the quality of the trial no.3 which is better than the one of the trial no.2, the quality for main highway and the local road is 0.56 and 0.19, respectively. It means that the length of matched or successful extraction network to the reference one of main highway is 56% of the total length of the extraction network while of the local road is 19%.

The correctness and the quality of the local road seem to be very low. This should be because of incomplete digitization of the reference data together with over-extraction. The process could extract many non-road features and claims them to be road network. For main highway, it can be discussed that the reference data are more complete digitization and the extraction is higher efficient due to better presentation of the candidate road network.



CHAPTER V

CONCLUSION AND RECOMMENDATIONS

5.1 Conclusion

The main objectives of this study are to propose the procedures for road extraction from the THEOS imagery and to develop extension modules to perform those methods. The procedures include image pan-sharpening process from multispectral images and panchromatic image, the clustering techniques applied to pan-sharpened images to generate clusters of candidate road network, the morphological operations and edge-aid segmentation applied to filtering and remove non-road objects. Finally, the morphological thinning is applied to road centerline extraction from the candidate road network. The results of those methods are concluded and few recommendations are given below for further research.

5.1.1 Pan-sharpening image

One of the objectives of this research was to improve the IHS pan-sharpening process for THEOS data in order to obtain the images with high spatial resolution and multi-spectral response. The trials were used to determine weighting parameters of certain bands to improve IHS transformation methods. There were three trials to perform. For trials no.1 and no.2, the Green and Blue bands were adjusted by multiplying with 0.75 and 0.25, respectively. No adjustment for these 2 bands in the Trail no.3. For all trials, Red and NIR bands are adjusted by multiplying with a and b ,

respectively. Using the highest average CC of original multispectral images and pan-sharpened images of each trial, $a = 0.05, 0.55, \text{ and } 1.05$ and $b = 0.95, 0.45, \text{ and } 1.45$ are applied to the trial no.1 to no.3, respectively. Pan-sharpened images resulted from each trial were examined by visual comparison of their color composite images and panchromatic image, comparing CCs of pan-sharpened and panchromatic images, clustering results comparison.

By visual comparison of color composite images from each trial, it reveals that the one from the trial no.3 is the best in terms of crispiness of feature appearance. Trial no.1 shows the highest color distortion.

By comparing CCs of pan-sharpened and panchromatic images, the trial no.3 shows the highest average CCs followed by the trial no.2. This conclusion was confirmed by comparing pan-sharpen images of Red, NIR bands and color composite image (R:G:B 4:2:1). All images of the trial no.3 were the best quality and their crispiness is very close to the panchromatic image.

By clustering comparison, the result from the trial no.3 shows that a smaller number of clusters can cover candidate road network and its connectivity was better than other trials.

This pan-sharpening process was operated using MATLAB.

5.1.2 Image clustering

In this study the FCM and SA is the newly proposed technique fit for THEOS image clustering. It provides the best result compared to the results using ISODATA and K-mean techniques. The results of image clustering from each

technique are examined by the descriptive statistics, visual comparison, and the accuracy assessment based on overall accuracy and the kappa statistics.

By the descriptive statistics, the FCM and SA technique shows obvious isolation separation of built-up area in the band NIR while all classes in each band of other technique are overlapped.

By visual comparison of the clustering results, the clusters resulted from FCM and SA technique is better than other 2 techniques in terms of being higher crispy and distinct.

By the accuracy assessment, the overall accuracy and kappa statistics using FCM and SA, were 66.50% and 0.60, respectively, which are higher than the ones from ISODATA and K-means techniques.

5.1.3 Road extraction

The extension module of automated road centerline extraction is developed to cover processes operating on pan-sharpened images. These processes include, in order, morphological Top-Hat operation, edge-aided segmentation, and morphological thinning operation. The module is applied for binary images of road candidate network resulted from the pan-sharpened images of the trials no.2 and no.3. The module can work very well as expected in the objective and the results from trials are discussed below.

The quality of extraction results from both trials is examined using completeness and correctness. The assessment reported that the completeness and the correctness of the extracted centerline of both types of road, main highway and local road, from the trial no.3 are better than the ones from the trial no.2.

For the trial no.3, the completeness for main highway and the local road is 0.72 and 0.61, respectively, while the correctness is 0.70 and 0.20, and the quality is 0.56 and 0.19, respectively. For the Trail no.2, the completeness for main highway and the local road is 0.62 and 0.56, respectively while the correctness is 0.69 and 0.19, and the quality is 0.52 and 0.17, respectively.

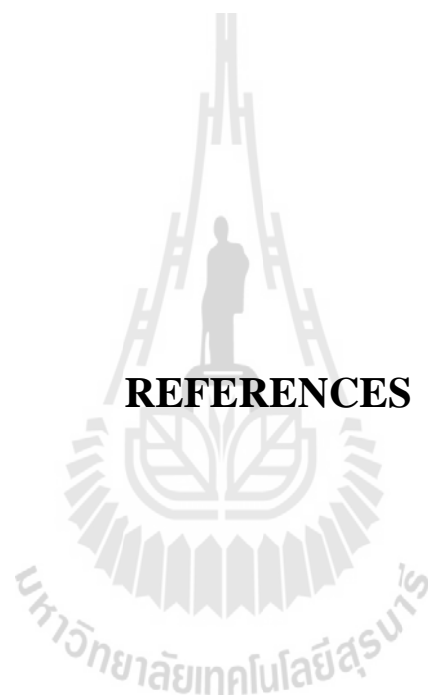
The completeness of the trial no.3 is considered good. The mismatching could be due to under-extraction of the process together with the quality of the candidate road network.

The correctness and the quality of the local road of the trial no.3 seem to be very low. This should be because of incomplete digitization of the reference data together with over-extraction. The process could extract many non-road features and claims them to be road network.

5.2 Recommendation

1. For pan-sharpening process, a number of pairs of varying weighting parameters (a and b) should be increased or other techniques such as wavelet transformation should be tried for experiments. The most proper or better parameters could be discovered. Apart from IHS transformation, other techniques should be tried and compared as well.

2. For road extraction, other mathematical and morphological operation(s) that can provide more complete candidate road network and increase its connectivity should be sought for. The method to connect more possible road line after thinning should be sought for as well.



REFERENCES

REFERENCES

- Ameri, F., Mobaraki, A.M., and Valadan Zoej, M.J. (2008). Semi automatic extraction of different-shaped road centerlines from MS and pan-sharped IKONOS images. **The International Archives of the Photogrammetry, Remote Sensing and Spatial Information Sciences**. 35(3b): 621-626.
- Bezdek, J.C. (1974). Cluster validity with fuzzy sets. **Journal of Cybernet**. 3(3): 58-72.
- Bezdek, J.C. (1981). **Pattern recognition with fuzzy objective function algorithm**. Plenum Press: New York.
- Bezdek, J.C., and Pal, S.K. (1992). **Fuzzy Models for Pattern Recognition**. IEEE Press: Piscataway, New York.
- Chavez, P.S., Berlin, G.L., and Sowers, L.B. (1984). Statistical method for selecting landsat MSS ratios. **Journal of Applied Photographic Engineering**. 8(1): 23-30.
- Choi, M., Kim, R.Y., Nam, M.Y., and Kim, H.O. (2005). Fusion of multispectral and panchromatic satellite images using the curvelet Transform. **IEEE Geoscience and Remote Sensing Letters**. 2: 136-140.
- Dal Poz, A.P., Gallis, R.A., and Silva, J.F.C. (2002). Semiautomatic road extraction by dynamic programming optimisation in the object space: single image case. **The International Archives of the Photogrammetry, Remote Sensing and Spatial Information Sciences**. 34(3): 215-220.
- Dunn, J.C. (1973). A fuzzy relative of the ISODATA process and its use in detecting compact well-separated clusters. **Journal of Cybernetics**. 3(3): 32-57.

- GISTDA. (2009). **THEOS user guide 2009** [Online]. Available: http://theos.gistda.or.th/download/THEOS_User_Guide_2009.pdf.
- Gonzalez-Audicana, M., Saleta, J.L., Catalan, R.G., and Garcia, R. (2004). Fusion of multi-spectral and panchromatic images using improve IHS and PCA merges based on wavelet decomposition. **IEEE transactions on Geoscience and Remote Sensing**. 42(6): 1291-1299.
- Grote, A., Butenuth, M., and Heipke, C. (2007). Road extraction in suburban areas based on normalized cuts. **The International Archives of the Photogrammetry, Remote Sensing and Spatial Information Sciences**. 36: 51-56.
- Gruen, A., and Li, H. (1997). Semi-automatic linear feature extraction by dynamic programming and LSB-snakes. **Photogrammetric Engineering and Remote Sensing**. 63(8): 985-995.
- Heipke, C., Mayer, H., and Wiedemann, C. (1996). Evaluation of automatic road extraction. **International achieves of Photogrammetry and remote sensing**. 323: 151-160.
- Hernandez, J., and Marcotegul, B. (2009). Filtering of artifact and pavement segmentation from mobile LIDAR data. **LaserScanning'09** [Online]. Available: <http://cmm.ensmp.fr/~hernandez/docs/LaserScanning2009.pdf>.
- Kirkpatrick, S., Gelatt, C.D. Jr., and Vecchi, M.P. (1983). Optimization by simulated annealing. **Science**. 220: 671-680.
- Kwon, S.H. (1998). Cluster validity index for fuzzy clustering. **IEEE Electronics Letter**. 34(22): 2176-2177.
- Li, J., Luo, J., Ming, D., and Shen, Z. (2005). **A new methods for merging IKONOS Panchromatic and Multispectral image data**. IEEE.

- Lizarazo, I., and Barros, J. (2008). Fuzzy image segmentation for urban land cover classification. **International Society for Photogrammetry and Remote Sensing** [Online]. Available: http://www.isprs.org/proceedings/XXXVIII/4-C1/Sessions/Session6/6669_Lizarazo_Proc.pdf.
- Ma, H., Zhao, Y., and Chen, Y. (2008). Road extraction from high resolution remote sensing image based on mathematical morphology. **Proc. SPIE**. 7147 [Online]. Available: 144.206.159.178/ft/CONF/16423743/16423767.pdf.
- Madhan, M., Dinesh, A., Ajay, S., Sathya, B., and Raju, S. (2005). Automatic road network extraction from high resolution multi-spectral satellite imagery based on fuzzy and mathematical morphology. **GIS Development March 2005** [Online]. Available: <http://www.gisdevelopment.net/technology/ip/mi05257pf.htm>.
- Marr, D., and Hildreth, E. (1980). Theory of Edge Detection. **Royal Society of London Proceedings Series**. 207: 187–217.
- Mena, J.B. (2003). State of the art on automatic road extraction for GIS update: A novel classification. **Pattern Recognition Letters**. 24(16): 3037-3057.
- Metropolis, N., Rosenbluth, A., Rosenbluth, M., Teller, A., and Teller, E. (1953). Equation of state calculations by fast computing machines. **The Journal of Chemical Physics**. 21(6):1087-1092.
- Mohammadzadeh, A., Tavakoli, A., and Valadan Zoej, M.J. (2004). Automatic linear feature extraction of IRANIAN road from high resolution multi-spectral satellite imagery. **The International Archives of the Photogrammetry, Remote Sensing and Spatial Information Sciences**. 35(3): 764-767.

- Mohammadzadeh, A., Tavakoli, A., and Valadan Zoej, M.J. (2006). Road extraction based on fuzzy logic and mathematical morphology from pan-sharpened IKONOS images. **The Photogrammetric Record**. 21(113): 44-60.
- Narasimhan, R. (2006). Computer vision. **Lecture note in computer vision** [Online]. Available: <http://www.cs.cmu.edu/afs/cs/academic/class/15385-s06/lectures/ppts/lec-7.ppt>.
- Park, S.R., and Kim, T. (2001). Semi-automatic road extraction algorithm from IKONOS images using template matching. **Proc 22nd Asian Conference on Remote Sensing** [Online]. Available: <http://www.a-a-r-s.org/acrs/proceeding/ACRS2001/Papers/VHR2-04.pdf>.
- Serra, J. (1982). **Image Analysis and Mathematical Morphology**. Academic Press: London.
- Shukla, S., ChandraKanth, R., and Ramachandran, R. (2002). Semi-automatic road extraction algorithm for high resolution images using path following approach. **Proc Indian conference on computer vision graphics and image processing** [Online]. Available: <http://www.ee.iitb.ac.in/~icvgip/PAPERS/311.pdf>.
- Song, M., and Civco, D. (2004). Road Extraction Using SVM and Image Segmentation. **Photogrammetric Engineering & Remote Sensing**. 70(12): 1365-1371.
- Teague, Z. (2001). IKONOS pan-sharpened products evaluation. **Proc.High Spatial Resolution Commercial Imagery Workshop** [Online]. Available: http://lscm.gsfc.nasa.gov/library/HSRCIW01/PanSharp_ProductsEval_Teague.pdf.
- Tu, T.M., Su, S.C., Shyu, H.C., and Huang P.S. (2001). A new look at IHS-like image fusion methods. **ELSEVIER in Information Fusion**. 2: 177-186.

- Tu, T.M., Huang, P.S., Hung, C.L., and Chang, C.P. (2004). A fast intensity-hue-saturation fusion technique with spectral adjustment for IKONOS imagery. **IEEE Geoscience and Remote Sensing Letters**. 1: 309-312.
- Veeraraghavan, V. (2004). **A Quantitative Analysis of Pan Sharpened Images**. Electrical Engineering , Mississippi State University. 80 pp.
- Wang, R., and Zhang, Y. (2003). Extraction of Urban Road Network Using QuickBird Pan-Sharpended Multispectral and Panchromatic Imagery by Performing Edge-aided Post-Classification. **ISPRS Joint Workshop on Spatial Temporal and Multi-Dimensional Data Modeling and Analysis** [Online]. Available: http://www.cim.mcgill.ca/~ruisheng/software/18-Wang_Extraction of Urban Road Edge-Aided Post Class.pdf.
- Wang, R., Hu, Y., and Zhang, X. (2005). Extraction of Road Networks Using Pan-Sharpended Multispectral and Panchromatic QuickBird Images. **Geomatica** [online]. <http://www.cim.mcgill.ca/~ruisheng/software/GeomaticaAccepted.pdf>.
- Wang, X., Zhao, H., Tang, Z., and Fu, G. (2009). Road extraction in remote sensing images based on PCNN and mathematical morphology. **Proc of SPIE** [Online]. Available: <http://144.206.159.178/ft/CONF/16436801/16436819.pdf>.
- Xie, X.L., and Beni, G. (1991). A validity measure for fuzzy clustering. **IEEE Pattern Analysis and Machine Intelligence**. 13: 841-847.
- Zeng, M., Li, J., and Peng Z. (2006). The design of Top-Hat morphological filter and application to infrared target detection. **ELSEVIER in infrared Physics & Technology**. 48(1): 67-76.
- Zhang, C., Murai, S., and Baltsavias, M. (1999). Road network detection by mathematical morphology. **Proc. Of ISPRS Workshop 3D Geospatial Data**

Production [Online]. Available: <http://e-collection.library.ethz.ch/eserv/eth:25218/eth-25218-01.pdf>.

Zhang, H., Xiao, Z., and Zhou, Q., (2008). Research on road extraction semi-automatically from high resolution remote sensing images. **The International Archives of the Photogrammetry, Remote Sensing and Spatial Information Sciences**. 37: 535-538.

Zhang, Y. (1999). A new merging method and its spectral and spatial effects. **International Journal of Remote Sensing**. 20: 2003-2014.

Zhang, Y. (2002). A new automatic approach for effectively fusing landsat 7 as well as IKONOS images. **IGARSS**. 4: 2429-2431.

Zhang, Y. (2002). Problems in the fusion of commercial high-resolution satellite as well as Landsat 7 images and initial solutions. **Proc. Of ISPRS, vol.34, part 4 Geospatial theory, processing and applications, Ottawa, July 8-12, 2002**, [Online]. Available: <http://www.isprs.org/proceedings/XXXIV/part4/pdppapers/220.pdf>.

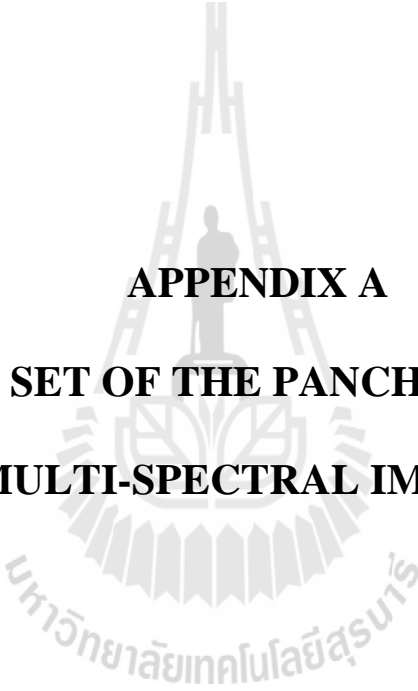
Zhang, Y., and Hong, G. (2005). An IHS and wavelet integrated approach to improve pan-sharpening visual quality of natural colour IKONOS and QuickBird images. **Information Fusion**. 6(3): 225-234.

Zhao, H., Kumagai, J., Nakagawa, M., and Shibasaki, R. (2002). Semi-automatic road extraction from high-resolution satellite image. **Proc. Of ISPRS**. 34(3): 406-411.

Zhou, J., Civco, D.L., and Silander, J.A. (1998). A wavelet transform method to merge landsat TM and SPOT panchromatic data. **International Journal of Remote Sensing**. 19: 743-757.



APPENDICES



APPENDIX A
THE DATA SET OF THE PANCHROMATIC AND
MULTI-SPECTRAL IMAGES

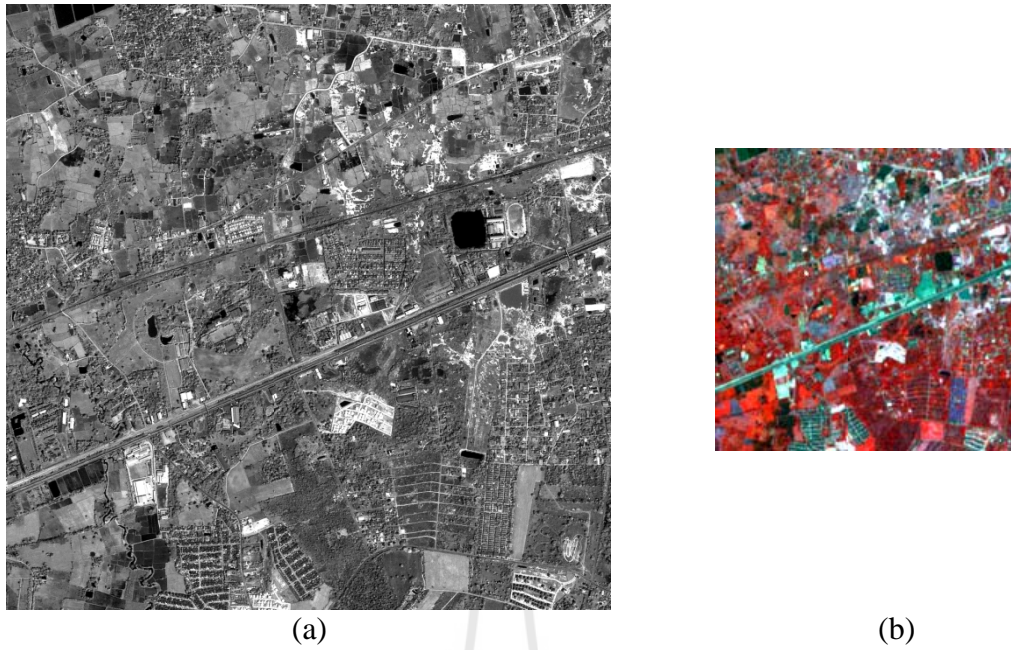


Figure A.1 The image data set 1 (a) Panchromatic image (b) Multispectral images.

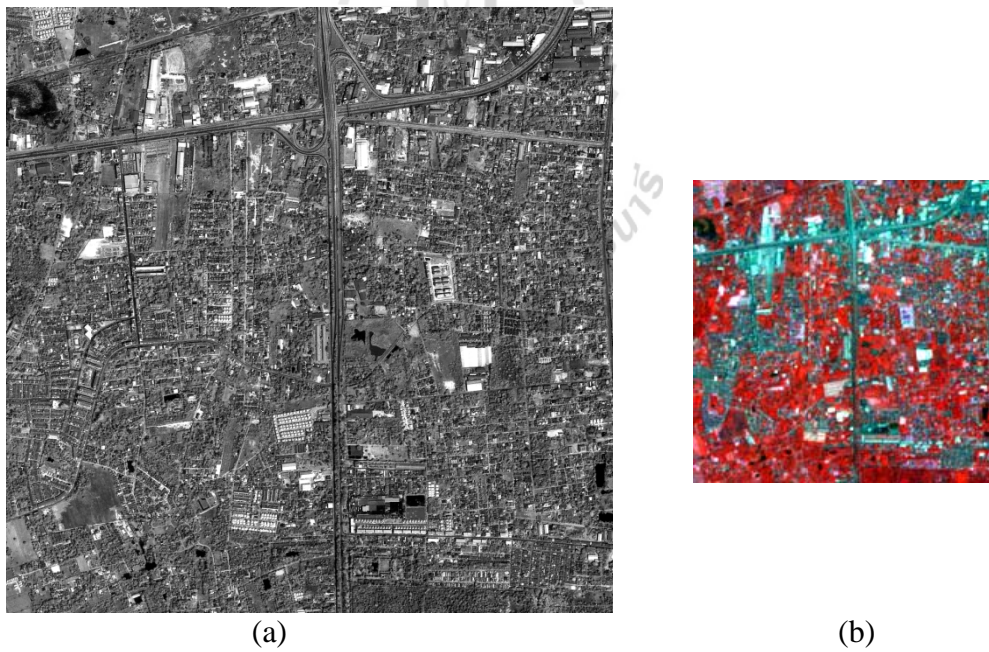


Figure A.2 The image data set 2 (a) Panchromatic image (b) Multispectral images.

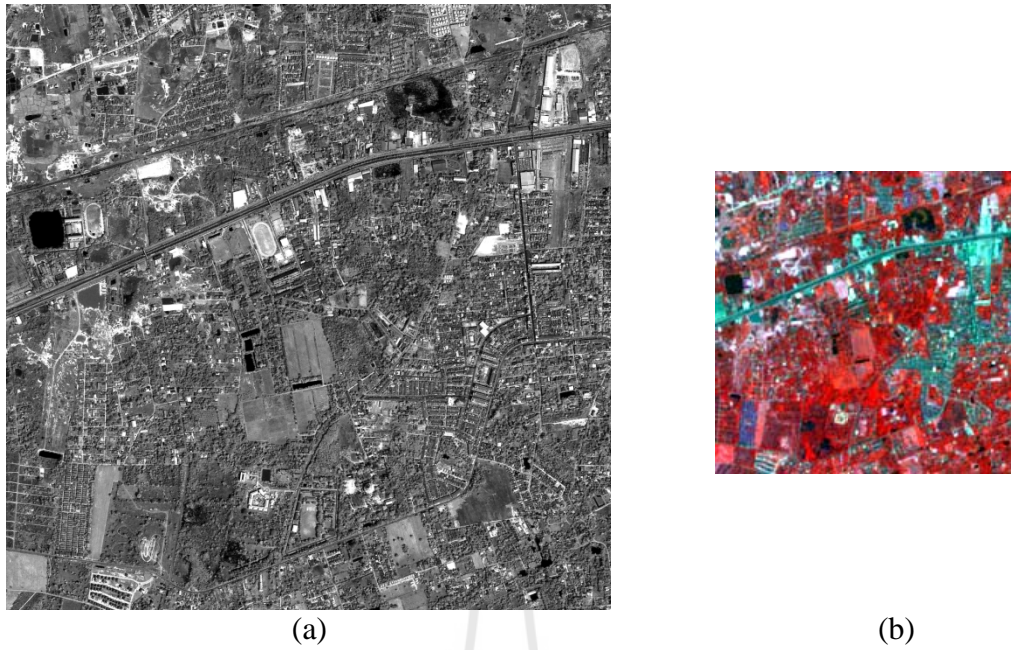


Figure A.3 The image data set 3 (a) Panchromatic image (b) Multispectral images.

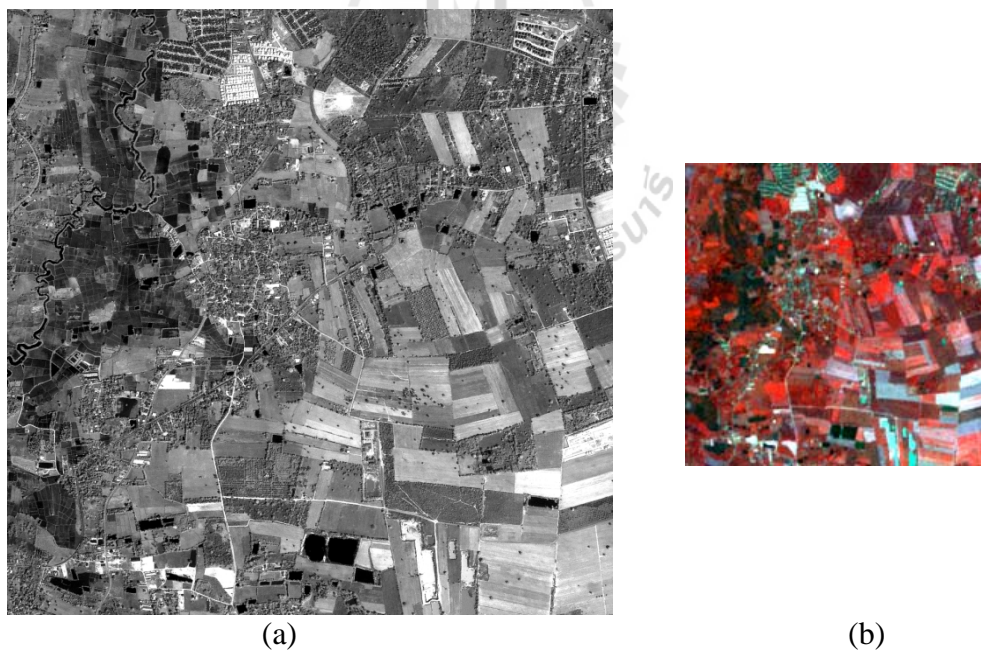
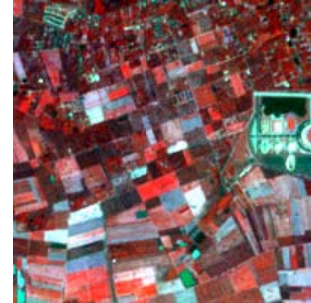


Figure A.4 The image data set 4 (a) Panchromatic image (b) Multispectral images.



(a)



(b)

Figure A.5 The image data set 5 (a) Panchromatic image (b) Multispectral images.



(a)



(b)

Figure A.6 The image data set 6 (a) Panchromatic image (b) Multispectral images.

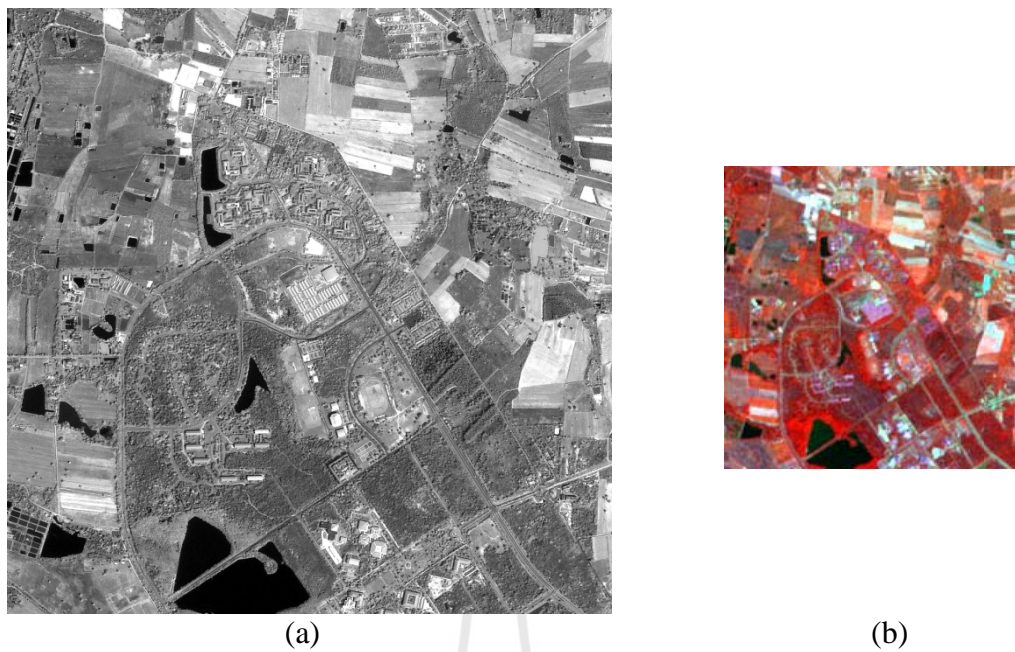


Figure A.7 The image data set 7 (a) Panchromatic image (b) Multispectral images.

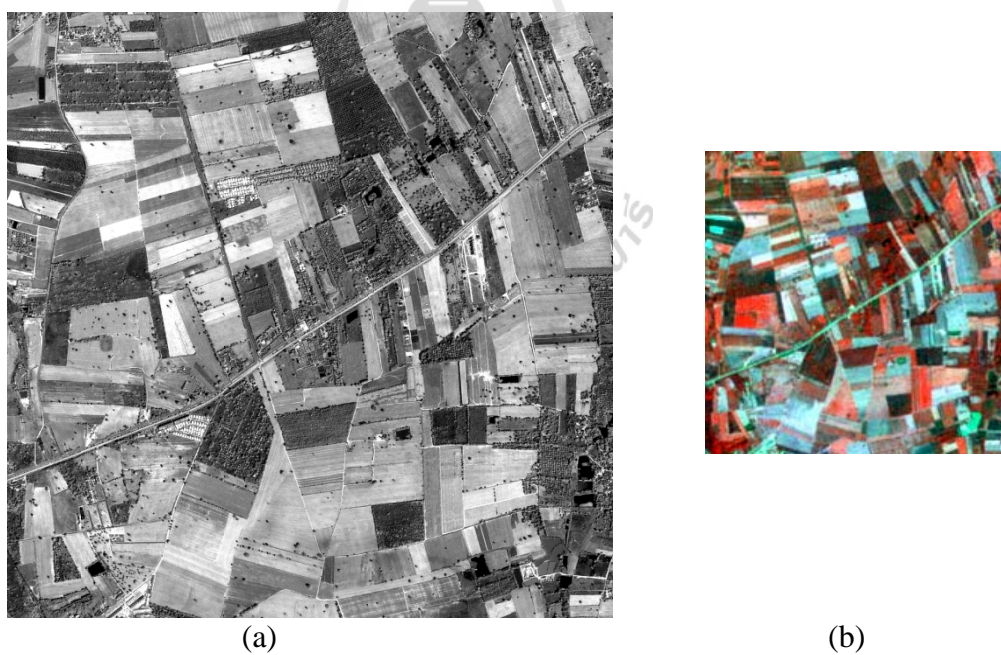


Figure A.8 The image data set 8 (a) Panchromatic image (b) Multispectral images.

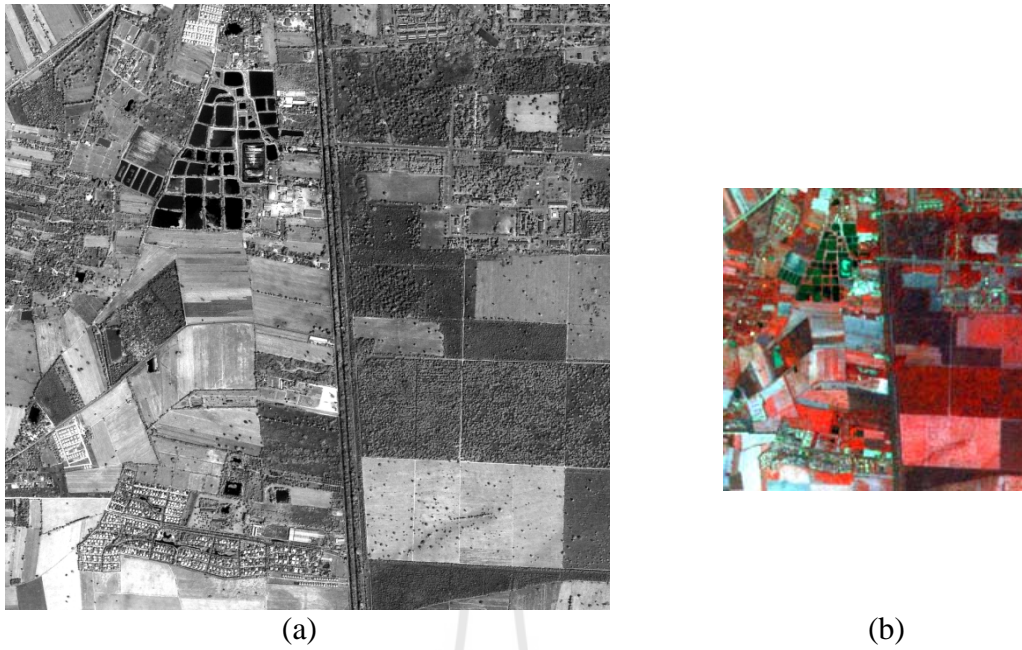


Figure A.9 The image data set 9 (a) Panchromatic image (b) Multispectral images.

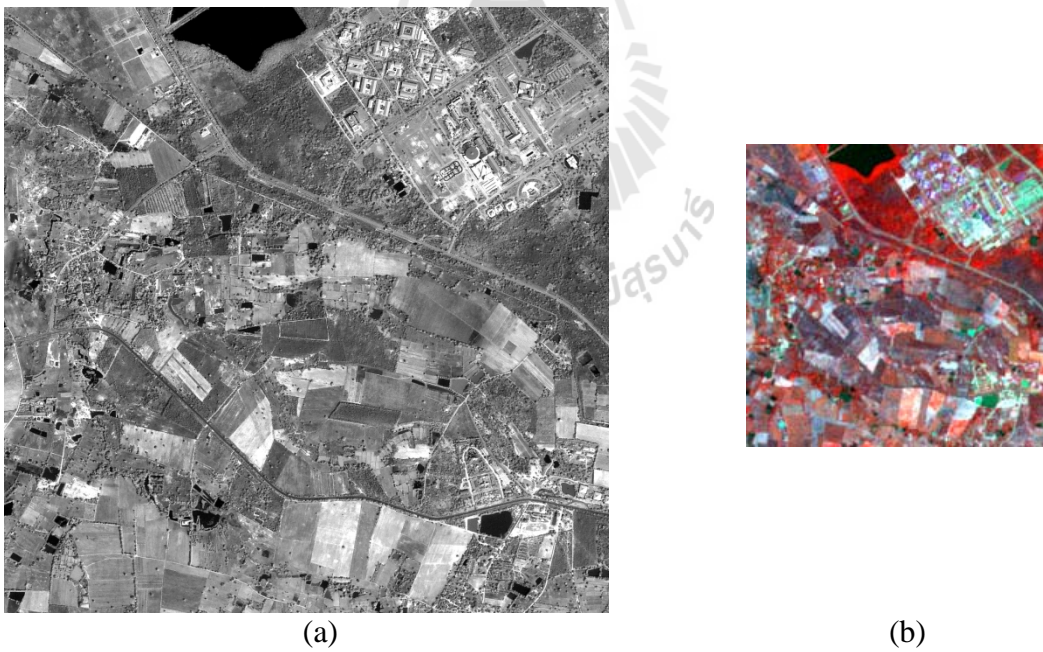


Figure A.10 The image data set 10 (a) Panchromatic image (b) Multispectral images.

APPENDIX B
THE COMPARISON OF THE CCs OF THE ORIGINAL
MULTI-SPECTRAL AND THE PAN-SHARPENED
IMAGES

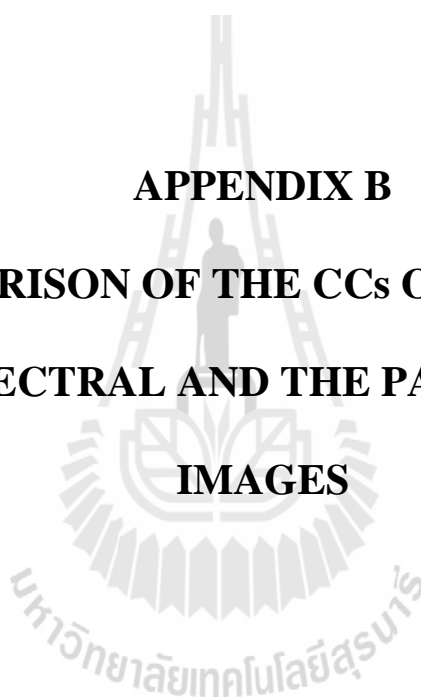


Table B.1 The comparison of the CCs resulted from the Trial no.1 and the FIHS method of Tu el al. (2004).

CCs	Data set 1		Data set 2		Data set 3		Data set 4		Data set 5		Data set 6		Data set 7		Data set 8		Data set 9		Data set 10	
	FIHS	Trial no.1	FIHS	Trial no.1	FIHS	Trial no.1	FIHS	Trial no.1	FIHS	Trial no.1	FIHS	Trial no.1	FIHS	Trial no.1	FIHS	Trial no.1	FIHS	Trial no.1	FIHS	Trial no.1
Band 1	0.1440	0.5600	0.2297	0.6682	0.1775	0.6194	0.0814	0.4654	0.1223	0.7870	0.1896	0.5742	0.2465	0.5986	0.1749	0.5986	0.2306	0.6025	0.1977	0.5616
Band 2	0.3874	0.7412	0.4536	0.7998	0.4088	0.7729	0.4332	0.7458	0.4864	0.5197	0.5137	0.8041	0.5457	0.8401	0.5615	0.8401	0.5355	0.8016	0.4691	0.7616
Band 3	0.7278	0.8989	0.7310	0.9085	0.7404	0.9099	0.7981	0.9202	0.8228	0.9342	0.8158	0.9341	0.8226	0.9585	0.8772	0.9585	0.8402	0.9367	0.7914	0.9176
Band 4	0.7564	0.8991	0.7313	0.8855	0.7432	0.8951	0.8439	0.9350	0.8400	0.9361	0.7962	0.9216	0.8984	0.9418	0.8440	0.9418	0.8822	0.9498	0.8364	0.9312
Average	0.5039	0.7748	0.5364	0.8155	0.5175	0.7993	0.5391	0.7666	0.5679	0.7943	0.5788	0.8085	0.6283	0.8347	0.6144	0.8347	0.6221	0.8226	0.5737	0.7930

Table B.2 The comparison of the CCs resulted from the Trial no.2 and the FIHS method of Tu el al. (2004).

CCs	Data set 1		Data set 2		Data set 3		Data set 4		Data set 5		Data set 6		Data set 7		Data set 8		Data set 9		Data set 10	
	FIHS	Trial no.1	FIHS	Trial no.1	FIHS	Trial no.1	FIHS	Trial no.1	FIHS	Trial no.1	FIHS	Trial no.1	FIHS	Trial no.1	FIHS	Trial no.1	FIHS	Trial no.1	FIHS	Trial no.1
Band 1	0.1440	0.3878	0.2297	0.4710	0.1775	0.4094	0.0814	0.3048	0.1223	0.3557	0.1896	0.4311	0.2465	0.3950	0.1749	0.3950	0.2306	0.4566	0.1977	0.4456
Band 2	0.3874	0.6840	0.4536	0.7134	0.4088	0.6906	0.4332	0.7136	0.4864	0.7552	0.5137	0.7683	0.5457	0.7931	0.5615	0.7931	0.5355	0.7810	0.4691	0.7406
Band 3	0.7278	0.8937	0.7310	0.8835	0.7404	0.8948	0.7981	0.9276	0.8228	0.9348	0.8158	0.9304	0.8226	0.9547	0.8772	0.3950	0.8402	0.9421	0.7914	0.9235
Band 4	0.7564	0.9025	0.7313	0.8776	0.7432	0.8912	0.8439	0.9439	0.8400	0.9399	0.7962	0.9207	0.8984	0.9401	0.8440	0.9401	0.8822	0.9570	0.8364	0.9398
Average	0.5039	0.7170	0.5364	0.7364	0.5175	0.7215	0.5391	0.7250	0.5679	0.7464	0.5788	0.7626	0.6283	0.7707	0.6144	0.7707	0.6221	0.7842	0.5737	0.7624

Table B.3 The comparison of the CCs resulted from the Trial no.3 and the FIHS method of Tu et al. (2004).

CCs	Data set 1		Data set 2		Data set 3		Data set 4		Data set 5		Data set 6		Data set 7		Data set 8		Data set 9		Data set 10	
	FIHS	Trial no.1	FIHS	Trial no.1	FIHS	Trial no.1	FIHS	Trial no.1	FIHS	Trial no.1	FIHS	Trial no.1	FIHS	Trial no.1	FIHS	Trial no.1	FIHS	Trial no.1	FIHS	Trial no.1
Band 1	0.1440	-0.0043	0.2297	0.0373	0.1775	0.0187	0.0814	-0.0199	0.1223	0.0028	0.1896	0.0529	0.2465	0.0722	0.1749	0.0722	0.2306	0.1069	0.1977	0.1069
Band 2	0.3874	0.1832	0.4536	0.2201	0.4088	0.1985	0.4332	0.2635	0.4864	0.3114	0.5137	0.3323	0.5457	0.4120	0.5615	0.4120	0.5355	0.3702	0.4691	0.3702
Band 3	0.7278	0.5552	0.7310	0.5448	0.7404	0.5714	0.7981	0.6725	0.8228	0.7086	0.8158	0.6953	0.8226	0.7992	0.8772	0.7992	0.8402	0.7356	0.7914	0.7356
Band 4	0.7564	0.5960	0.7313	0.5704	0.7432	0.5865	0.8439	0.7318	0.8400	0.7309	0.7962	0.6635	0.8984	0.7447	0.8440	0.7447	0.8822	0.7963	0.8364	0.7963
Average	0.5039	0.3325	0.5364	0.3431	0.5175	0.3438	0.5391	0.4120	0.5679	0.4384	0.5788	0.4360	0.6283	0.5070	0.6144	0.5070	0.6221	0.5022	0.5737	0.5022





APPENDIX C

THE MODULE OF FCM AND SA, ROAD EXTRACTION

DEVELOPED BY IDL PROGRAMMING

File name : fcmsa_ru.pro

```

PRO fcmsa_run_define_buttons, buttonInfo
  ENVI_DEFINE_MENU_BUTTON, buttonInfo, $
    VALUE = 'Fuzzy C-Means', $
    REF_VALUE = 'K-Means', $
    EVENT_PRO = 'fcmsa_run', $
    UVALUE = 'FKCMM', $
    POSITION = 'after'
END

pro fcmsa_run, event

COMPILE_OPT STRICTARR

print, '-----'
print, 'Fuzzy-C-Means Clustering'
print, systime(0)
print, '-----'

catch, theError
if theError ne 0 then begin
  void = Dialog_Message(!Error_State.Msg, /error)
  return
endif

envi_select, title='Choose multispectral image for clustering', $
  fid=fid, dims=dims, pos=pos
if (fid eq -1) then begin
  print, 'cancelled'
  return
endif

envi_file_query, fid, fname=fname, xstart=xstart, ystart=ystart
print, 'Selected image: ', fname
print, 'Selected bands: ', pos + 1

; tie point
map_info = envi_get_map_info(fid=fid)
envi_convert_file_coordinates, fid, dims[1], dims[3], e, n, /to_map
map_info.mc[2:3]= [e,n]

; number of clusters
base = widget_auto_base(title='Number of Classes')
wg = widget_sslider(base, title='Classes', min=2, max=15, $
  value=6, dt=1, uvalue='slide', /auto)
result = auto_wid_mng(base)

```



```

if (result.accept eq 0) then begin
    print, 'cancelled'
    return
endif
K = byte(result.slide)
print, 'Number of clusters', K

; init temperature
map_info = envi_get_map_info(fid=fid)
envi_convert_file_coordinates, fid, dims[1], dims[3], e, n, /to_map
map_info.mc[2:3]= [e,n]

base = widget_auto_base(title='Clustering parameters')
list = ['T0', 'Beta']
vals = [100,0.5]
we = widget_edit(base, list=list, uvalue='edit', $
    vals=vals, field= 2, dt=4, /auto)
result = auto_wid_mng(base)
if (result.accept eq 0) then begin
    print,'cancelled'
    return
endif
T0 = result.edit[0]
beta = result.edit[1]

query=dialog_message('Export clusters to ROIs',/question)
if query eq 'Yes' then roi_flag=1 else roi_flag=0

; output destination
base = widget_auto_base(title='FCM SA Output')
sb = widget_base(base, /row, /frame)
wp = widget_outfm(sb, uvalue='outf', /auto)
result = auto_wid_mng(base)
if (result.accept eq 0) then begin
    print, 'cancelled'
    return
endif

c_names = strarr(K+1)
fhvs = ftarr(K)
c_names[0] = 'unclassified'
for i=1,K do c_names[i]='cluster: '+strtrim(i,2)

num_cols = dims[2]-dims[1]+1L
num_rows = dims[4]-dims[3]+1L
num_pixels = (num_cols*num_rows)
num_bands = n_elements(pos)

```

```

s_image = fltarr(num_bands,num_pixels)
widget_control, /hourglass

if num_pixels gt 100000 then $
; random sample of 100000 pixels
  indices = randomu(seed, 100000, /long) mod num_pixels $
; all pixels
else indices = lindgen(num_pixels)

G = fltarr(num_bands,n_elements(indices))
image = fltarr(num_bands,num_pixels)
for i=0,num_bands-1 do begin
  temp= envi_get_data(fid=fid,dims=dims,pos=pos[i])
  image[i,*] = temp
  G[I,*]=temp[indices]
endfor

; initialize memberships at random
U = randomu(seed,n_elements(indices),K)
for j=0,K-1 do U[*,j]=U[*,j]/total(U,2)

sizeG=size(G)
sizeU=size(U)
print,'size G',sizeG
print,'size U',sizeU
print,'t0',T0
FCMSA, G, U, Ms, T0=T0

; export clusters to ROIs
if roi_flag then begin
  envi_delete_rois, envi_get_roi_ids()
  labels = cluster_fcm(G, Ms) + 1B
  if n_elements(labels) eq 1 then return
  for i=1,K do begin
    roi_id = envi_create_roi(color=i+1, name=c_names[i], ns=num_cols,
nl=num_rows)
    ind = where(labels eq i,count)
    if count gt 0 then begin
      xpts = indices[ind] mod num_cols
      ypts = indices[ind]/num_cols
    endif
    envi_define_roi, roi_id, /point, xpts=xpts, ypts=ypts
  endfor
endif

; classify the image
print, 'classifying...'

```

```

labels = cluster_fcm(image, Ms) + 1B
if n_elements(labels) eq 1 then return

; write result to memory or disk
if (result.outf.in_memory eq 1) then begin
  envi_enter_data, byte(reform(labels,num_cols,num_rows)), $
    file_type=3, $
    map_info=map_info, $
    bnames=['FCM('+fname+')'],$
    num_classes=K+1, $
    class_names=c_names, $
    xstart=xstart+dims[1], $
    ystart=ystart+dims[3], $
    lookup=class_lookup_table(indgen(K+1))
  print, 'Result written to memory'
endif else begin
  openw, unit, result.outf.name, /get_lun
  writeu, unit, byte(reform(labels,num_cols,num_rows))
  envi_setup_head ,fname=result.outf.name, ns=num_cols, nl=num_rows, nb=1, $
    data_type=1, $
    interleave=2, $
    file_type=3, $
    map_info=map_info, $
    bnames=['FCM('+fname+')'],$
    num_classes=K+1, $
    class_names=c_names, $
    xstart=xstart+dims[1], $
    ystart=ystart+dims[3], $
    lookup=class_lookup_table(indgen(K+1)), $
    descrip='FCM clustering of ' + result.outf.name, $
    /write
  print, 'File created ', result.outf.name
  free_lun, unit
endelse

end

// end of file fcmsa_run.pro

```

File name : fcmsa.pro

```

pro FCMSA, G, U, Ms, niter=niter, unfrozen=unfrozen,T0=T0

n = (size(G))[2]
NN = (size(G))[1]
K = (size(U))[2]
MsNew=fltarr(NN,K)
if n_elements(niter) eq 0 then niter = 500 ;500
if n_elements(unfrozen) eq 0 then unfrozen = lindgen(n)

; vector distances to cluster centers
Ds = fltarr(n,NN)
; work array
W = fltarr(n,NN)

; iteration
progressbar = Obj_New('progressbar', Color='blue', Text='0',$
    title='FCM clustering: delta_U...',xsize=250,ysize=20)
progressbar->start
dU = 1.0 & iter=0L
dMs=1.0
T = T0
SSnew=0
;while ((dMs gt 0.001) or (iter lt 20)) and (iter lt niter) do begin
while (T gt 0.0001) do begin
    if progressbar->CheckCancel() then begin
        print,'clustering aborted'
        progressbar->Destroy
        return
    endif
    progressbar->Update,(iter*100)/niter,text=strtrim(dMs,2)
    Uold = U
    UU = U*U
    Msold=Msnew
    SSold=SSnew
    ; update means and distances
    Ms = transpose(UU##G)
    for j=0,K-1 do begin
        Ms[j,*]=Ms[j,;]/total(UU[*],j)
        for i=0,NN-1 do W[*],i]=replicate(Ms[j],i),n)
        Ds = transpose(G)-W
        Dspi=(U*U)*(Ds*Ds)
        dd = 1/total(Ds*Ds,2)
        U[unfrozen,j] = dd[unfrozen]
    endfor
; normalize
    prixb=total(Dspi)/n
    Msnew=Ms

```

```

for j=0,K-1 do U[* ,j]=U[* ,j]/total(U,2)
dU = max(abs(U-Uold))
iter=iter+1

dMs=min(abs(MsOld-MsNew))
dMss=dMs*dMs
SS=prixb/dMss

print,"SS",SS
print,"SSold",SSold
SSnew=SS
;cal Dss
Dss=SSnew-SSold
print,"distanc ss",Dss
RanPs=RANDOMU(seed,1)
print,"random",RanPs
if Dss gt 0 then begin
  P=1/(1+exp(-(Dss/T)))
  print,"p",P
  if RanPs lt P then SSnew=SSold else SSnew=SSnew
endif else begin SSnew=SSnew
endelse

print,"SSnew",SSnew
iter=iter+1
T = 0.8*T

print,"Tnew",T
print,"loop",iter
endwhile

Ms = transpose(Ms)
progressbar->destroy

end

//end of file fcmsa.pro

```

The module for automated road extraction

File name : autoroadextraction.pro

```

PRO autoroadextraction_define_buttons,buttoninfo
  ENVI_DEFINE_MENU_BUTTON, buttonInfo, $
  VALUE = 'autoroadextraction', $
  REF_VALUE = 'autoroadextraction', $
  EVENT_PRO = 'autoroadextraction', $
  UVALUE = 'MM',$
  POSITION = 'after'
END
pro autoroadextraction,event
  COMPILE_OPT STRICTARR
  print, '-----'
  print, 'automatic road extraction module'
  print, systime(0)
  print, '-----'

  catch, theError
  if theError ne 0 then begin
    void = Dialog_Message(!Error_State.Msg, /error)
    return
  endif

  envi_select, title='Choose Binary image ', $
    fid=fid, dims=dims,pos=pos
  if (fid eq -1) then begin
    print, 'cancelled'
    return
  endif

  envi_file_query, fid, fname=fname, xstart=xstart, ystart=ystart
    print, 'Selected image: ',fname
    print, 'Selected bands: ',pos + 1
  imroad=READ_IMAGE(fname)
  envi_select, title='Choose edge image', $
    fid=fid_edge, dims=dims_edge,pos=pos_edge
  if (fid_edge eq -1) then begin
    print, 'cancelled'
    return
  endif

  envi_file_query, fid_edge, fname=fname_edge, xstart=xstart, ystart=ystart
    print, 'Selected image: ',fname_edge
    print, 'Selected bands: ',pos + 1

  imedge=READ_IMAGE(fname_edge)

  base = widget_auto_base(title='The structure element')
  list = ['structure element']

```

```

vals = [3]
we = widget_edit(base, list=list, uvalue='edit', $
  vals=vals, field= 1, dt=4, /auto)
result = auto_wid_mng(base)
if (result.accept eq 0) then begin
  print,'cancelled'
  return
endif

query=dialog_message('Export road centerline ',/question)
if query eq 'Yes' then roi_flag=1 else roi_flag=0

; output destination
topLB = WIDGET_AUTO_BASE(title='Enter Output Filename')
out = WIDGET_OUTF(topLB, /auto, uvalue='outf', xsize=30)
result2 = AUTO_WID_MNG(topLB)
if (result2.accept eq 0) then begin
  print, 'cancelled'
  return
endif

;start define structure large area
stre =3
strucElem = DIST(stre) LE stre
print,strucElem
stre2 =4
strucElem2 = DIST(stre2) LE stre2
print,strucElem2
stre1 = result.edit[0]
strucElem1 = DIST(stre1) LE stre1
print,strucElem1

imdilate=DILATE(imroad,strucElem)
tophatImgb = MORPH_TOPHAT(imdilate, strucElem1)
imopen=MORPH_OPEN(tophatImgb, strucElem)
tophatImgs = MORPH_TOPHAT(imopen, strucElem2)
mask= tophatImgs LT 200
newmask=imopen*mask
imclose=MORPH_CLOSE(newmask,strucElem)

sz = SIZE(imroad)
imagebw = BYTARR(1,sz[1], sz[2])
for i=0,sz[1]-1 do begin
  for j=0,sz[2]-1 do begin
    if(imroad[i,j] GT 200) AND (imedge[i,j] GT 200) then begin
      imagebw[0,i,j]=255
    end else begin

```

```

        imagebw[0,i,j]=0
    endelse

    endfor
endfor

h0 = [[0b, 0, 0], [0, 1, 0], [1, 1, 1]]
m0 = [[1b, 1, 1], [0, 0, 0], [0, 0, 0]]
h1 = [[0b, 0, 0], [1, 1, 0], [1, 1, 0]]
m1 = [[0b, 1, 1], [0, 0, 1], [0, 0, 0]]
h2 = [[1b, 0, 0], [1, 1, 0], [1, 0, 0]]
m2 = [[0b, 0, 1], [0, 0, 1], [0, 0, 1]]
h3 = [[1b, 1, 0], [1, 1, 0], [0, 0, 0]]
m3 = [[0b, 0, 0], [0, 0, 1], [0, 1, 1]]
h4 = [[1b, 1, 1], [0, 1, 0], [0, 0, 0]]
m4 = [[0b, 0, 0], [0, 0, 0], [1, 1, 1]]
h5 = [[0b, 1, 1], [0, 1, 1], [0, 0, 0]]
m5 = [[0b, 0, 0], [1, 0, 0], [1, 1, 0]]
h6 = [[0b, 0, 1], [0, 1, 1], [0, 0, 1]]
m6 = [[1b, 0, 0], [1, 0, 0], [1, 0, 0]]
h7 = [[0b, 0, 0], [0, 1, 1], [0, 1, 1]]
m7 = [[1b, 1, 0], [1, 0, 0], [0, 0, 0]]

; Iterate until the thinned image is identical to
; the input image for a given iteration.
bCont = 1b
iIter = 1

B=replicate(1,3,3)
im1=DILATE(ERODE(img2,B),B)
;im1=MORPH_OPEN(imagebw,B)
thinImg = im1

WHILE bCont EQ 1b DO BEGIN
    PRINT,'Iteration: ', iIter
    inputImg = thinImg

    ; Perform the thinning using the first pair
    ; of structure elements.
    thinImg = MORPH_THIN(inputImg, h0, m0)

    ; Perform the thinning operation using the
    ; remaining structural element pairs.
    thinImg = MORPH_THIN(thinImg, h1, m1)
    thinImg = MORPH_THIN(thinImg, h2, m2)
    thinImg = MORPH_THIN(thinImg, h3, m3)

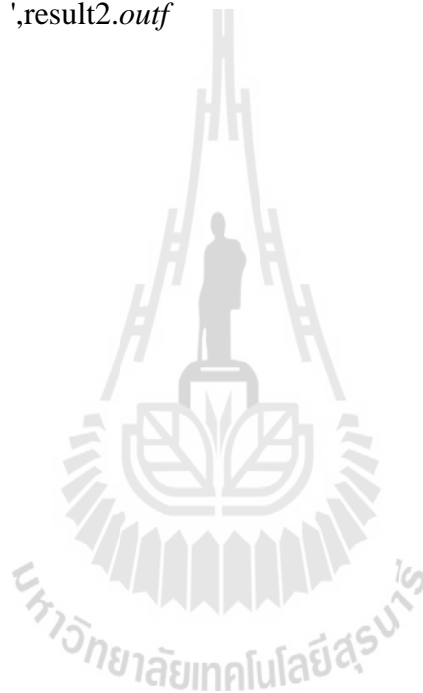
```



```
thinImg = MORPH_THIN(thinImg, h4, m4)
thinImg = MORPH_THIN(thinImg, h5, m5)
thinImg = MORPH_THIN(thinImg, h6, m6)
thinImg = MORPH_THIN(thinImg, h7, m7)
; Test the condition and increment the loop.
bCont = MAX(inputImg - thinImg)
iIter = iIter + 1

; End WHILE loop statements.
ENDWHILE

write_image,result2.outf,'tiff',thinImg
print, 'output image: ',result2.outf
end
```



CURRICULUM VITAE

Name Satith Sangpradid

Birthday 14 November 1976

Birth Place 137 Moo 12, Khok Sung Sub-district, Ubonratana District, Khon Kaen, Thailand

Education

1998 Bachelor of Science (Management Information Systems): Faculty of Sciences, Maharakham University Thailand

2003 Master of Science (Information Technology): Faculty of Information Technology, King Mongkut's University of Technology North Bangkok, Thailand

2006 Certificate Advanced of Studied in Remote Sensing and Geographic Information Systems School of Engineering and Technology Asian institute of Technology (AIT), Thailand

Scholarship

The financial support from Maharakham University, Thailand

Position and Place of Work

Lecturer in Faculty of Informatics, Maharakham University, Thailand.